Introduction to Gravitational Wave Data Analysis

真貝寿明　Hisaaki Shinkai

大阪工業大学情報科学部

http://www.oit.ac.jp/is/shinkai/

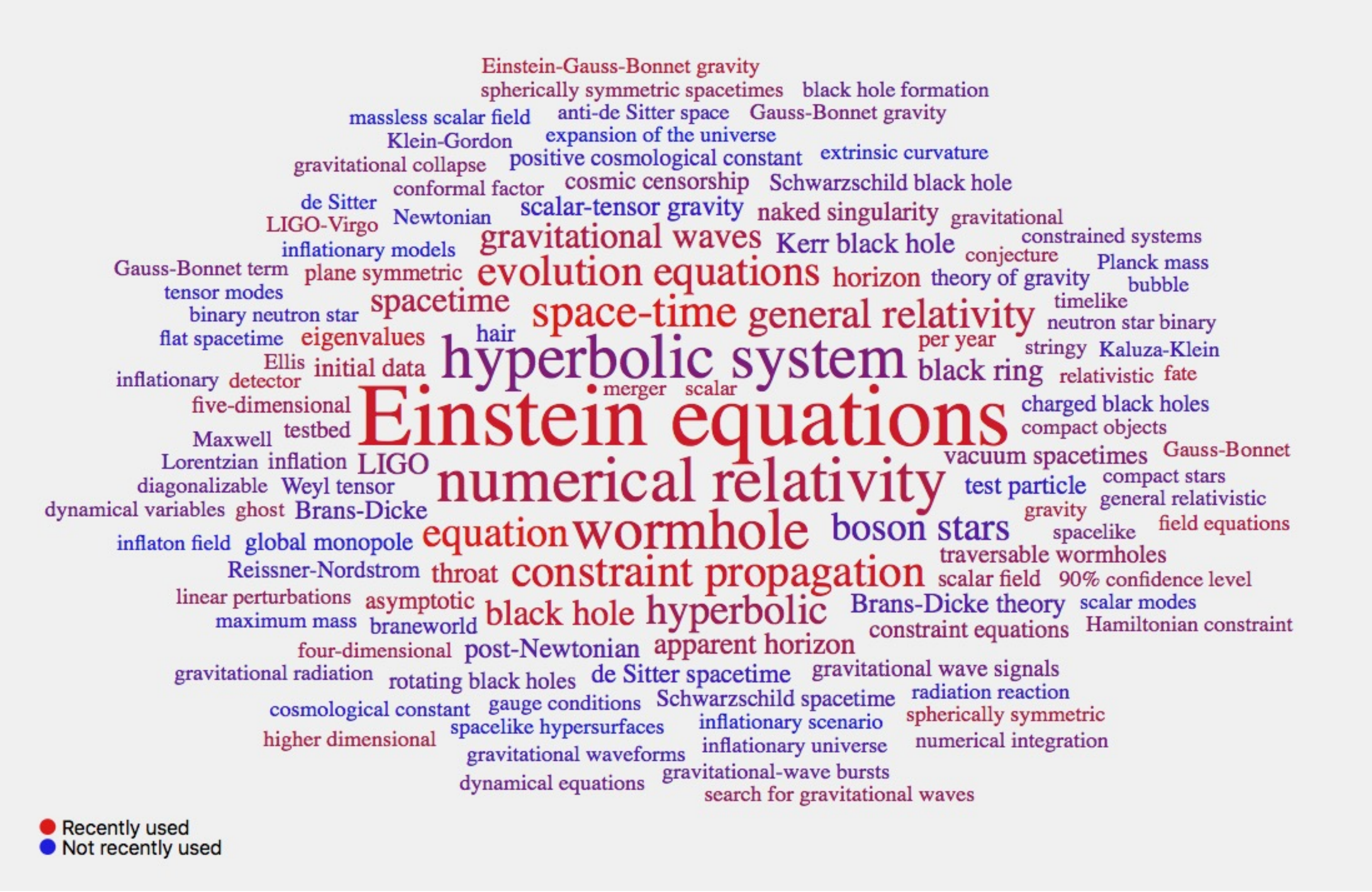

https://scimeter.org says.

references

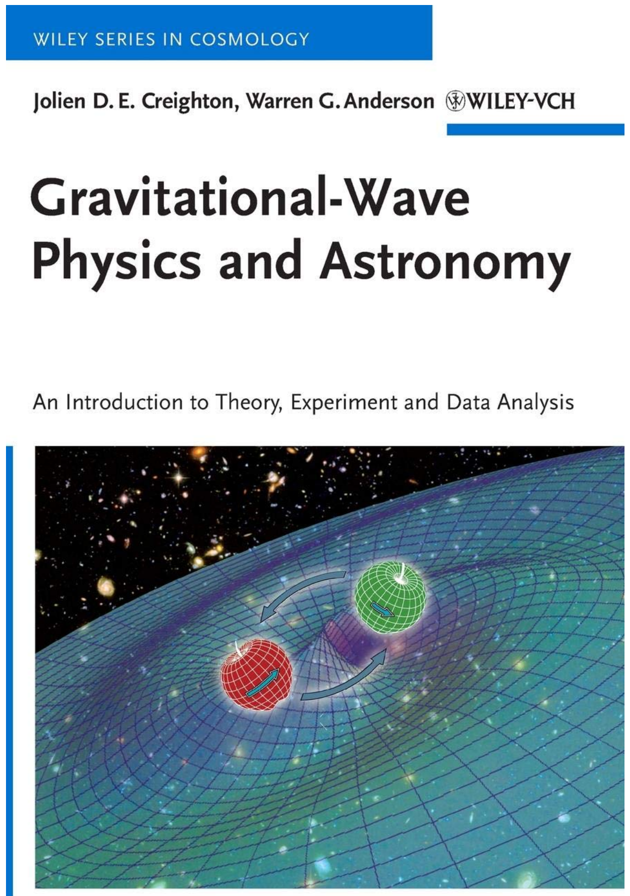

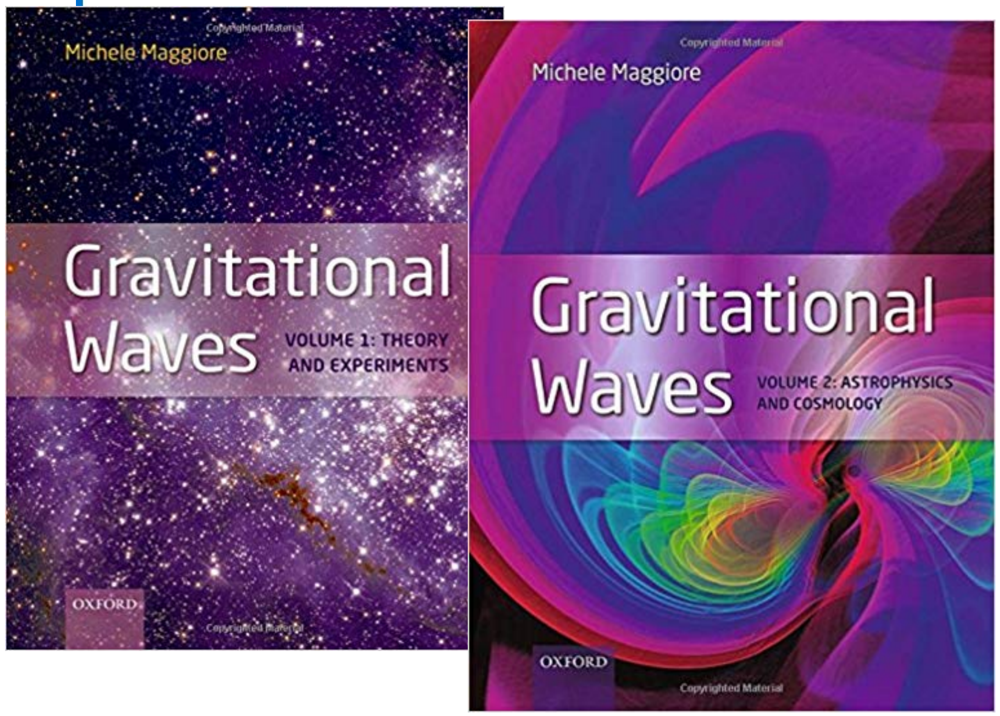

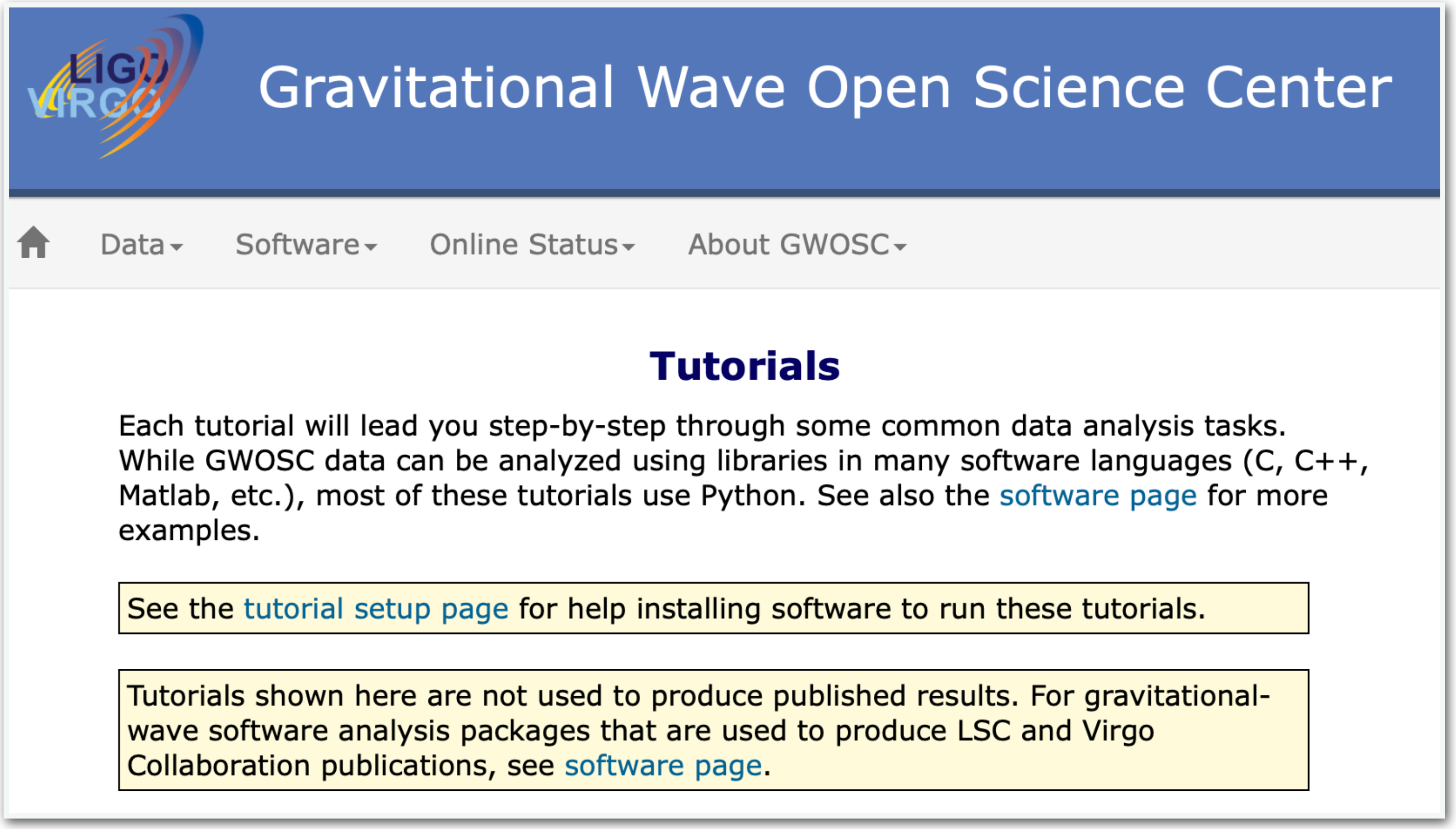

https://www.gw-openscience.org/tutorials/

references

370 システム/制御/情報, Vol. 62, No. 9, pp. 370–375, 2018

解　説

重力波の直接検出とデータ解析

真貝　寿明*

一般社団法人
システム制御情報学会
The Institute of Systems, Control and Information Engineers

https://www.iscie.or.jp/pub/journal

http://www.oit.ac.jp/is/~shinkai/

◆◆◆◆解説◆◆◆◆

重力波の観測とデータ解析

日本物理学会誌　Vol. 72, No. 3, 2017

田越秀行
大阪市立大学大学院理学研究科
tagoshi@sci.osaka-cu.ac.jp

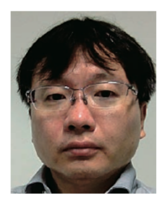

伊藤洋介
東京大学大学院理学系研究科附属ビッグバン宇宙国際研究センター
yousuke_itoh@resceu.s.u-tokyo.ac.jp

端山和大
東京大学宇宙線研究所重力波観測研究施設
hayama@icrr.u-tokyo.ac.jp

428 情報処理 Vol.57 No.5 May 2016

特別解説　応 専

重力波の初検出と情報処理技術

―LIGO と KAGRA で活用されている情報処理技術―

Kipp Cannon[*1]　端山和大[*1]　伊藤洋介[*1]　高橋弘毅[*2]
[*1] 東京大学
[*2] 長岡技術科学大学

重力波の波源 (GW sources)

http://gwcenter.icrr.u-tokyo.ac.jp

supernovae — 超新星爆発（写真出典:NASA）

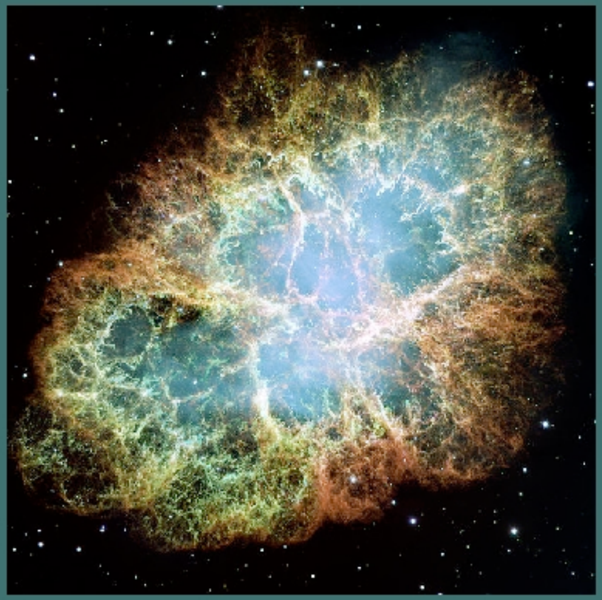

予測が難しい

hard to predict

pulsars — パルサー（写真出典:NASA）

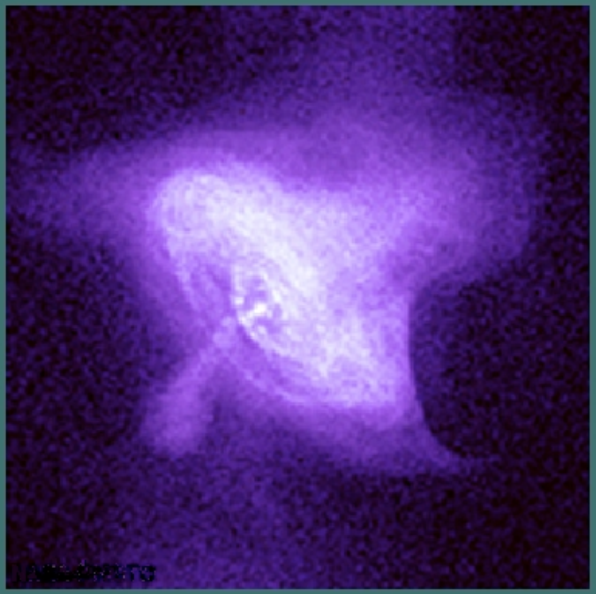

振幅が小さい

too small amplitude

black hole — ブラックホール（想像図）

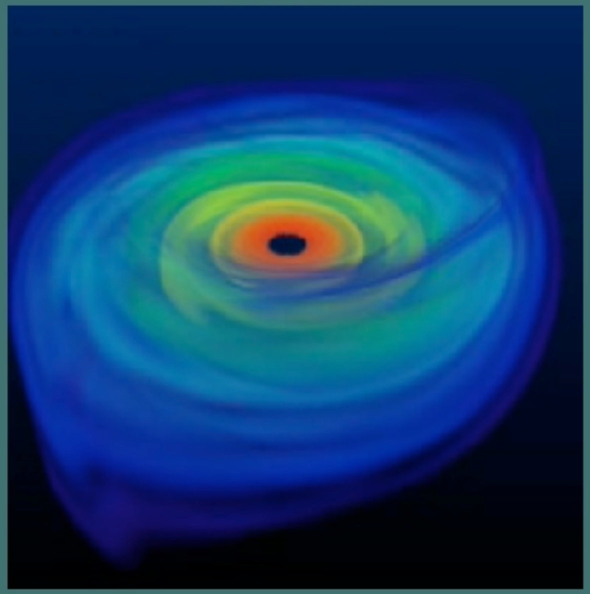

振幅が小さい

too small amplitude

binary neutron stars — 連星中性子星合体（想像図）

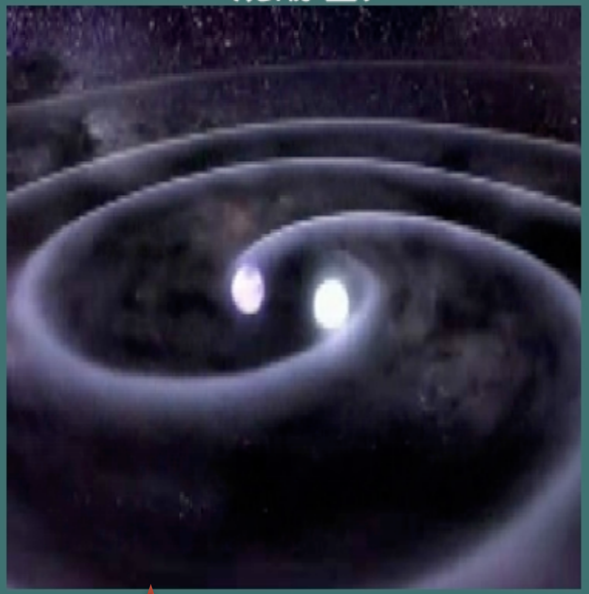

連星合体を
ターゲットに

binary coalescence

重力波の分類 (GW classification)

	sources	waveform prediction	data analysis	projects/codes
CBC	binary BHBH/ NSNS/BHNS	so so	so so	LALInference pyCBC, gstLAL BayesWave
Burst	supernovae	hard	unknown	cWB
CW	pulsars, rotating stars	easy	hard	Einstein@Home
Stochastic	cosmological	model dependent	hard	
unknown	unknown	unknown	unknown	

CBC: compact binary coalescence

連星系のパラメータ． $\boldsymbol{s}_1, \boldsymbol{s}_2, \boldsymbol{n}$ はベクトル量

2 つの天体の質量	m_1, m_2
2 つの天体の回転角運動量	$\boldsymbol{s}_1, \boldsymbol{s}_2$
連星軌道面の傾斜角	ι
合体時刻と合体時の位相	t_c, φ_c
観測地点からの波源方向	$-\hat{\boldsymbol{n}}$
2 つの重力波モードの偏角	ψ
観測地点からの距離	r

GW151226 (S/N=13.0)

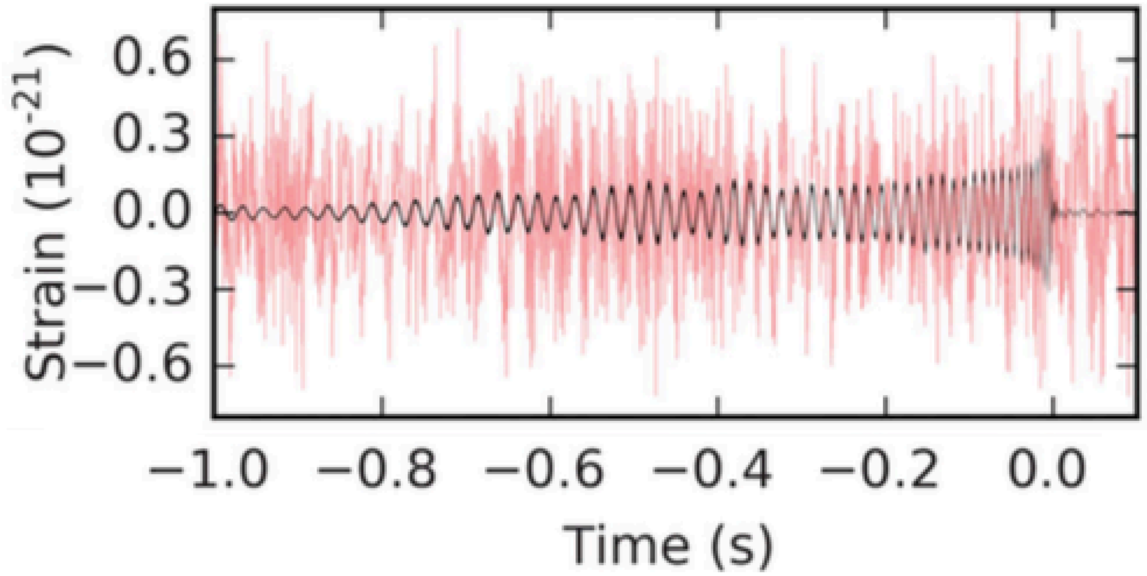

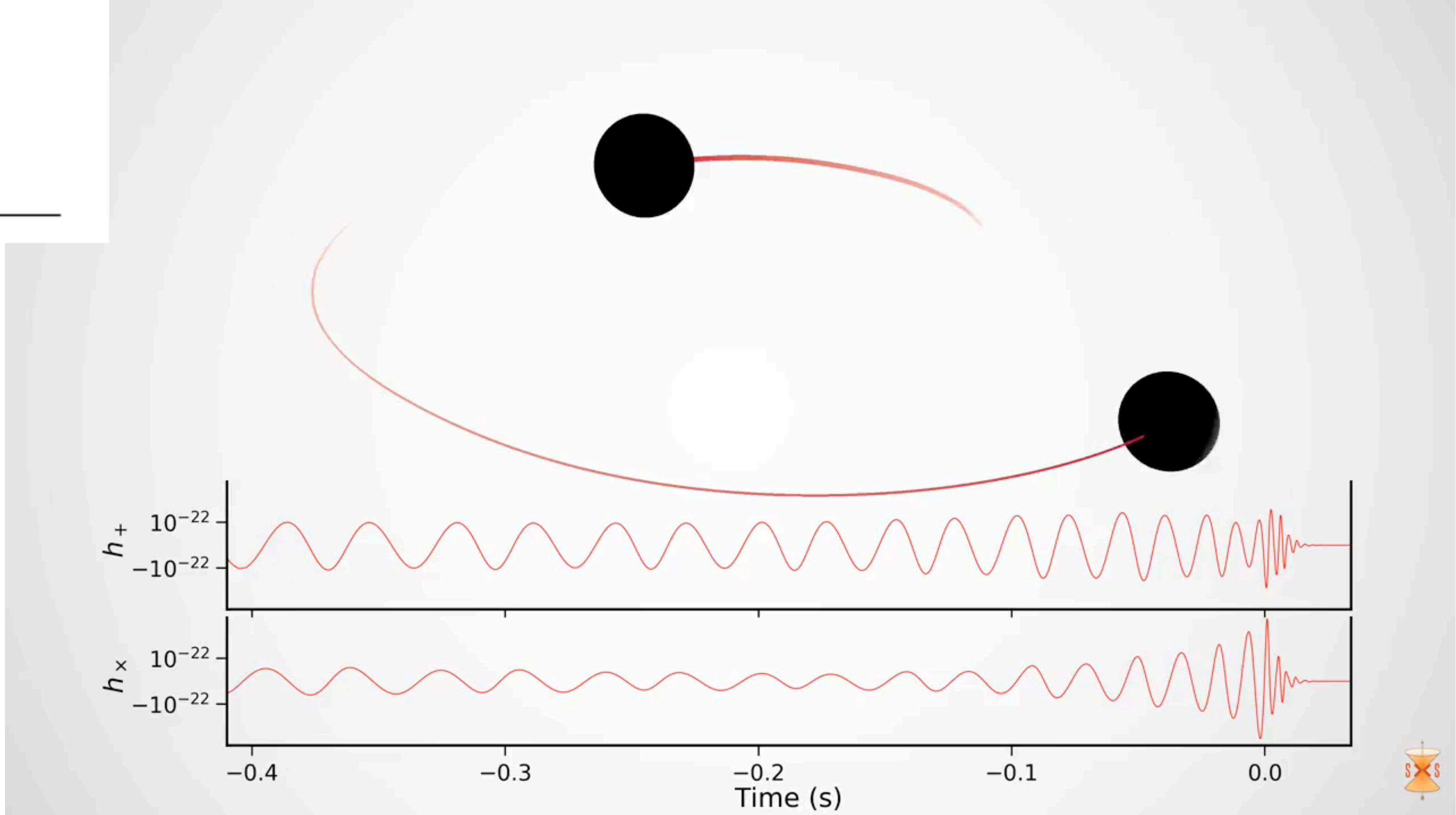

http://ligo.org/detections/GW170104.php

CBC: compact binary coalescence

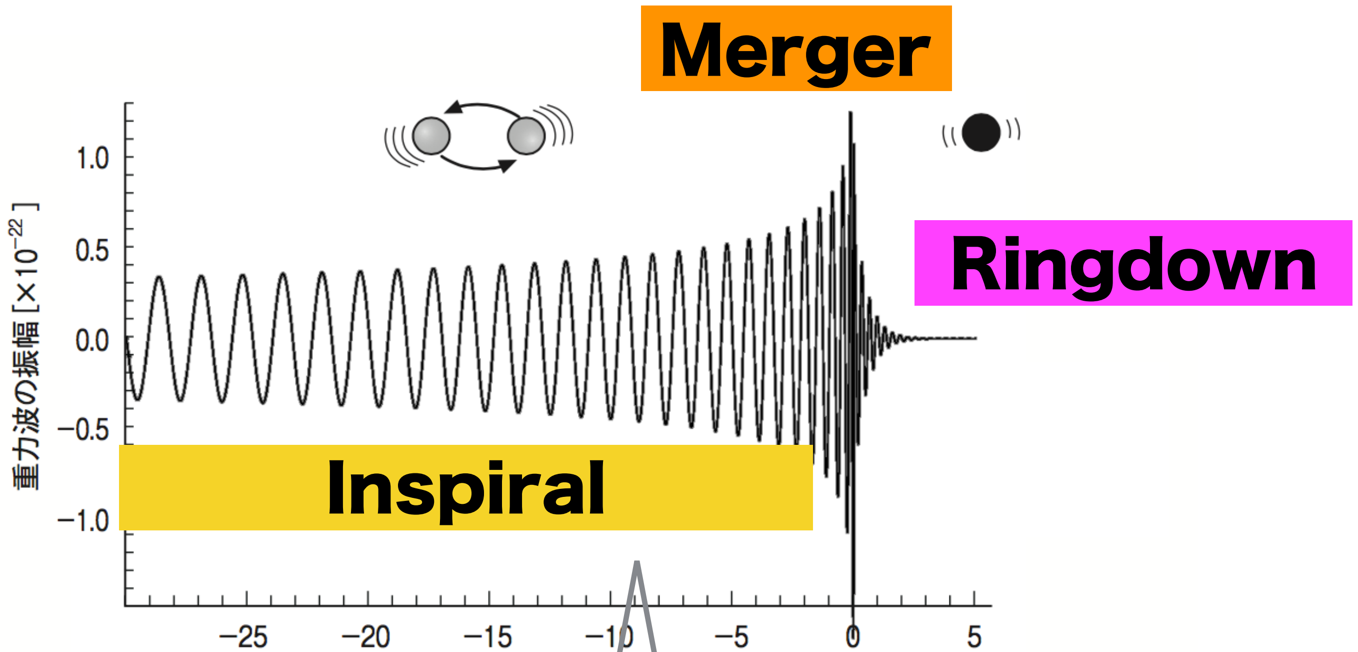

quadrupole formula

$$h_+(t) = -\frac{G\mathcal{M}}{c^2 r}\frac{1+\cos^2\iota}{2}\left(\frac{t_c - t}{5G\mathcal{M}/c^3}\right)^{-1/4}\cos 2\varphi$$

$$h_\times(t) = -\frac{G\mathcal{M}}{c^2 r}\cos\iota\left(\frac{t_c - t}{5G\mathcal{M}/c^3}\right)^{-1/4}\sin 2\varphi$$

chirp mass

$$\mathcal{M} = \frac{(m_1 m_2)^{3/5}}{(m_1+m_2)^{1/5}}$$

$$h(t+\tau) = F_+(\hat{\boldsymbol{n}},\psi)\, h_+(t) + F_\times(\hat{\boldsymbol{n}},\psi)\, h_\times(t)$$

$$h(t) = -\frac{G\mathcal{M}}{c^2 D}\left(\frac{t_c - t}{5G\mathcal{M}/c^3}\right)^{-1/4}\cos 2[\varphi(t)+\Delta\varphi]$$

where

$$D \equiv r\left[F_+^2\left(\frac{1+\cos^2\iota}{2}\right)^2 + F_\times^2\ \cos^2\iota\right]^{-1/2}$$

and

$$2\Delta\varphi \equiv -\tan^{-1}\left(\frac{F_x}{F_+}\frac{2\cos\iota}{1+\cos^2\iota}\right)$$

CBC: compact binary coalescence

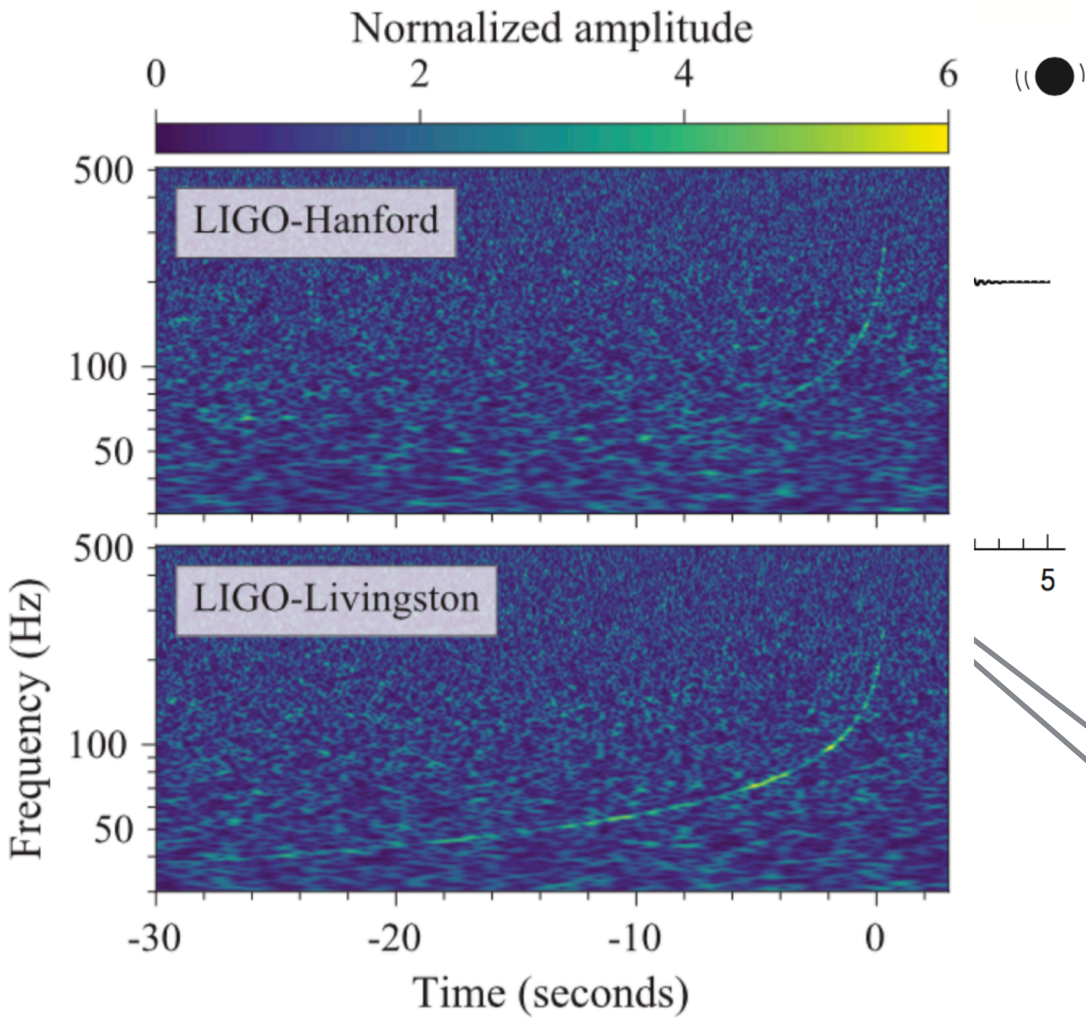

spectrogram

2nd PN 近似までで,

$$\tilde{g}(f) = -\sqrt{\frac{5\pi}{24}\frac{G^2\mathcal{M}^2}{c^5}}\left(\frac{\pi G\mathcal{M}f}{c^3}\right)^{-7/6} e^{-i\Psi(f)}$$

where

$$\Psi(f) = -\frac{\pi}{4} + \frac{3}{128\eta}\left[x^{-5/2} + \left(\frac{3715}{756} + \frac{55}{9}\eta\right)x^{-3/2} - 16\pi x^{-1} + \left(\frac{15293365}{508032} + \frac{27145}{504}\eta + \frac{3085}{72}\eta^2\right)x^{-1/2}\right]$$

$$h(t+\tau) = F_+(\hat{\boldsymbol{n}},\psi)\,h_+(t) + F_\times(\hat{\boldsymbol{n}},\psi)\,h_\times(t)$$

$$h(t) = -\frac{G\mathcal{M}}{c^2 D}\left(\frac{t_c - t}{5G\mathcal{M}/c^3}\right)^{-1/4}\cos 2[\varphi(t) + \Delta\varphi]$$

where

$$D \equiv r\left[F_+^2\left(\frac{1+\cos^2\iota}{2}\right)^2 + F_\times^2\,\cos^2\iota\right]^{-1/2}$$

and

$$2\Delta\varphi \equiv -\tan^{-1}\left(\frac{F_x}{F_+}\frac{2\cos\iota}{1+\cos^2\iota}\right)$$

Fourier Transform

$$\begin{cases} \tilde{x}(f) = \displaystyle\int_{-\infty}^{\infty} x(t)\,e^{-2\pi i f t}\,dt \\ x(t) = \displaystyle\int_{-\infty}^{\infty} \tilde{x}(f)\,e^{2\pi i f t}\,df \end{cases}$$

Sensitivity curves

BH-BH 質量	$50R_g$	$10R_g$	$5R_g$
$10^8 M_\odot + 10^8 M_\odot$	244 yr	142 day	8.91 day
$10^7 M_\odot + 10^7 M_\odot$	24.4 yr	14.3 day	21.4 hr
$10^6 M_\odot + 10^6 M_\odot$	2.44 yr	1.43 day	2.14 hr
$10^5 M_\odot + 10^5 M_\odot$	89.1 day	3.42 hr	12.8 min
$10^4 M_\odot + 10^4 M_\odot$	8.91 day	20.5 min	77.0 sec
$10^3 M_\odot + 10^3 M_\odot$	21.4 hr	2.05 min	7.70 sec
$10^2 M_\odot + 10^2 M_\odot$	2.14 hr	12.3 sec	0.77 sec
$10 M_\odot + 10 M_\odot$	12.8 min	1.23 sec	77 msec

各質量の BH 連星の separation について，合体までの時間を

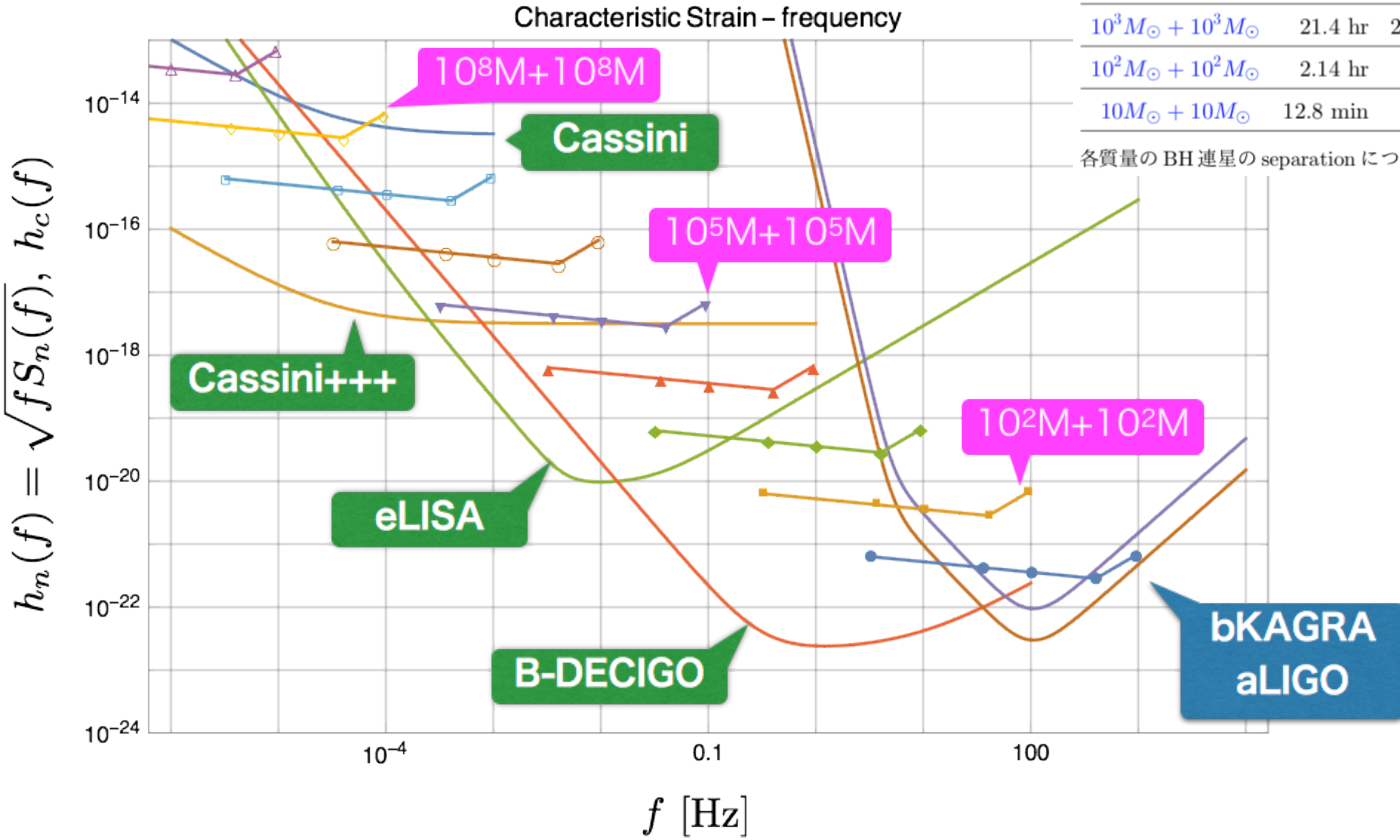

Sensitivity curve with characteristic strain

http://gwplotter.com

(dimensionless)

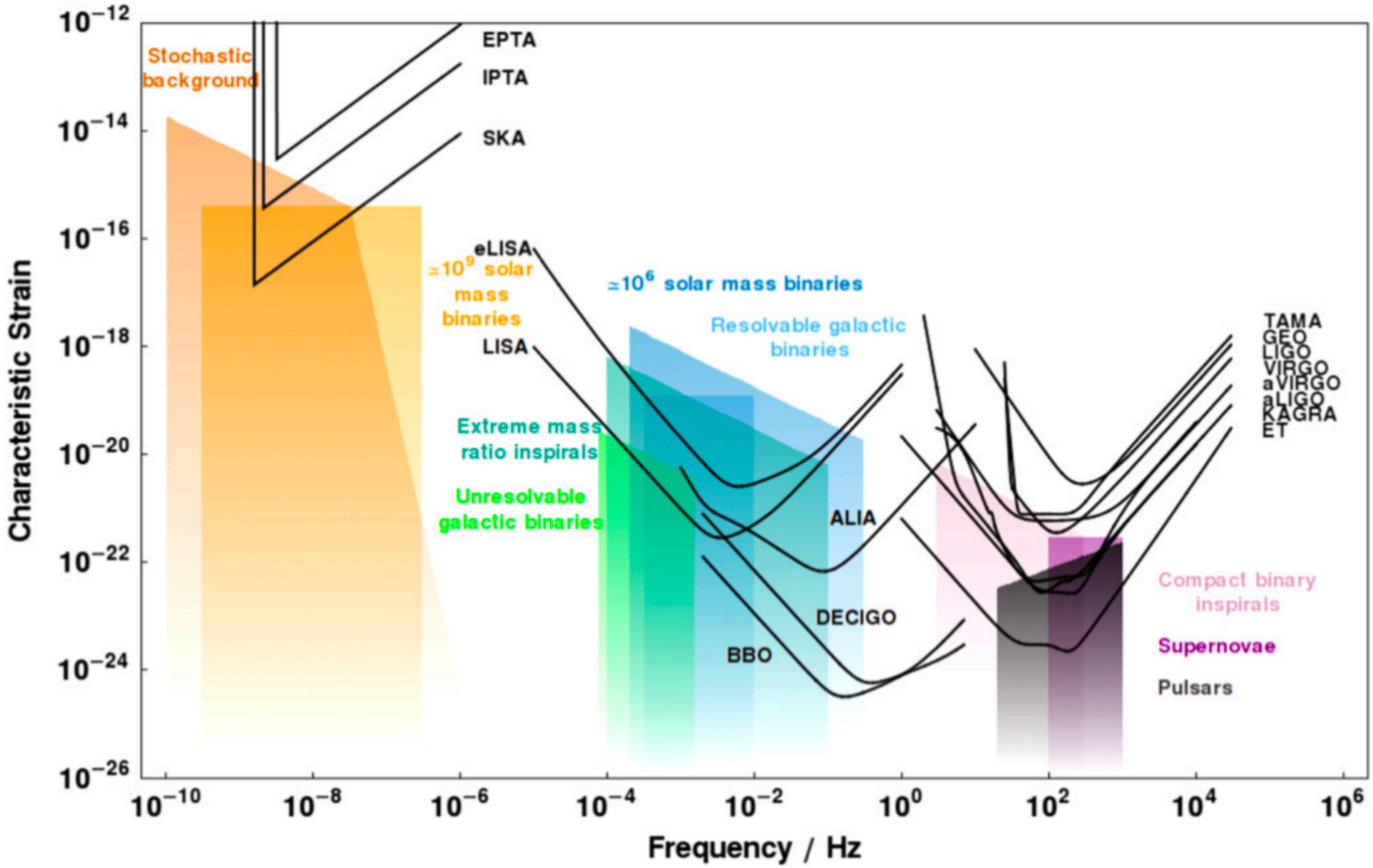

Figure A1. A plot of characteristic strain against frequency for a variety of detectors and sources.

Sensitivity curve with Power Spectral Density

http://gwplotter.com

/sqrt(Hz)

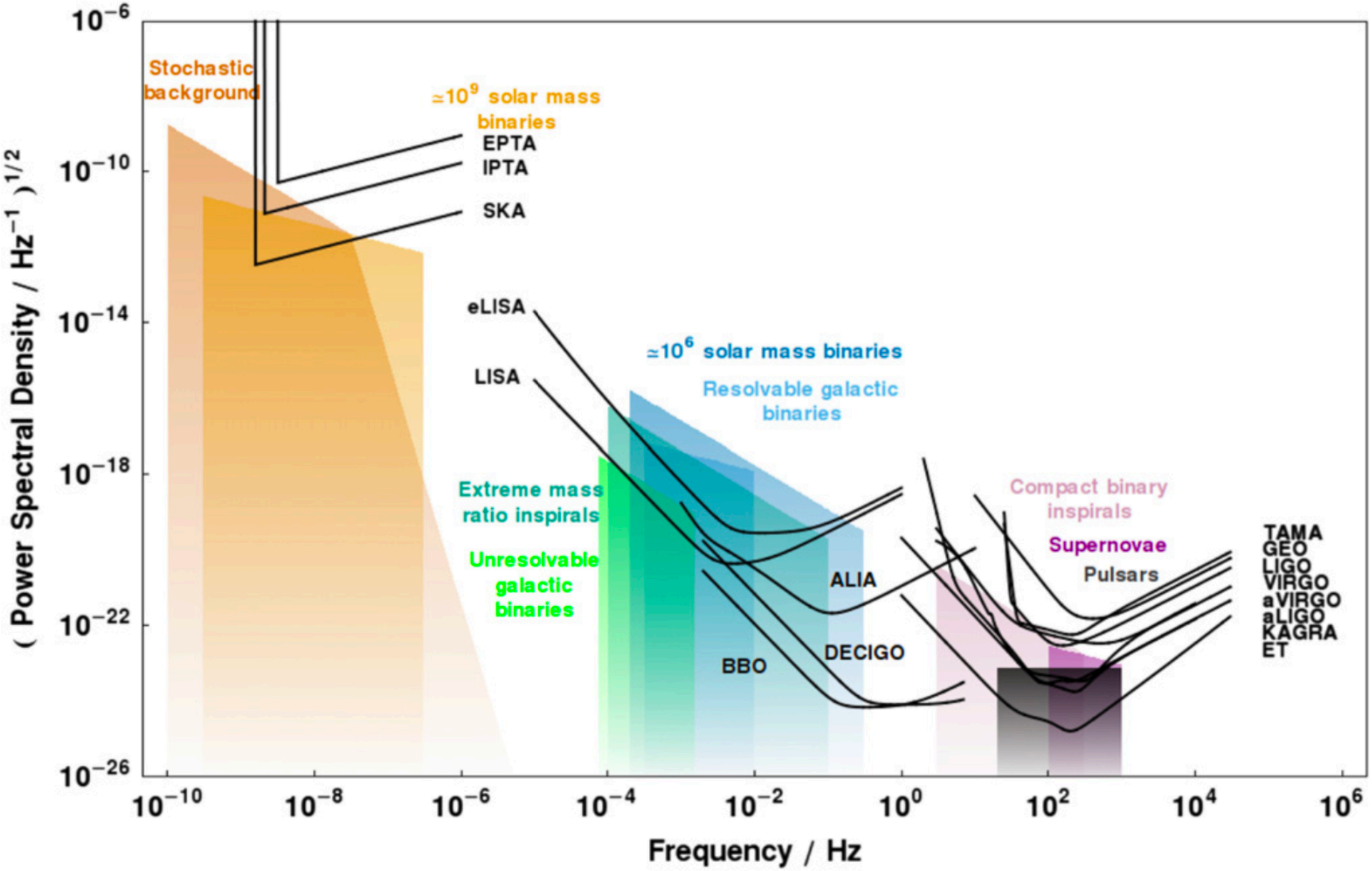

Figure A2. A plot of the square root of PSD against frequency for a variety of detectors and sources.

Sensitivity curve with dimensionless energy density

http://gwplotter.com

(dimensionless)

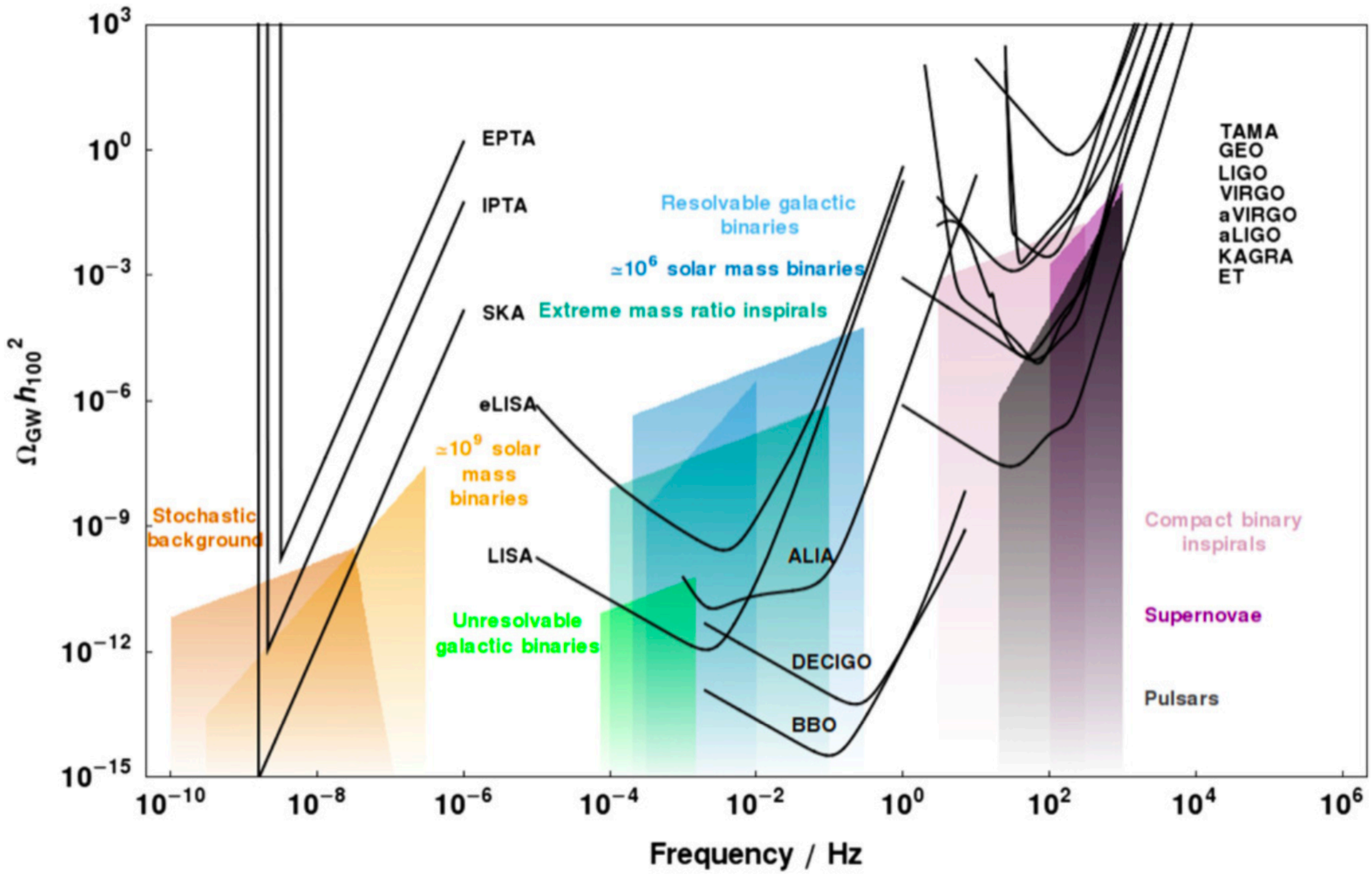

Figure A3. A plot of the dimensionless energy density in GWs against frequency for a variety of detectors and sources.

Ideal vs Reality (Theory vs Data Analysis)

GW150914 (S/N=23.7)

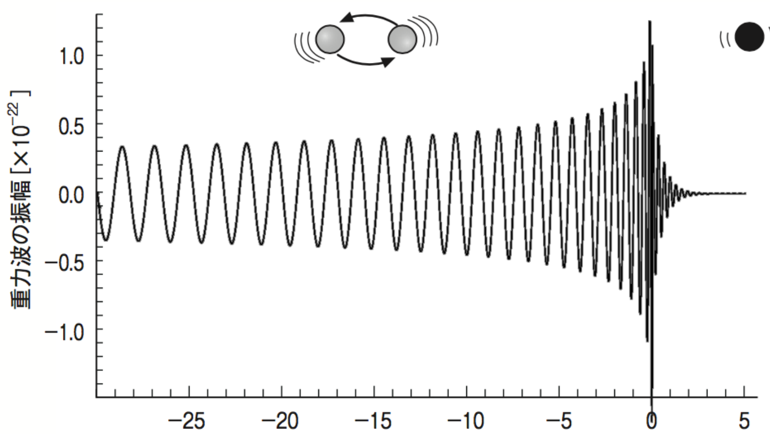

h(t)

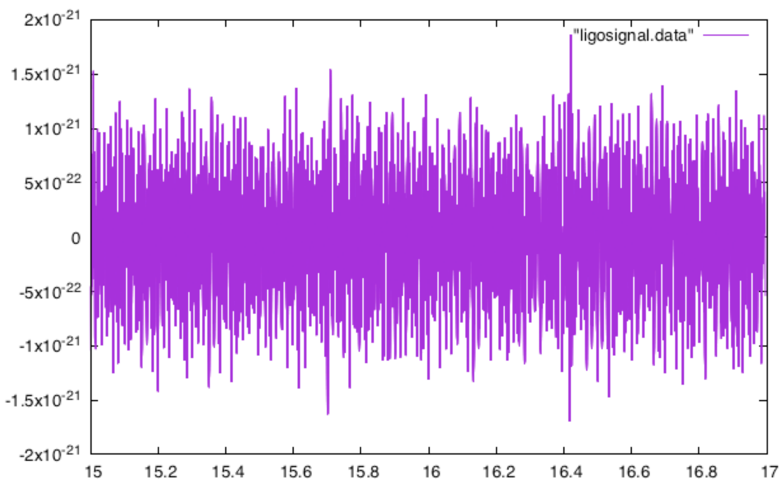

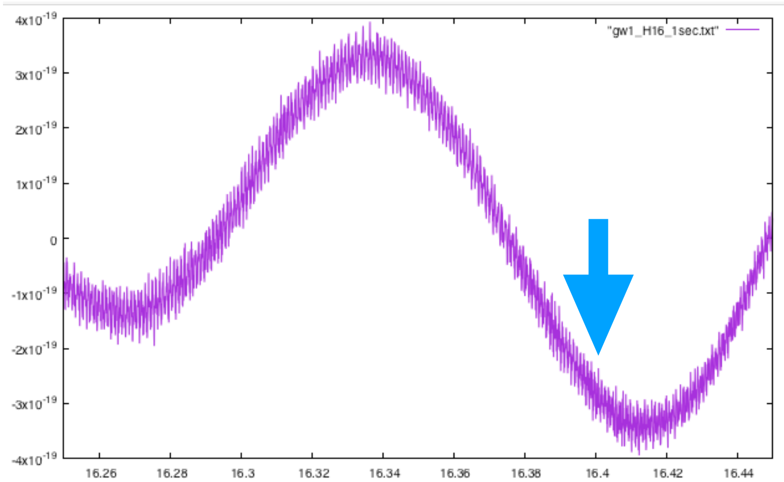

16.25 16.45

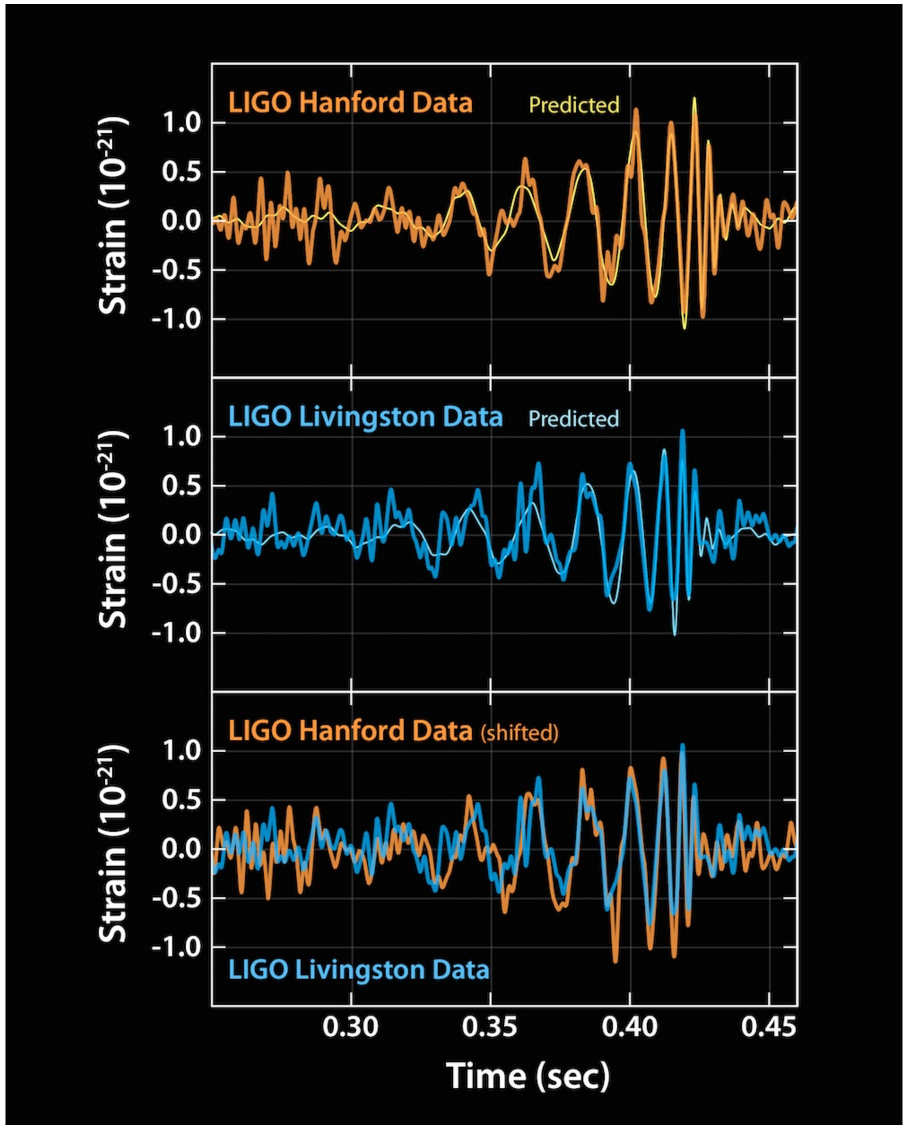

challenging for data analysis

GW data is with noise

signal quickly decays

(M=60Msun, a=0.75 —> 300Hz, tau = 3 ms)

Power spectrum of Noise

Parseval id. ▶ $$\int_{-\infty}^{\infty} [x(t)]^2\, dt = \int_{-\infty}^{\infty} [\tilde{x}(f)]^2\, df$$

power spectrum density

$$\langle x^2 \rangle = \lim_{T\to\infty} \frac{1}{T} \int_{-T/2}^{T/2} [x(t)]^2\, dt = \int_{-\infty}^{\infty} P(f) df$$

$$P(f) = \lim_{T\to\infty} \frac{1}{T} \left[\tilde{x}(f)\tilde{x}^*(f)\right]$$

if stationary prob. process

Wiener-Khinchin theorem ▶ $$P(f) = \int_{-\infty}^{\infty} R_x(\tau) e^{-2\pi i f \tau}\, d\tau$$

$$R_x(\tau) = \langle x(t)\, x(t+\tau) \rangle = \lim_{T\to\infty} \frac{1}{T} \int_{-T/2}^{T/2} x(t) x(t+\tau)\, dt$$

auto-correlation func.

$$\langle x^2 \rangle = 2 \int_0^{\infty} P(f)\, df = \int_0^{\infty} S_x(f)\, df$$

if noise is Gaussian

$$S_x(f) = 2 \int_{-\infty}^{\infty} R_x(\tau) e^{-2\pi i f \tau}\, d\tau = \lim_{\Delta t\to 0} 2\sigma^2 \Delta t$$

Power spectrum of Noise

$$\langle x^2 \rangle = 2\int_0^\infty P(f)\,df = \int_0^\infty S_x(f)\,df$$

if noise is Gaussian

$$S_x(f) = 2\int_{-\infty}^{\infty} R_x(\tau) e^{-2\pi i f \tau}\,d\tau = \lim_{\Delta t \to 0} 2\sigma^2 \Delta t$$

$$p_x[x(t)] \propto \exp\left[-\frac{1}{2\sigma^2}\sum_j x_j^2\right] \propto \exp\left[-\int_{-\infty}^{\infty} \frac{|\tilde{x}(f)|^2}{S_x}\,df\right]$$

$$p_x[x(t)] \propto e^{-(x,x)/2}$$

define the noise-weighed inner product

$$(a,b) \equiv 4\,\mathcal{R}e \int_0^\infty \frac{\tilde{a}(f)\,\tilde{b}^*(f)}{S(f)} df$$

$$= 2\int_{-\infty}^{\infty} \frac{\tilde{a}(f)\,\tilde{b}^*(f)}{S(|f|)} df$$

$$= \int_{-\infty}^{\infty} \frac{\tilde{a}(f)\,\tilde{b}^*(f) + \tilde{a}^*(f)\,\tilde{b}(f)}{S(|f|)} df$$

Matched Filter

ヌル仮説 $\mathcal{H}_0 : \quad s(t) = n(t)$

対立仮説 $\mathcal{H}_1 : \quad s(t) = n(t) + h(t)$

signal = gw + noise

$$s(t) = h(t) + n(t)$$

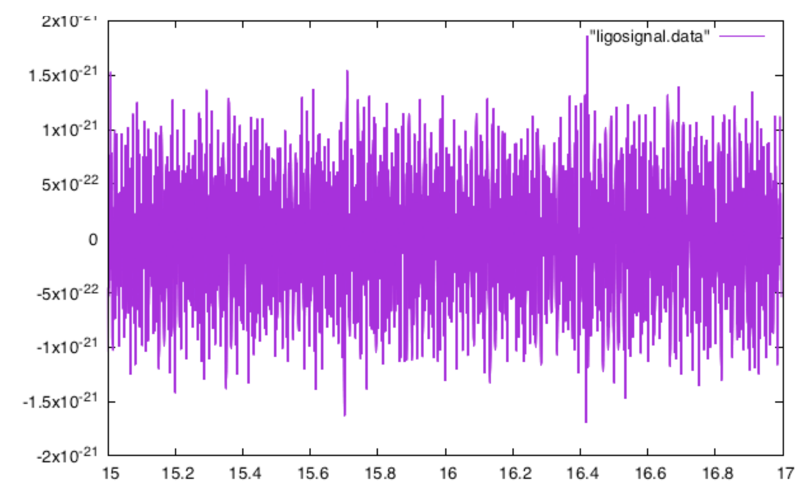

Odds Ratio

$$O(\mathcal{H}_1|s) = \frac{P(\mathcal{H}_1|s)}{P(\mathcal{H}_0|s)}$$

Likelihood

$$\Lambda(\mathbf{B}|\mathbf{A}) = \frac{P(\mathbf{A}|\mathbf{B})}{P(\mathbf{A}|\overline{\mathbf{B}})}$$

$$\Lambda(\mathcal{H}_1|s) = \frac{p(s|\mathcal{H}_1)}{p(s|\mathcal{H}_0)}$$

$$p(s|\mathcal{H}_1) = p_n[s(t) - h(t)] \propto e^{-(s-h,s-h)/2}$$

$$p(s|\mathcal{H}_0) = p_n[s(t)] \propto e^{-(s,s)/2}$$

$$\Lambda(\mathcal{H}_1|s) = \frac{e^{-(s-h,s-h)/2}}{e^{-(s,s)/2}} = e^{(s,h)} e^{-(h,h)/2}$$

Matched Filter
(signal-noise ratio)

$$(s,h) = 4\,\mathcal{R}e \int_0^\infty \frac{\tilde{s}(f)\,\tilde{h}^*(f)}{S_n(f)}\,df$$

Bayes Theorem

$$P(B_k|A) = \frac{P(A \cap B_k)}{P(A)}$$

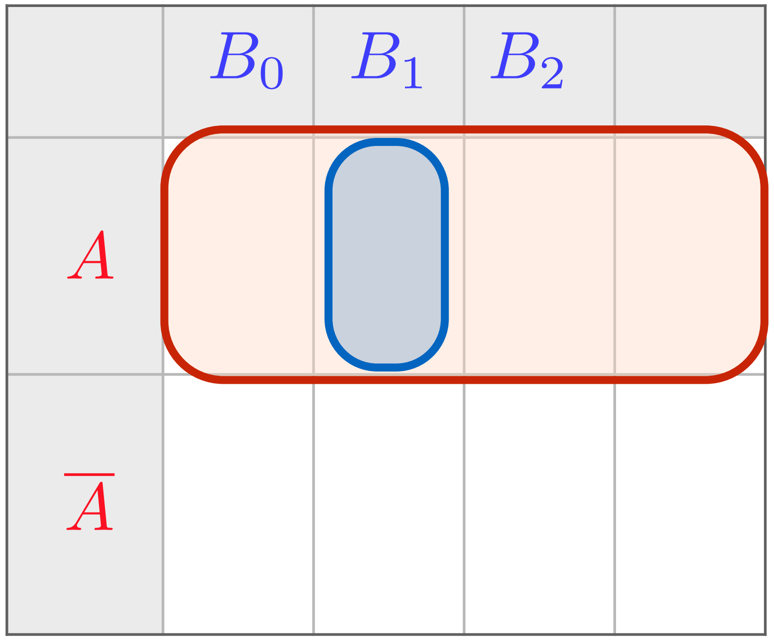

$$P(A \cap B_k) = P(A|B_k)P(B_k)$$

$$P(A) = \sum_k P(A \cap B_k)$$

$$P(B_k|A) = \frac{P(A|B_k)P(B_k)}{\sum_k P(A|B_k)P(B_k)}$$

A→B **B→A**

原因→結果 **結果→原因**

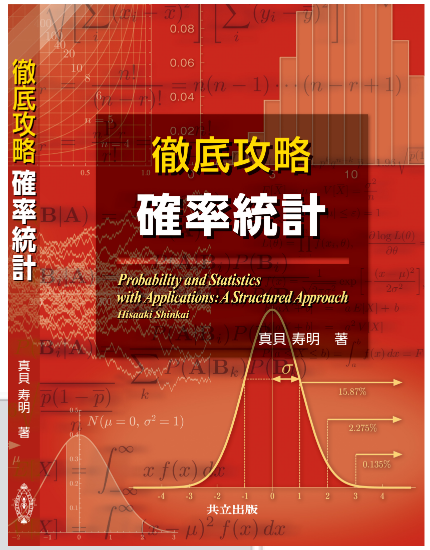

応用例

インターネットでの個別広告の実現

本屋や音楽ダウンロードサイトで「おすすめ」

迷惑メールフィルタ

ユーザに合わせた設定

Matched Filter

signal = gw + noise

$$s(t) = h(t) + n(t)$$

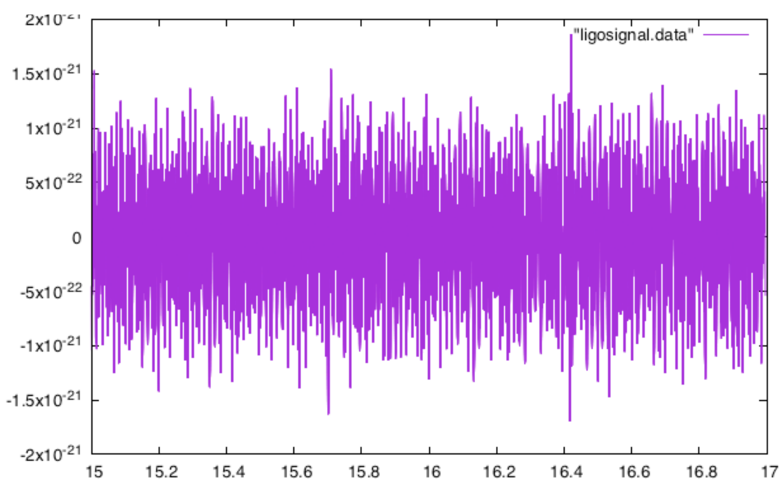

gw template

$$h(t)$$

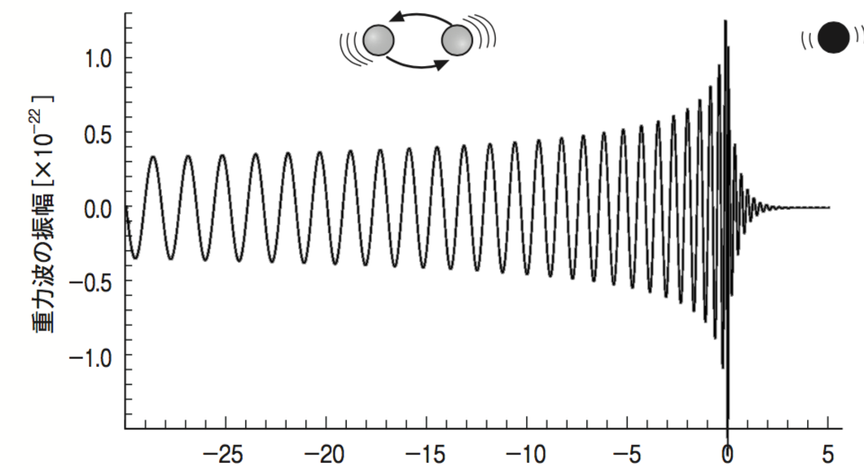

$$\rho = 2 \int_{-\infty}^{\infty} \frac{\tilde{s}(f)\tilde{h}^*(f)}{S_h(|h|)} df$$

signal/noise ratio

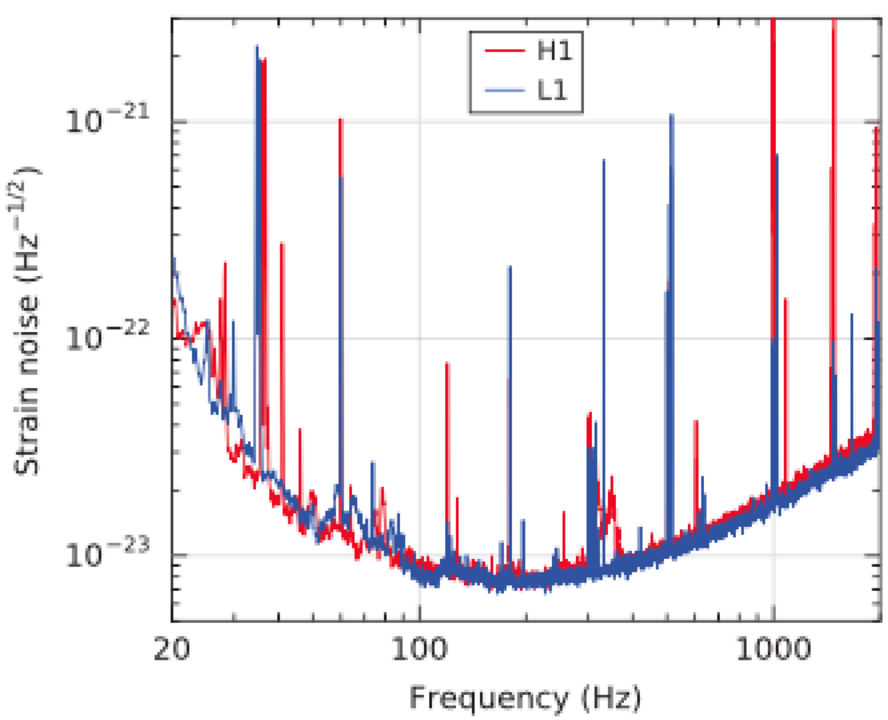

GW151226 (S/N=13.0)

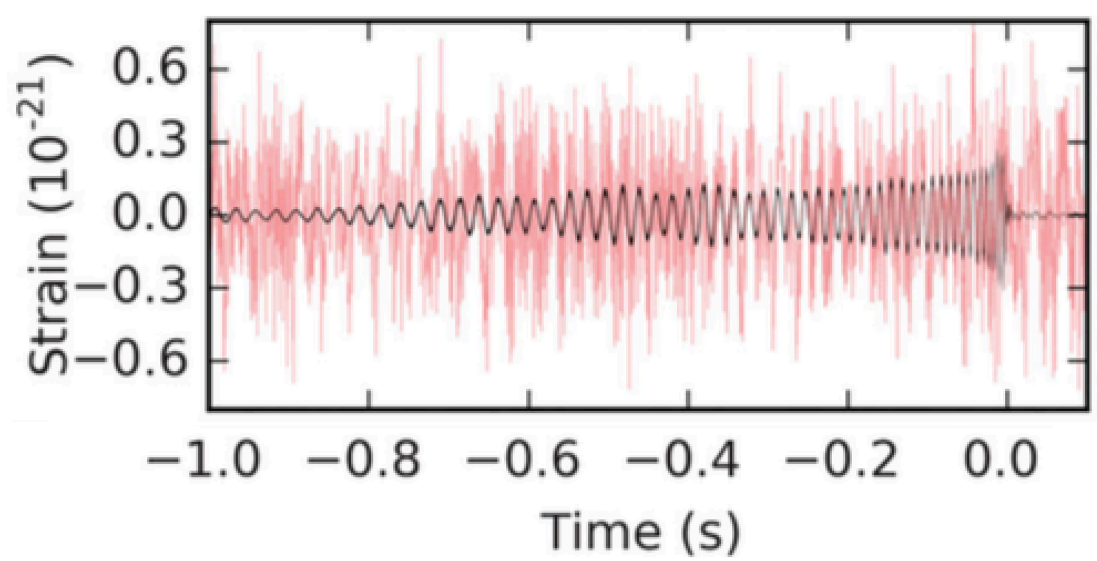

Parameter Estimation

Likelihood

$$\Lambda(\mathcal{H}_1|s) = \frac{p(s|\mathcal{H}_1)}{p(s|\mathcal{H}_0)}$$

$$s(t) = n(t) + h_\theta(t)$$

パラメータ θ^i

$$\Lambda(\mathcal{H}_\theta|s) = \frac{p(s|\mathcal{H}_\theta)}{p(s|\mathcal{H}_0)}$$

$$\log \Lambda(\mathcal{H}_\theta|s) = (s, h_\theta) - \frac{1}{2}(h_\theta, h_\theta)$$

deriv. local max

$$(s - h_\theta, \frac{\partial}{\partial \theta^i} h_\theta)\Big|_{\theta=\theta_{\rm max}} = 0$$

連星系のパラメータ． $\boldsymbol{s}_1, \boldsymbol{s}_2, \boldsymbol{n}$ はベクトル量

2 つの天体の質量	m_1, m_2
2 つの天体の回転角運動量	$\boldsymbol{s}_1, \boldsymbol{s}_2$
連星軌道面の傾斜角	ι
合体時刻と合体時の位相	t_c, φ_c
観測地点からの波源方向	$-\hat{\boldsymbol{n}}$
2 つの重力波モードの偏角	ψ
観測地点からの距離	r

Fisher matrix

$$\Gamma_{ij} \equiv \overline{v_i v_j} = \overline{(n, \frac{\partial h_{\theta_{\rm max}}}{\partial \theta^i})(\frac{\partial h_{\theta_{\rm max}}}{\partial \theta^j}, n)} = (\frac{\partial h_{\theta_{\rm max}}}{\partial \theta^i}, \frac{\partial h_{\theta_{\rm max}}}{\partial \theta^j}) \qquad v_i \equiv (n, \frac{\partial h_{\theta_{\rm max}}}{\partial \theta^i})$$

$$p(\boldsymbol{v}) = \frac{1}{\sqrt{2\pi \det \Gamma}} \exp\left[-\frac{1}{2} V^{ij} v_i v_j\right]$$

$$V^{ij} \equiv (\Gamma^{-1})^{ij}$$

uncertainty

$$(\Delta\theta^i)_{\rm rms} = \sqrt{V^{ii}} \quad \text{(no summation)}$$

correlation coef.

$$c_{ij} = \frac{\overline{\Delta\theta^i \Delta\theta^j}}{V^{ii} V^{jj}} = \frac{V^{ij}}{\sqrt{V^{ii} V^{jj}}}$$

Markov Chain Monte Carlo (MCMC)

確率分布を見つける力業

マルコフ連鎖モンテカルロ法（MCMC）の考え方

問題発生

山田君は誤って大きな洞穴に落ちて気を失ってしまった。気付けば夜で、中は真っ暗に。落ちた穴をどう見つければいいのか。

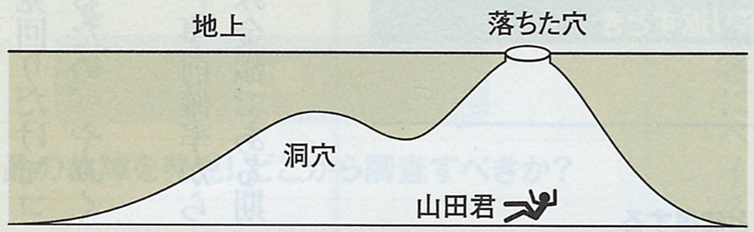

ランダムに歩いて（乱数発生）、小石を投げる（計測）

そこで山田君は、ランダムに歩き、近くの小石を拾って真上に投げ、小石が天井にぶつかり落ちてくる時間を測った。「ここが高いな」と思ったら、その付近に集中的に小石を投げた。合計で20回小石を投げ上げた。

足跡を数える（確率分布〈P（x）〉の推測）

暗闇の中、山田君が注目したのは足元だった。スマートフォンの明かりで足跡を調べ、その分布を見て洞穴の形状を推測。右から2番目の足跡までの確率を2／20、すなわち0.1とみた。

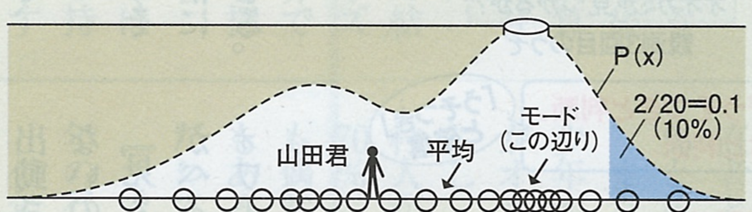

本質

天井ではなく足元を見る。これがMCMCの発想だ。小石を投げる回数を20回から1000回にすれば、推測の精度は上がる。体力勝負の力業であり、コンピューターとの相性が抜群だ

＊藤田一弥・フォワードネットワーク代表への取材を基に本誌編集部作成

Column

コンピューターで大進化を遂げ重力波観測に貢献するベイズ

今年2月、米国を中心とした国際チームによって、アインシュタインの予測した「重力波」が史上初めて観測されたことが明らかになった。

米国の観測装置は、13億年前に二つのブラックホールが衝突、合体したことで生じた重力波を捉えた。それが事前に予想された波形と見事に合致したのである。

そんな科学の大きな進歩につながる歴史的な発見に、実はベイズの理論が大きく貢献していた。詳細は統計専門誌「SIGNIFICANCE（4月号）」に譲るが、約250年前に発見されて〝追放〟された理論が今、再び脚光を浴びている。

その理由をひもとくのが、「マルコフ連鎖モンテカルロ法（MCMC）」と呼ばれる確率分布を求める手法だ。

そもそも、ベイズの理論は数学を基礎としており理論的に完成度が高かった。だが、実際に応用するとなると、あまりに高度な積分計算をしなければ解けない。そのため、複雑なモデルを組むことができず、1980年代まで注目されなかった。

その壁を越えたのが、MCMCとコンピューターの力であった。

ここでMCMCの原理について数式を使わずに触れよう。

左図に「山田君が洞穴に落ちてそこが真っ暗な場合、穴の場所をどう推定するか」という事例を掲載した。

LIGO Computing Latencies

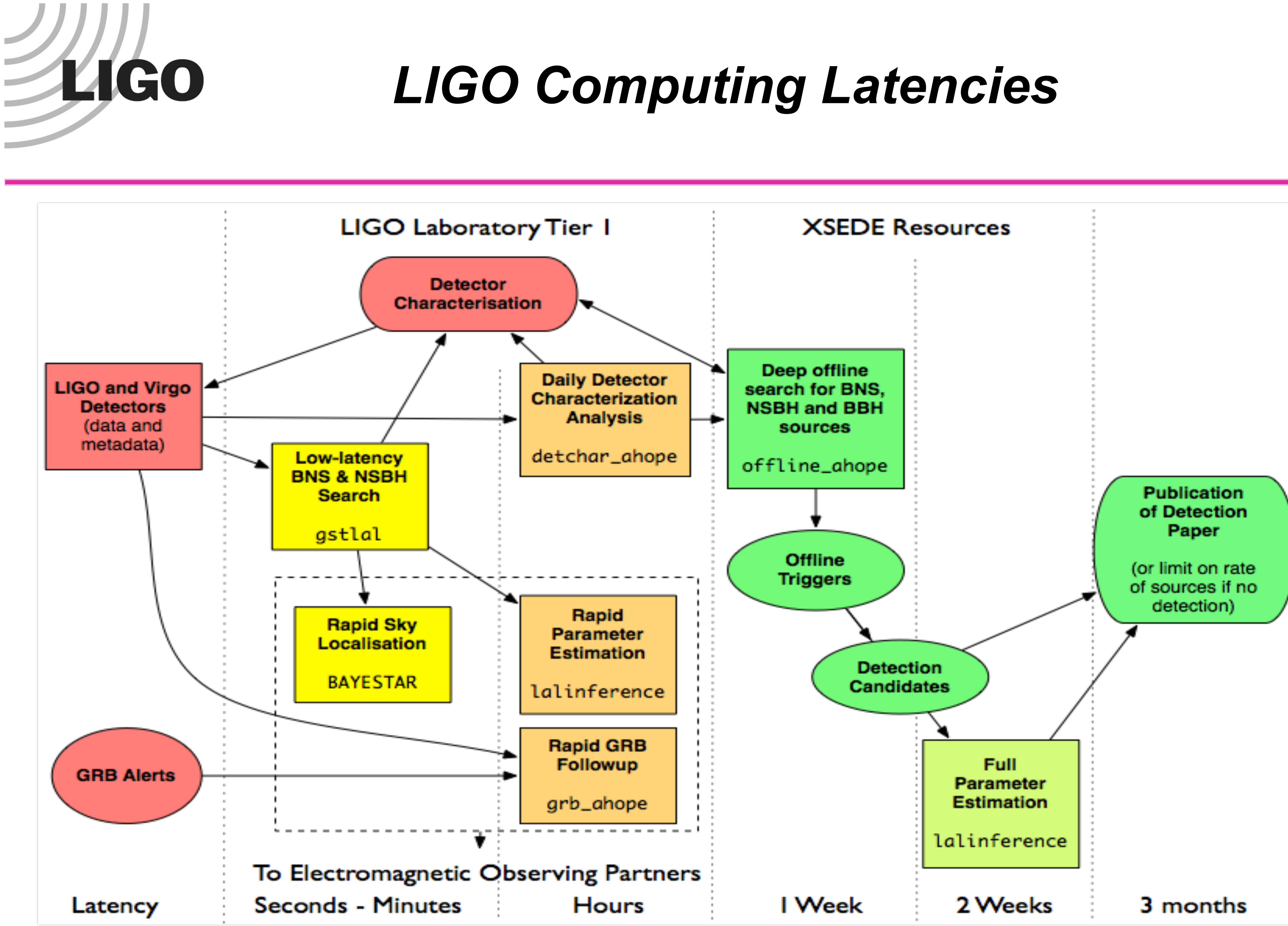

Sharon Brunett, 2015/10

CBC: compact binary coalescence

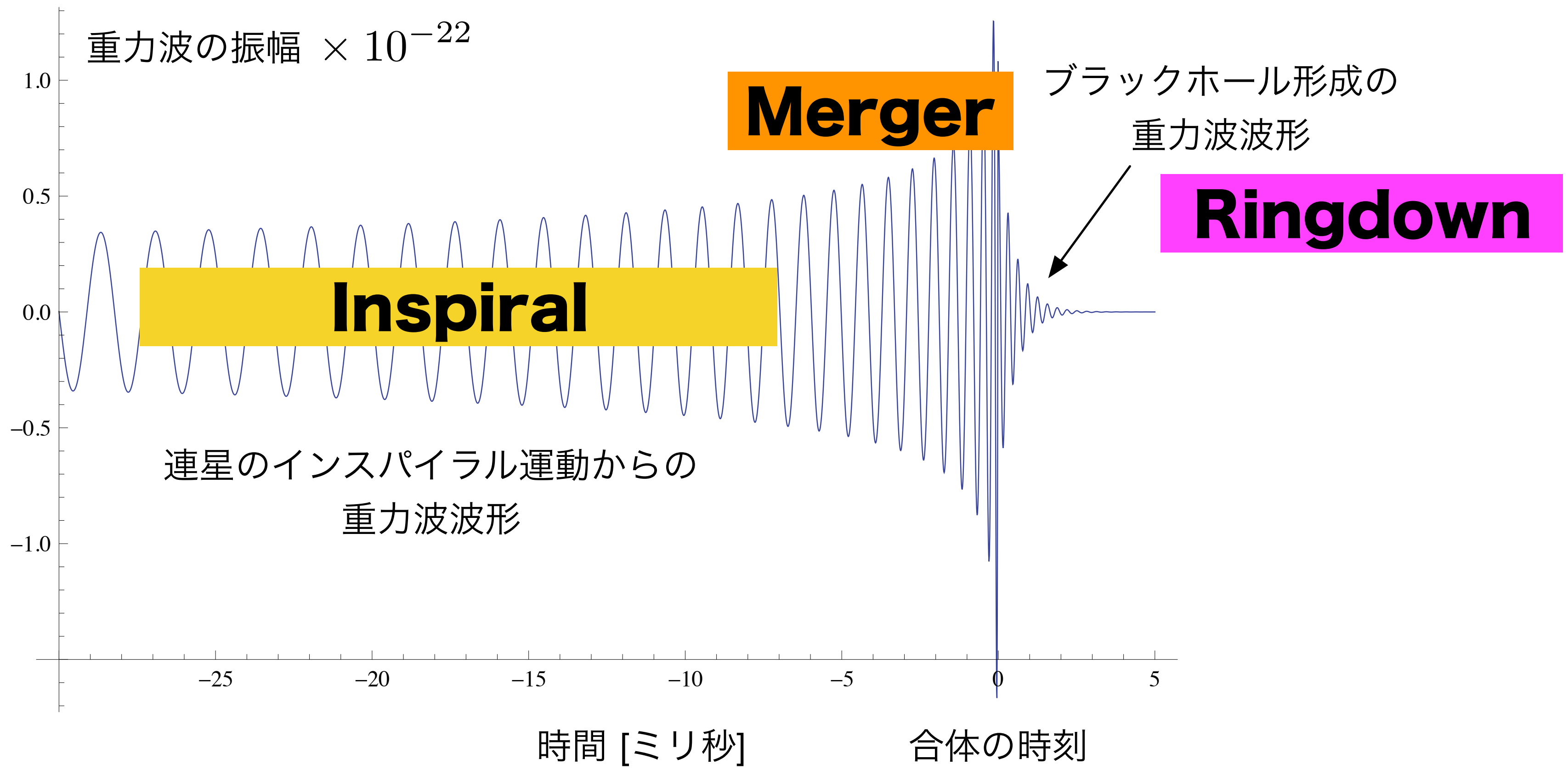

$$h(t) = -\frac{G\mathcal{M}}{c^2 D}\left(\frac{t_c - t}{5G\mathcal{M}/c^3}\right)^{-1/4} \cos 2[\varphi(t) + \Delta\varphi]$$

where

$$D \equiv r\left[F_+^2\left(\frac{1+\cos^2\iota}{2}\right)^2 + F_\times^2\ \cos^2\iota\right]^{-1/2}$$

and

$$2\Delta\varphi \equiv -\tan^{-1}\left(\frac{F_x}{F_+}\frac{2\cos\iota}{1+\cos^2\iota}\right)$$

Horizon distance (Observational range)

$$D_{\rm horizon} = \frac{2}{5}\sqrt{\frac{5}{6}}\frac{c}{\pi^{2/3}}\left(\frac{G\mathcal{M}}{c^3}\right)^{5/6}\left[\int_{f_{\rm min}}^{f_{\rm max}}\frac{f^{7/3}}{S_n(f)}df\right]^{1/2}\frac{1}{\rho}$$

Horizon distance

LVK, 1304.0670 (2020/1 update)

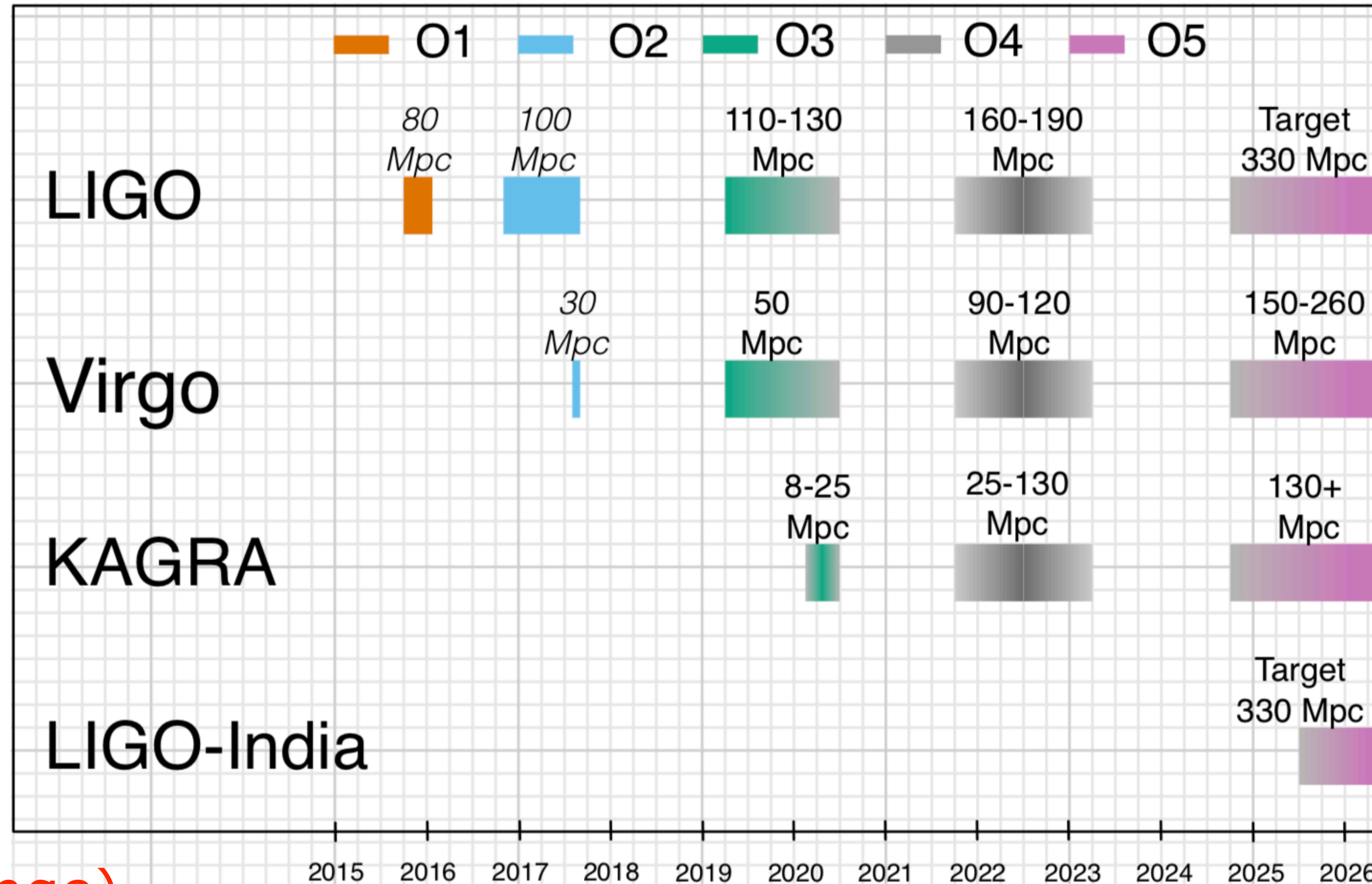

Horizon distance (Observational range)

		O1	O2	O3	O4	O5
BNS Range (Mpc)	aLIGO	80	100	110 – 130	160 – 190	330
	AdV	-	30	50	90 – 120	150 – 260
	KAGRA	-	-	8 – 25	25 – 130	130+
BBH Range (Mpc)	aLIGO	740	910	990 – 1200	1400 – 1600	2500
	AdV	-	270	500	860 – 1100	1300 – 2100
	KAGRA	-	-	80 – 260	260 – 1200	1200+
NSBH Range (Mpc)	aLIGO	140	180	190 – 240	300 – 330	590
	AdV	-	50	90	170 – 220	270 – 480
	KAGRA	-	-	15 – 45	45 – 290	290+
Burst Range (Mpc)	aLIGO	50	60	80 – 90	110 – 120	210
$[E_{\rm GW}=10^{-2}M_\odot c^2]$	AdV	-	25	35	65 – 80	100 – 155
	KAGRA	-	-	5 – 25	25 – 95	95+
Burst Range (kpc)	aLIGO	15	20	25 – 30	35 – 40	70
$[E_{\rm GW}=10^{-9}M_\odot c^2]$	AdV	-	10	10	20 – 25	35 – 50
	KAGRA	-	-	0 – 10	10 – 30	30+

Table 2 Achieved and projected detector sensitivities for a $1.4M_\odot$+$1.4M_\odot$ BNS system, a $30M_\odot$+$30M_\odot$ BBH system, a $1.4M_\odot$+$10M_\odot$ NSBH system, and for an unmodeled burst signal. The quoted ranges correspond to the orientation-averaged spacetime volumes surveyed per unit detector time. For the burst ranges, we assume an emitted energy in GWs at 140 Hz of $E_{\rm GW}=10^{-2}M_\odot c^2$ and of $E_{\rm GW}=10^{-9}M_\odot c^2$. The later is consistent with the order of magnitude of the energy expected from core-collapse of massive stars (see footnote 4). Both CBC and burst ranges are obtained using a single-detector SNR threshold of 8. The O1 and O2 numbers are representative of the best ranges for the LIGO detectors: Hanford in O1 and Livingston in O2. The O3 numbers for aLIGO and AdV reflect recent average performance of each of the three detectors. Range intervals are quoted for future observing runs due to uncertainty about the sequence and impact of upgrades.

rho=8

$$D_{\rm horizon}=\frac{2}{5}\sqrt{\frac{5}{6}}\frac{c}{\pi^{2/3}}\left(\frac{G\mathcal{M}}{c^3}\right)^{5/6}\left[\int_{f_{\rm min}}^{f_{\rm max}}\frac{f^{7/3}}{S_n(f)}df\right]^{1/2}\frac{1}{\rho}$$

CBC: compact binary coalescence

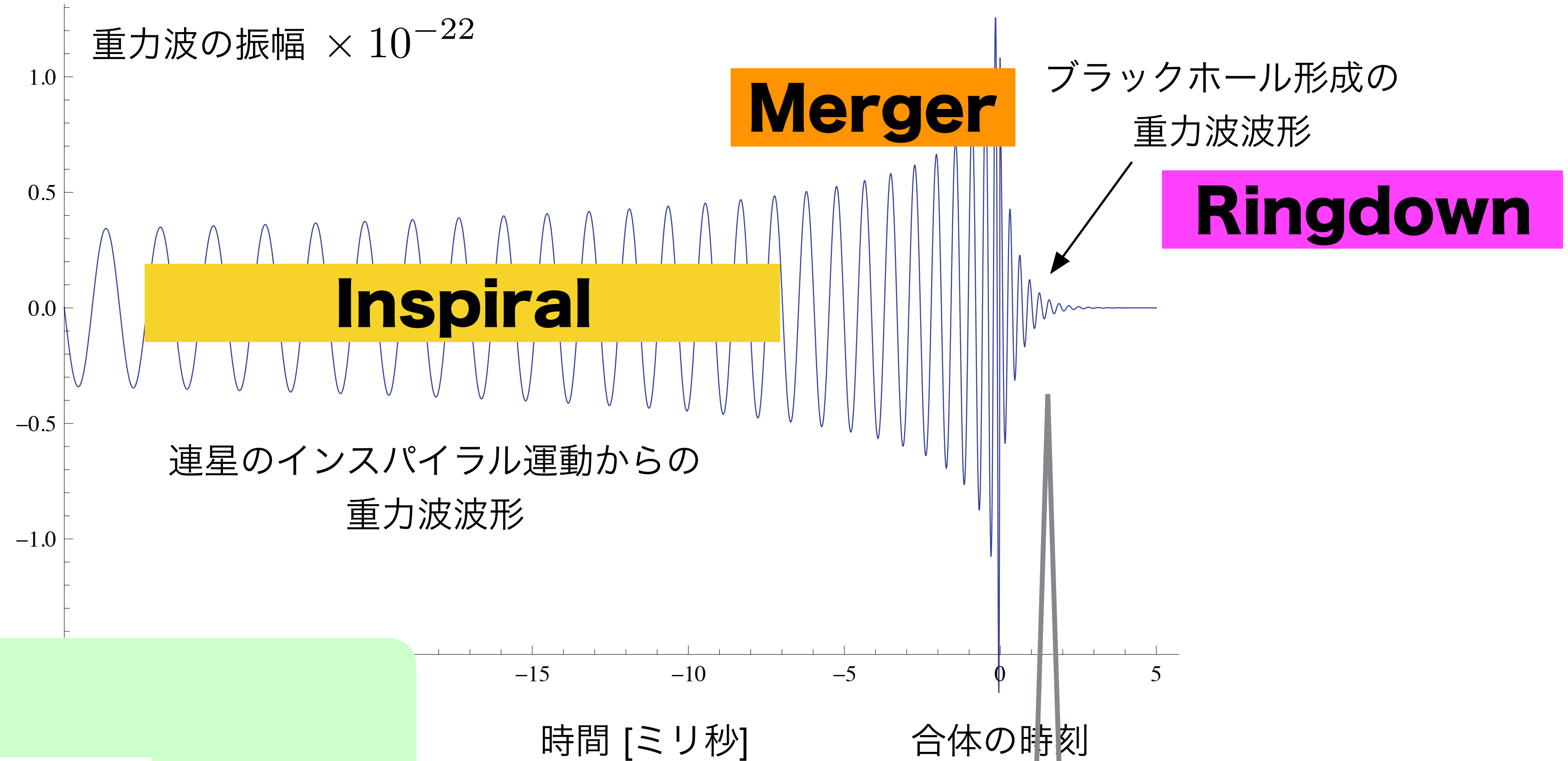

Fitting formula

$$f_R = f_1 + f_2(1-a)^{f_3}$$

$$Q \equiv \frac{f_R}{2f_I} = q_1 + q_2(1-a)^{q_3}$$

$f_1 = 1.5251, \quad f_2 = -1.1568, \quad f_3 = 0.1292$

$q_1 = 0.7000, \quad q_2 = 1.4187, \quad q_3 = -0.4990.$

$$h(t) = Ae^{-(t-t_0)/\tau}\cos(2\pi f_R(t-t_0) - \phi_0)$$

$$h(t) \sim Ae^{i2\pi f_{\rm qnm} t} = Ae^{i2\pi(f_R + i f_I)t}$$

$$a = 1 - \left(\frac{Q-q_1}{q_2}\right)^{1/q_3}$$

$$M[M_\odot] = \frac{c^3}{2\pi G}\frac{f_1 + f_2(1-a)^{f_3}}{f_{\rm qnm}[{\rm Hz}]}$$

BH mass and spin.

CBC: compact binary coalescence

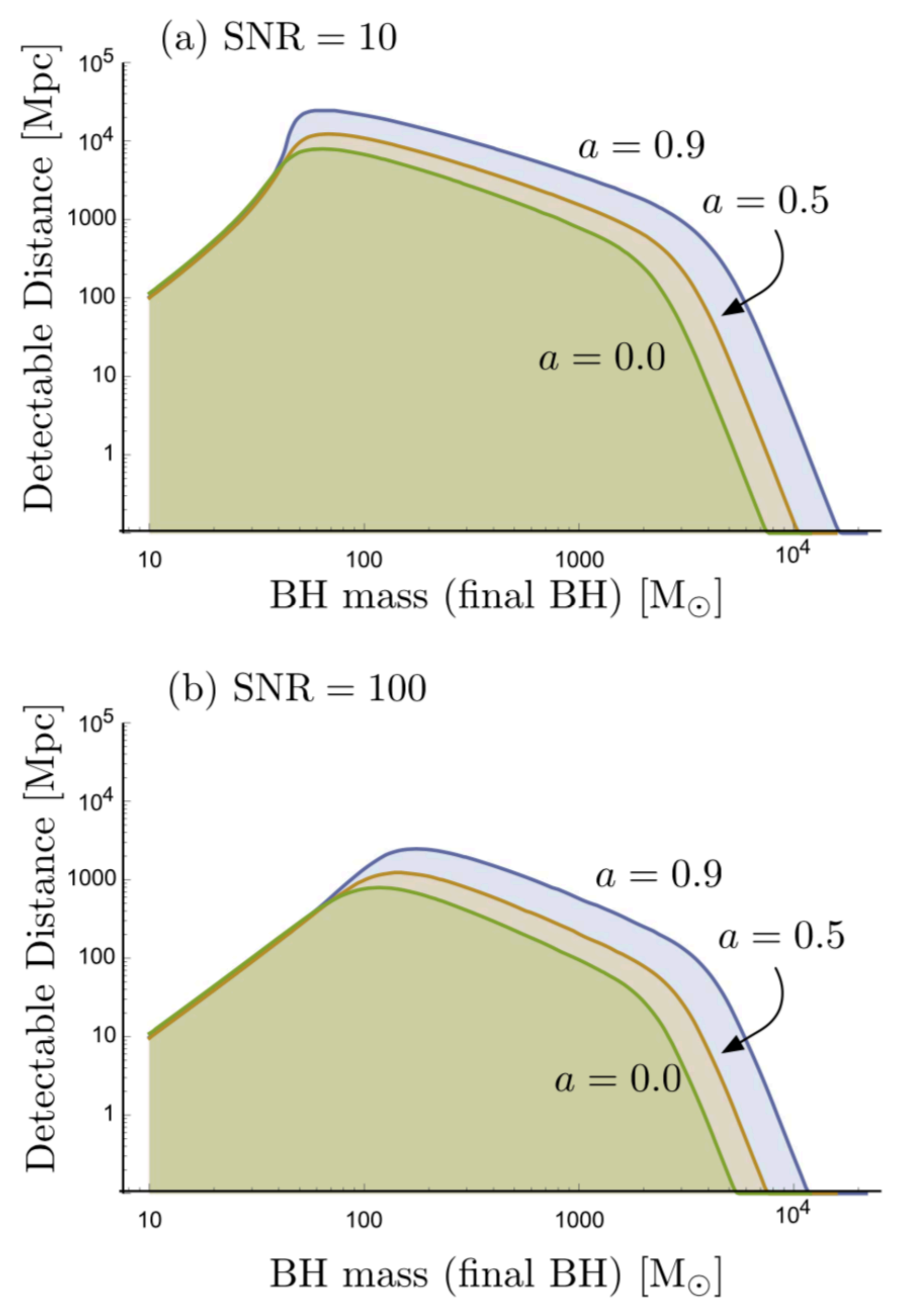

Figure 8. Detectable distance D of the ring-down signal at KAGRA. S/N is set to (a) 10 and (b) 100.

HS+, ApJ 835 (2017)276

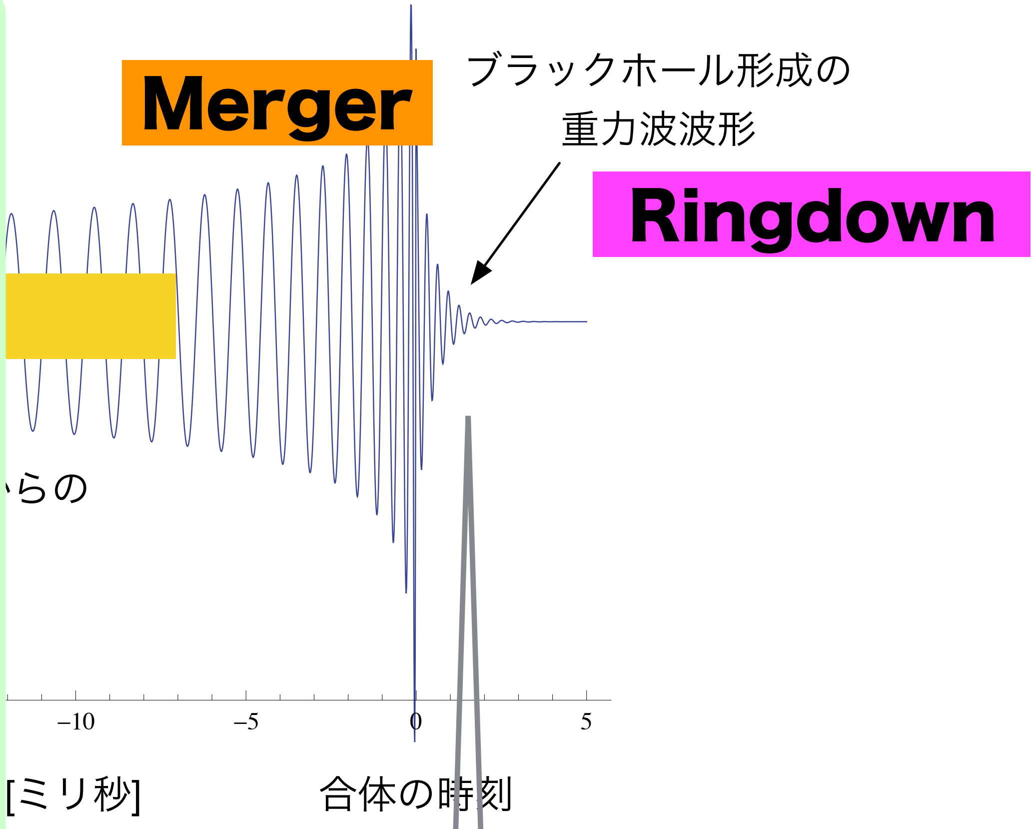

$$h(t) = Ae^{-(t-t_0)/\tau}\cos(2\pi f_R(t-t_0)-\phi_0)$$

Horizon distance (Observational range)

$$\rho^2 = \frac{8}{5}\frac{\epsilon_r(a)}{f_R^2}\frac{(1+z)M}{S_h(f_R/(1+z))} \times \left(\frac{(1+z)M}{d_L(z)}\right)^2\left(\frac{4\mu}{M}\right)^2.$$

GWTC-1

PHYSICAL REVIEW X **9**, 031040 (2019)

GWTC-1: A Gravitational-Wave Transient Catalog of Compact Binary Mergers Observed by LIGO and Virgo during the First and Second Observing Runs

B. P. Abbott *et al.*[*]
(LIGO Scientific Collaboration and Virgo Collaboration)

(Received 14 December 2018; revised manuscript received 27 March 2019; published 4 September 2019)

O1: September 12, 2015 -- January 19, 2016

▶ GW150914 BHBH

O2: November 30, 2016 -- August 25, 2017

▶ GW170817 NSNS

▶ **GWTC-1 catalogue paper [arXiv:1811.12907]**

▶ **data released to public Feb, 2019**

O3a: April 1, 2019 -- September 30, 2019

▶ data released to public April, 2021

O3b: November 1, 2019 -- May 1, 2020

GWTC-1 : False Alarm Rate, Signal-Noise-Ratio

GWTC-1: A GRAVITATIONAL-WAVE TRANSIENT CATALOG … PHYS. REV. X **9**, 031040 (2019)

TABLE I. Search results for the 11 GW events. We report a false-alarm rate for each search that found a given event; otherwise, we display ⋯. The network SNR for the two matched-filter searches is that of the template ranked highest by that search, which is not necessarily the template with the highest SNR. Moreover, the network SNR is the quadrature sum of the detectors coincident in the highest-ranked trigger; in some cases, only two detectors contribute, even if all three are operating nominally at the time of that event.

		FAR $[y^{-1}]$			Network SNR		
Event	UTC time	PyCBC	GstLAL	cWB	PyCBC	GstLAL	cWB
GW150914	09:50:45.4	$<1.53 \times 10^{-5}$	$<1.00 \times 10^{-7}$	$<1.63 \times 10^{-4}$	23.6	24.4	25.2
GW151012	09:54:43.4	0.17	7.92×10^{-3}	⋯	9.5	10.0	⋯
GW151226	03:38:53.6	$<1.69 \times 10^{-5}$	$<1.00 \times 10^{-7}$	0.02	13.1	13.1	11.9
GW170104	10:11:58.6	$<1.37 \times 10^{-5}$	$<1.00 \times 10^{-7}$	2.91×10^{-4}	13.0	13.0	13.0
GW170608	02:01:16.5	$<3.09 \times 10^{-4}$	$<1.00 \times 10^{-7}$	1.44×10^{-4}	15.4	14.9	14.1
GW170729	18:56:29.3	1.36	0.18	0.02	9.8	10.8	10.2
GW170809	08:28:21.8	1.45×10^{-4}	$<1.00 \times 10^{-7}$	⋯	12.2	12.4	⋯
GW170814	10:30:43.5	$<1.25 \times 10^{-5}$	$<1.00 \times 10^{-7}$	$<2.08 \times 10^{-4}$	16.3	15.9	17.2
GW170817	12:41:04.4	$<1.25 \times 10^{-5}$	$<1.00 \times 10^{-7}$	⋯	30.9	33.0	⋯
GW170818	02:25:09.1	⋯	4.20×10^{-5}	⋯	⋯	11.3	⋯
GW170823	13:13:58.5	$<3.29 \times 10^{-5}$	$<1.00 \times 10^{-7}$	2.14×10^{-3}	11.1	11.5	10.8

GWTC-1 : Parameters

B. P. ABBOTT *et al.* PHYS. REV. X **9,** 031040 (2019)

TABLE III. Selected source parameters of the 11 confident detections. We report median values with 90% credible intervals that include statistical errors and systematic errors from averaging the results of two waveform models for BBHs. For GW170817, credible intervals and statistical errors are shown for IMRPhenomPv2NRT with a low spin prior, while the sky area is computed from TaylorF2 samples. The redshift for NGC 4993 from Ref. [94] and its associated uncertainties are used to calculate source-frame masses for GW170817. For BBH events, the redshift is calculated from the luminosity distance and assumed cosmology as discussed in Appendix B. The columns show source-frame component masses m_i and chirp mass $\mathcal{M}$, dimensionless effective aligned spin $\chi_{\rm eff}$, final source-frame mass M_f, final spin a_f, radiated energy $E_{\rm rad}$, peak luminosity $l_{\rm peak}$, luminosity distance d_L, redshift z, and sky localization $\Delta\Omega$. The sky localization is the area of the 90% credible region. For GW170817, we give conservative bounds on parameters of the final remnant discussed in Sec. V E.

Event	$m_1/M_\odot$	$m_2/M_\odot$	$\mathcal{M}/M_\odot$	$\chi_{\rm eff}$	$M_f/M_\odot$	a_f	$E_{\rm rad}/(M_\odot c^2)$	$\ell_{\rm peak}/({\rm erg\ s^{-1}})$	$d_L/{\rm Mpc}$	z	$\Delta\Omega/{\rm deg}^2$
GW150914	$35.6^{+4.7}_{-3.1}$	$30.6^{+3.0}_{-4.4}$	$28.6^{+1.7}_{-1.5}$	$-0.01^{+0.1}_{-0.1}$	$63.1^{+3.4}_{-3.0}$	$0.69^{+0.05}_{-0.04}$	$3.1^{+0.4}_{-0.4}$	$3.6^{+0.4}_{-0.4}\times10^{56}$	440^{+150}_{-170}	$0.09^{+0.03}_{-0.03}$	182
GW151012	$23.2^{+14.9}_{-5.5}$	$13.6^{+4.1}_{-4.8}$	$15.2^{+2.1}_{-1.2}$	$0.05^{+0.31}_{-0.20}$	$35.6^{+10.8}_{-3.8}$	$0.67^{+0.13}_{-0.11}$	$1.6^{+0.6}_{-0.5}$	$3.2^{+0.8}_{-1.7}\times10^{56}$	1080^{+550}_{-490}	$0.21^{+0.09}_{-0.09}$	1523
GW151226	$13.7^{+8.8}_{-3.2}$	$7.7^{+2.2}_{-2.5}$	$8.9^{+0.3}_{-0.3}$	$0.18^{+0.20}_{-0.12}$	$20.5^{+6.4}_{-1.5}$	$0.74^{+0.07}_{-0.05}$	$1.0^{+0.1}_{-0.2}$	$3.4^{+0.7}_{-1.7}\times10^{56}$	450^{+180}_{-190}	$0.09^{+0.04}_{-0.04}$	1033
GW170104	$30.8^{+7.3}_{-5.6}$	$20.0^{+4.9}_{-4.6}$	$21.4^{+2.2}_{-1.8}$	$-0.04^{+0.1}_{-0.2}$	$48.9^{+5.1}_{-4.0}$	$0.66^{+0.08}_{-0.11}$	$2.2^{+0.5}_{-0.5}$	$3.3^{+0.6}_{-1.0}\times10^{56}$	990^{+440}_{-430}	$0.20^{+0.08}_{-0.08}$	921
GW170608	$11.0^{+5.5}_{-1.7}$	$7.6^{+1.4}_{-2.2}$	$7.9^{+0.2}_{-0.2}$	$0.03^{+0.19}_{-0.07}$	$17.8^{+3.4}_{-0.7}$	$0.69^{+0.04}_{-0.04}$	$0.9^{+0.0}_{-0.1}$	$3.5^{+0.4}_{-1.3}\times10^{56}$	320^{+120}_{-110}	$0.07^{+0.02}_{-0.02}$	392
GW170729	$50.2^{+16.2}_{-10.2}$	$34.0^{+9.1}_{-10.1}$	$35.4^{+6.5}_{-4.8}$	$0.37^{+0.21}_{-0.25}$	$79.5^{+14.7}_{-10.2}$	$0.81^{+0.07}_{-0.13}$	$4.8^{+1.7}_{-1.7}$	$4.2^{+0.9}_{-1.5}\times10^{56}$	2840^{+1400}_{-1360}	$0.49^{+0.19}_{-0.21}$	1041
GW170809	$35.0^{+8.3}_{-5.9}$	$23.8^{+5.1}_{-5.2}$	$24.9^{+2.1}_{-1.7}$	$0.08^{+0.17}_{-0.17}$	$56.3^{+5.2}_{-3.8}$	$0.70^{+0.08}_{-0.09}$	$2.7^{+0.6}_{-0.6}$	$3.5^{+0.6}_{-0.9}\times10^{56}$	1030^{+320}_{-390}	$0.20^{+0.05}_{-0.07}$	308
GW170814	$30.6^{+5.6}_{-3.0}$	$25.2^{+2.8}_{-4.0}$	$24.1^{+1.4}_{-1.1}$	$0.07^{+0.12}_{-0.12}$	$53.2^{+3.2}_{-2.4}$	$0.72^{+0.07}_{-0.05}$	$2.7^{+0.4}_{-0.3}$	$3.7^{+0.4}_{-0.5}\times10^{56}$	600^{+150}_{-220}	$0.12^{+0.03}_{-0.04}$	87
NSNS GW170817	$1.46^{+0.12}_{-0.10}$	$1.27^{+0.09}_{-0.09}$	$1.186^{+0.001}_{-0.001}$	$0.00^{+0.02}_{-0.01}$	≤ 2.8	≤ 0.89	≥ 0.04	$\geq 0.1\times10^{56}$	40^{+7}_{-15}	$0.01^{+0.00}_{-0.00}$	16
GW170818	$35.4^{+7.5}_{-4.7}$	$26.7^{+4.3}_{-5.2}$	$26.5^{+2.1}_{-1.7}$	$-0.09^{+0.1}_{-0.2}$	$59.4^{+4.9}_{-3.8}$	$0.67^{+0.07}_{-0.08}$	$2.7^{+0.5}_{-0.5}$	$3.4^{+0.5}_{-0.7}\times10^{56}$	1060^{+420}_{-380}	$0.21^{+0.07}_{-0.07}$	39
GW170823	$39.5^{+11.2}_{-6.7}$	$29.0^{+6.7}_{-7.8}$	$29.2^{+4.6}_{-3.6}$	$0.09^{+0.22}_{-0.26}$	$65.4^{+10.1}_{-7.4}$	$0.72^{+0.09}_{-0.12}$	$3.3^{+1.0}_{-0.9}$	$3.6^{+0.7}_{-1.1}\times10^{56}$	1940^{+970}_{-900}	$0.35^{+0.15}_{-0.15}$	1666

GWTC-1 : Spectrograms

GWTC-1: A GRAVITATIONAL-WAVE TRANSIENT CATALOG … PHYS. REV. X **9,** 031040 (2019)

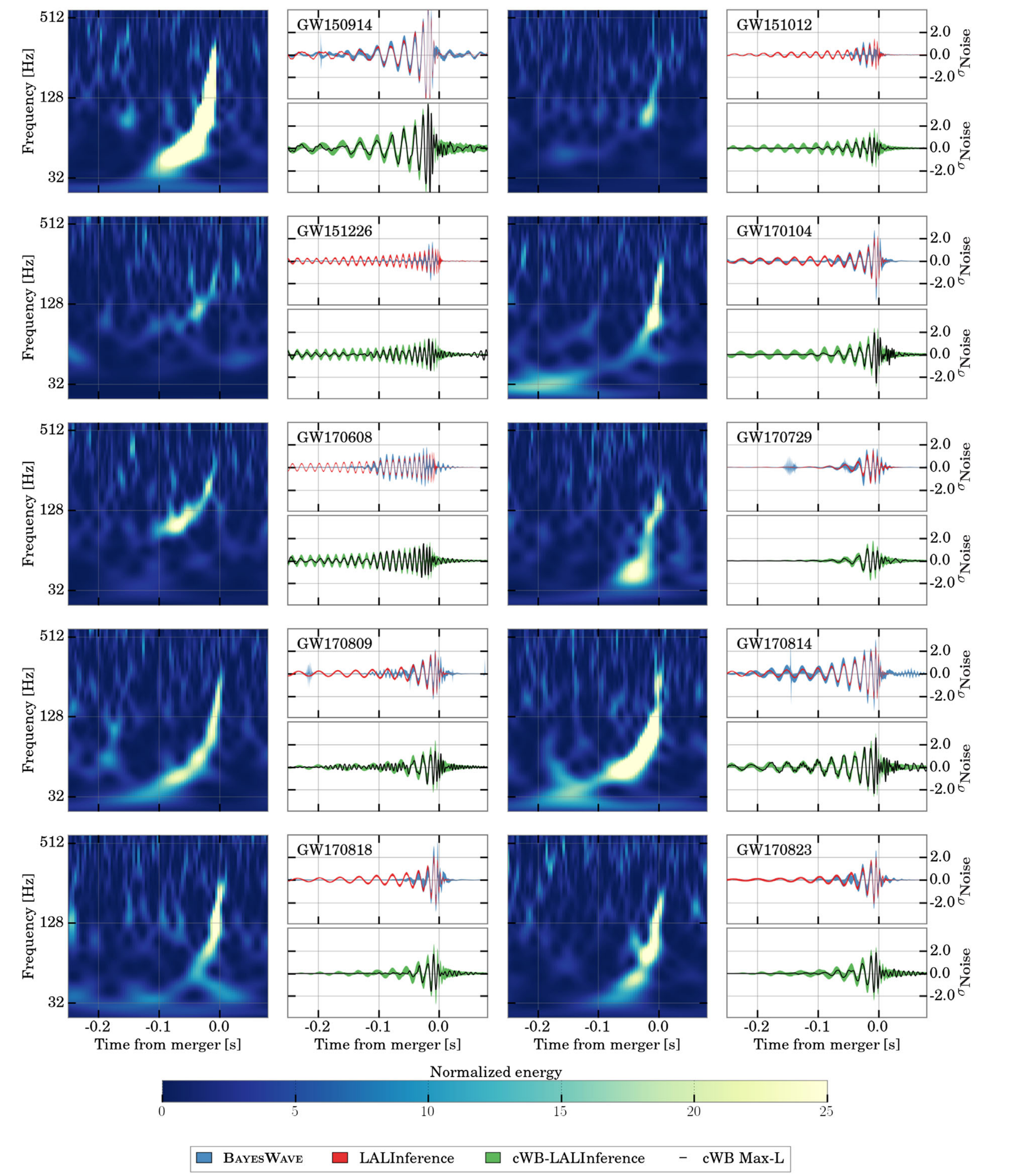

FIG. 10. Time-frequency maps and reconstructed signal waveforms for the ten BBH events. Each event is represented with three panels showing whitened data from the LIGO detector where the higher SNR is recorded. The first panel shows a normalized time-frequency power map of the GW strain. The remaining pair of panels shows time-domain reconstructions of the whitened signal, in units of the standard deviation of the noise. The upper panels show the 90% credible intervals from the posterior probability density functions of the waveform time series, inferred using CBC waveform templates from Bayesian inference (LALInference) with the PhenomP model (red band) and by the BayesWave wavelet model (blue band) [53]. The lower panels show the point estimates from the cWB search (solid lines), along with a 90% confidence interval (green band) derived from cWB analyses of simulated waveforms from the LALInference CBC parameter estimation injected into data near each event. Visible differences between the different reconstruction

GWTC-1 : Signal-Noise-Ratio of 3-detectors

TABLE V. KL divergences (in bits) between the prior and posterior for the effective aligned spin χ_{eff} and the effective precession spin χ_p. For the computation of the KL divergence for χ_p, we quote the KL divergence with the prior conditioned on the χ_{eff} posterior, $D_{\mathrm{KL}}^{\chi_p}(\chi_{\mathrm{eff}})$, and without conditioning, $D_{\mathrm{KL}}^{\chi_p}$. For GW170817, $D_{\mathrm{KL}}^{\chi_p}$ is given for the high spin prior. The median and 90% interval for the KL divergences is estimated by computing the statistic for repeated draws of a subset of the posterior and prior PDFs. Single-detector optimal SNRs from parameter-estimation analyses for Hanford (H), Livingston (L), and Virgo (V).

Event	GW150914	GW151012	GW151226	GW170104	GW170608	GW170729	GW170809	GW170814	GW170817	GW170818	GW170823
$D_{\mathrm{KL}}^{\chi_{\mathrm{eff}}}$	$0.71^{+0.04}_{-0.03}$	$0.23^{+0.03}_{-0.02}$	$1.32^{+0.11}_{-0.06}$	$0.54^{+0.03}_{-0.03}$	$0.97^{+0.03}_{-0.05}$	$1.83^{+0.07}_{-0.09}$	$0.71^{+0.03}_{-0.03}$	$0.99^{+0.05}_{-0.07}$	$2.32^{+0.08}_{-0.10}$	$0.50^{+0.04}_{-0.03}$	$0.32^{+0.04}_{-0.03}$
$D_{\mathrm{KL}}^{\chi_p}$	$0.16^{+0.03}_{-0.02}$	$0.09^{+0.03}_{-0.02}$	$0.17^{+0.03}_{-0.04}$	$0.05^{+0.01}_{-0.01}$	$0.07^{+0.01}_{-0.02}$	$0.09^{+0.02}_{-0.02}$	$0.05^{+0.01}_{-0.01}$	$0.02^{+0.01}_{-0.01}$	$0.19^{+0.04}_{-0.03}$	$0.06^{+0.02}_{-0.01}$	$0.03^{+0.01}_{-0.01}$
$D_{\mathrm{KL}}^{\chi_p}(\chi_{\mathrm{eff}})$	$0.09^{+0.02}_{-0.02}$	$0.08^{+0.02}_{-0.01}$	$0.12^{+0.05}_{-0.02}$	$0.07^{+0.02}_{-0.01}$	$0.08^{+0.02}_{-0.02}$	$0.03^{+0.01}_{-0.01}$	$0.06^{+0.01}_{-0.01}$	$0.13^{+0.03}_{-0.02}$	$0.07^{+0.01}_{-0.02}$	$0.09^{+0.02}_{-0.01}$	$0.03^{+0.01}_{-0.01}$
H SNR	$20.6^{+1.6}_{-1.6}$	$6.4^{+1.3}_{-1.3}$	$9.8^{+1.5}_{-1.4}$	$9.5^{+1.3}_{-1.6}$	$12.1^{+1.6}_{-1.6}$	$5.9^{+1.1}_{-1.1}$	$5.9^{+1.4}_{-1.4}$	$9.3^{+1.0}_{-1.2}$	$18.9^{+1.0}_{-1.0}$	$4.6^{+0.9}_{-0.8}$	$6.8^{+1.4}_{-1.2}$
L SNR	$14.2^{+1.6}_{-1.4}$	$5.8^{+1.2}_{-1.2}$	$6.9^{+1.2}_{-1.1}$	$9.9^{+1.5}_{-1.3}$	$9.2^{+1.5}_{-1.2}$	$8.3^{+1.4}_{-1.4}$	$10.7^{+1.6}_{-1.8}$	$14.3^{+1.5}_{-1.4}$	$26.3^{+1.4}_{-1.3}$	$9.7^{+1.5}_{-1.5}$	$9.2^{+1.7}_{-1.5}$
V SNR	...	...	...	...	...	$1.7^{+1.0}_{-1.1}$	$1.1^{+1.2}_{-0.8}$	$4.1^{+1.1}_{-1.1}$	$3.0^{+0.2}_{-0.2}$	$4.2^{+0.8}_{-0.7}$	...

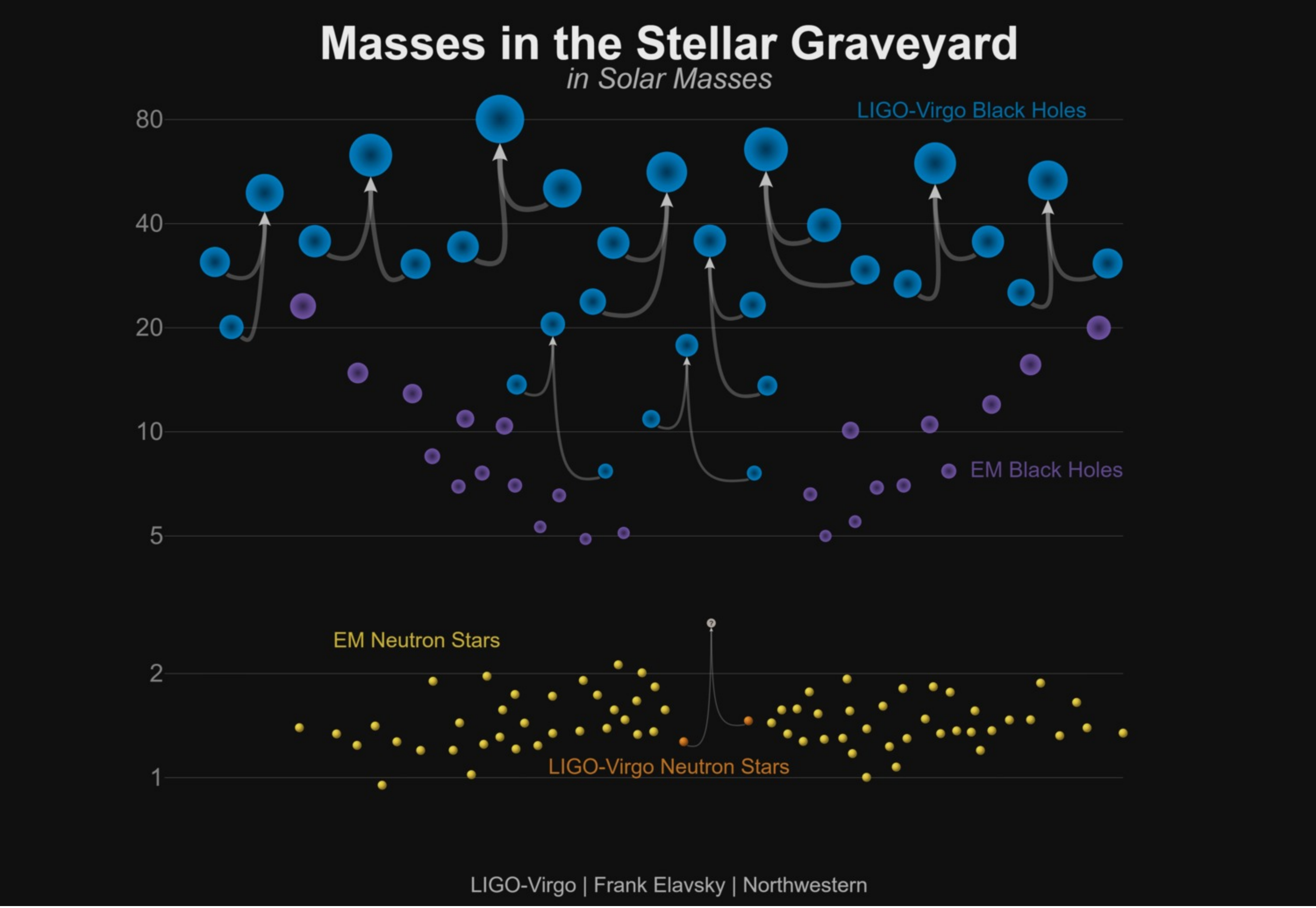

https://www.ligo.caltech.edu/image/ligo20181203a

Event	Primary mass (M_sun)	Secondary mass (M_sun)	Effective inspiral spin	chirp mass (M_sun)	Final spin	Final mass (M_sun)	Luminosity distance (Mpc)	GPS time (s)
GW150914	$35.6^{+4.8}_{-3.0}$	$30.6^{+3.0}_{-4.4}$	$-0.01^{+0.12}_{-0.13}$	$28.6^{+1.6}_{-1.5}$	$0.69^{+0.05}_{-0.04}$	$63.1^{+3.3}_{-3.0}$	430^{+150}_{-170}	1126259462.4
GW151012	$23.3^{+14.0}_{-5.5}$	$13.6^{+4.1}_{-4.8}$	$0.04^{+0.28}_{-0.19}$	$15.2^{+2.0}_{-1.1}$	$0.67^{+0.13}_{-0.11}$	$35.7^{+9.9}_{-3.8}$	1060^{+540}_{-480}	1128678900.4
GW151226	$13.7^{+8.8}_{-3.2}$	$7.7^{+2.2}_{-2.6}$	$0.18^{+0.20}_{-0.12}$	$8.9^{+0.3}_{-0.3}$	$0.74^{+0.07}_{-0.05}$	$20.5^{+6.4}_{-1.5}$	440^{+180}_{-190}	1135136350.6
GW170104	$31.0^{+7.2}_{-5.6}$	$20.1^{+4.9}_{-4.5}$	$-0.04^{+0.17}_{-0.20}$	$21.5^{+2.1}_{-1.7}$	$0.66^{+0.08}_{-0.10}$	$49.1^{+5.2}_{-3.9}$	960^{+430}_{-410}	1167559936.6
GW170608	$10.9^{+5.3}_{-1.7}$	$7.6^{+1.3}_{-2.1}$	$0.03^{+0.19}_{-0.07}$	$7.9^{+0.2}_{-0.2}$	$0.69^{+0.04}_{-0.04}$	$17.8^{+3.2}_{-0.7}$	320^{+120}_{-110}	1180922494.5
GW170729	$50.6^{+16.6}_{-10.2}$	$34.3^{+9.1}_{-10.1}$	$0.36^{+0.21}_{-0.25}$	$35.7^{+6.5}_{-4.7}$	$0.81^{+0.07}_{-0.13}$	$80.3^{+14.6}_{-10.2}$	2750^{+1350}_{-1320}	1185389807.3
GW170809	$35.2^{+8.3}_{-6.0}$	$23.8^{+5.2}_{-5.1}$	$0.07^{+0.16}_{-0.16}$	$25.0^{+2.1}_{-1.6}$	$0.70^{+0.08}_{-0.09}$	$56.4^{+5.2}_{-3.7}$	990^{+320}_{-380}	1186302519.8
GW170814	$30.7^{+5.7}_{-3.0}$	$25.3^{+2.9}_{-4.1}$	$0.07^{+0.12}_{-0.11}$	$24.2^{+1.4}_{-1.1}$	$0.72^{+0.07}_{-0.05}$	$53.4^{+3.2}_{-2.4}$	580^{+160}_{-210}	1186741861.5
GW170817	$1.46^{+0.12}_{-0.10}$	$1.27^{+0.09}_{-0.09}$	$0.00^{+0.02}_{-0.01}$	$1.186^{+0.001}_{-0.001}$	≤ 0.89	≤ 2.8	40^{+10}_{-10}	1187008882.4
GW170818	$35.5^{+7.5}_{-4.7}$	$26.8^{+4.3}_{-5.2}$	$-0.09^{+0.18}_{-0.21}$	$26.7^{+2.1}_{-1.7}$	$0.67^{+0.07}_{-0.08}$	$59.8^{+4.8}_{-3.8}$	1020^{+430}_{-360}	1187058327.1
GW170823	$39.6^{+10.0}_{-6.6}$	$29.4^{+6.3}_{-7.1}$	$0.08^{+0.20}_{-0.22}$	$29.3^{+4.2}_{-3.2}$	$0.71^{+0.08}_{-0.10}$	$65.6^{+9.4}_{-6.6}$	1850^{+840}_{-840}	1187529256.5

https://www.gw-openscience.org/catalog/GWTC-1-confident/html/

Event	GPS time (s)	FAR (yr^-1)	Pipeline	Network SNR	Detector frame chirp mass (M_sun)	Data Quality
151008	**1128348574.5**	**10.17**	**pycbc**	**8.8**	**5.12**	**No artifacts**
151012A	**1128666662.2**	**8.56**	**gstlal**	**9.6**	**2.01**	**Artifacts present**
151116	**1131748925.7**	**4.77**	**pycbc**	**9.0**	**1.24**	**No artifacts**
161202	**1164686041.9**	**6.00**	**gstlal**	**10.5**	**1.54**	**Artifacts can account for**
161217	**1165994201.4**	**10.12**	**gstlal**	**10.7**	**7.86**	**Artifacts can account for**
170208	**1170585583.8**	**11.18**	**gstlal**	**10.0**	**7.39**	**Artifacts present**
170219	**1171548267.0**	**6.26**	**gstlal**	**9.6**	**1.53**	**No artifacts**
170405	**1175425510.7**	**4.55**	**gstlal**	**9.3**	**1.44**	**Artifacts present**
170412	**1176047817.0**	**8.22**	**gstlal**	**9.7**	**4.36**	**Artifacts can account for**
170423	**1176984663.0**	**6.47**	**gstlal**	**8.9**	**1.17**	**No artifacts**
170616	**1181677658.8**	**1.94**	**pycbc**	**9.1**	**2.75**	**Artifacts present**
170630	**1182874645.8**	**10.46**	**gstlal**	**9.7**	**0.90**	**Artifacts present**
170705	**1183279534.3**	**10.97**	**gstlal**	**9.3**	**3.40**	**No artifacts**
170720	**1184625889.8**	**10.75**	**gstlal**	**13.0**	**5.96**	**Artifacts can account for**

https://www.gw-openscience.org/catalog/GWTC-1-marginal/html/

Sky Localization

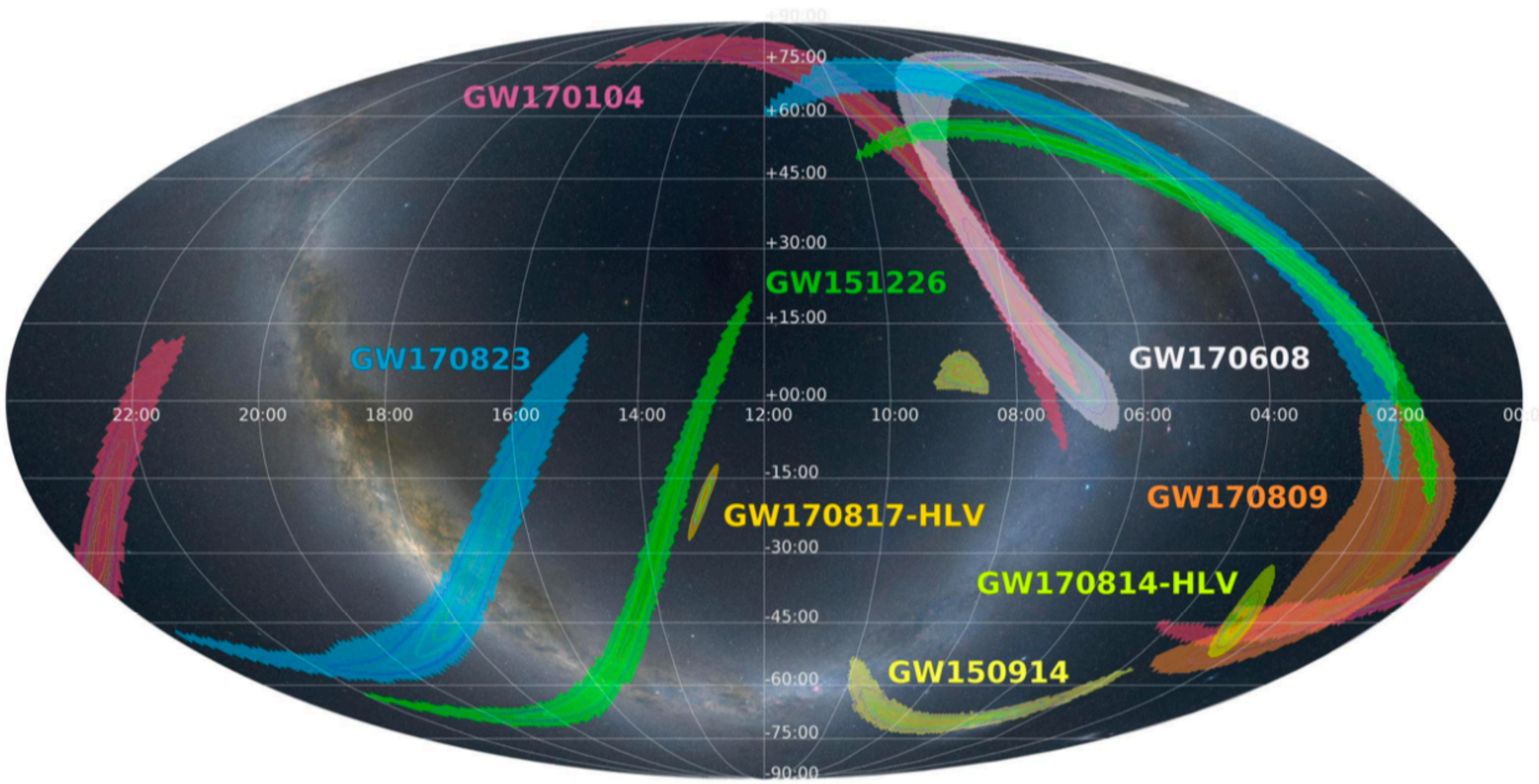

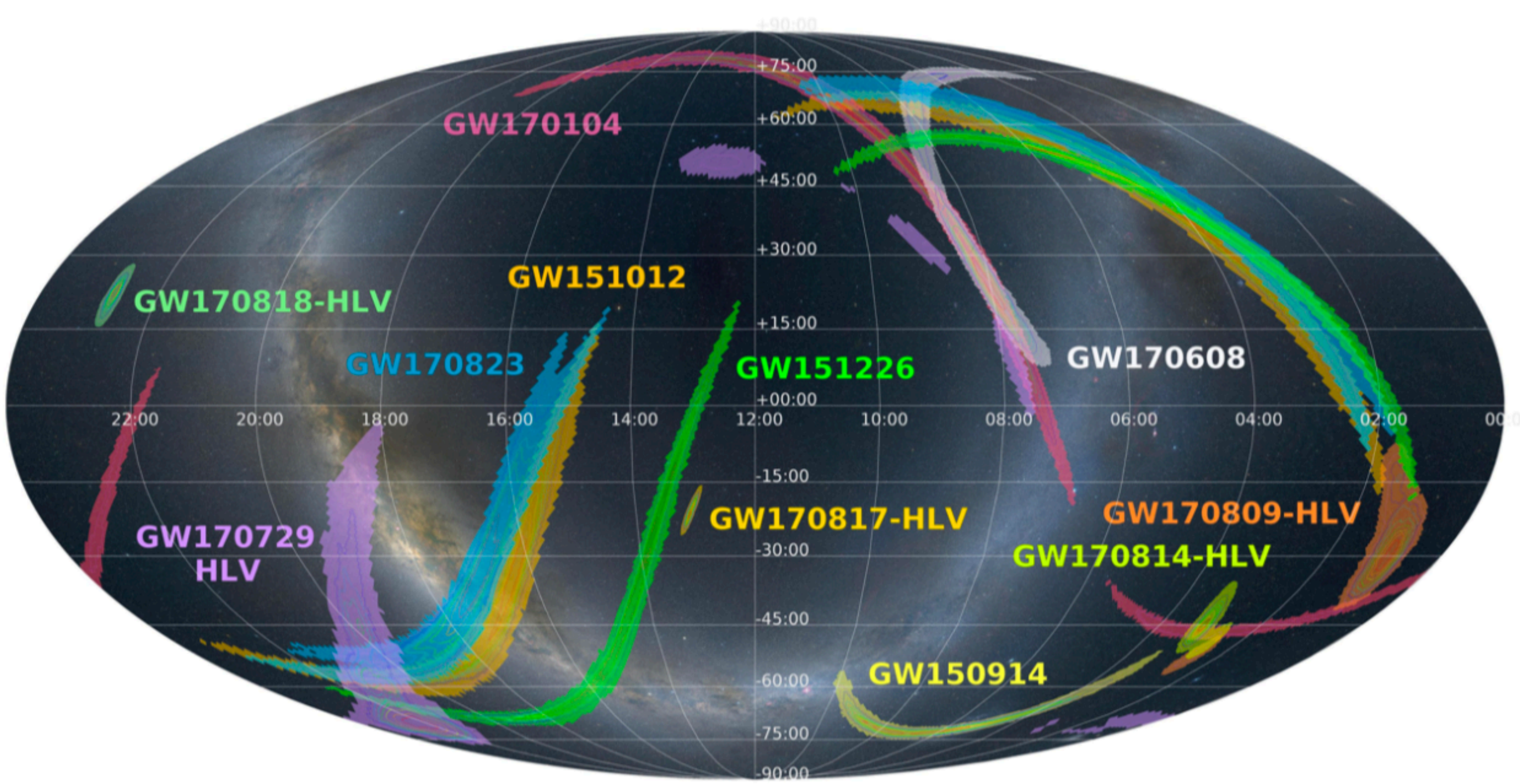

	Low-latency analyisis			Refined analysis		
Event	d_L(Mpc)	$\Delta\Omega\,(\mathrm{deg}^2)$	IFOs	d_L(Mpc)	$\Delta\Omega\,(\mathrm{deg}^2)$	IFOs
GW150914	—	307	HL	440^{+150}_{-170}	182	HL
GW151012	—	—	—	1080^{+550}_{-490}	1523	HL
GW151226	—	1337	HL	490^{+180}_{-190}	1033	HL
GW170104	730^{+340}_{-320}	1632	HL	990^{+440}_{-430}	921	HL
GW170608	310^{+200}_{-120}	864	HL	320^{+120}_{-110}	392	HL
GW170729	—	—	—	2840^{+1400}_{-1360}	1041	HLV
GW170809	1080^{+520}_{-470}	1155	HL	1030^{+320}_{-390}	308	HLV
GW170814	480^{+190}_{-170}	97	HLV	600^{+150}_{-220}	87	HLV
GW170817	40^{+10}_{-10}	31	HLV	40^{+7}_{-15}	16	HLV
GW170818	—	—	—	1060^{+420}_{-380}	39	HLV
GW170823	1380^{+700}_{-670}	2145	HL	1940^{+970}_{-900}	1666	HL

False Alarm Rate

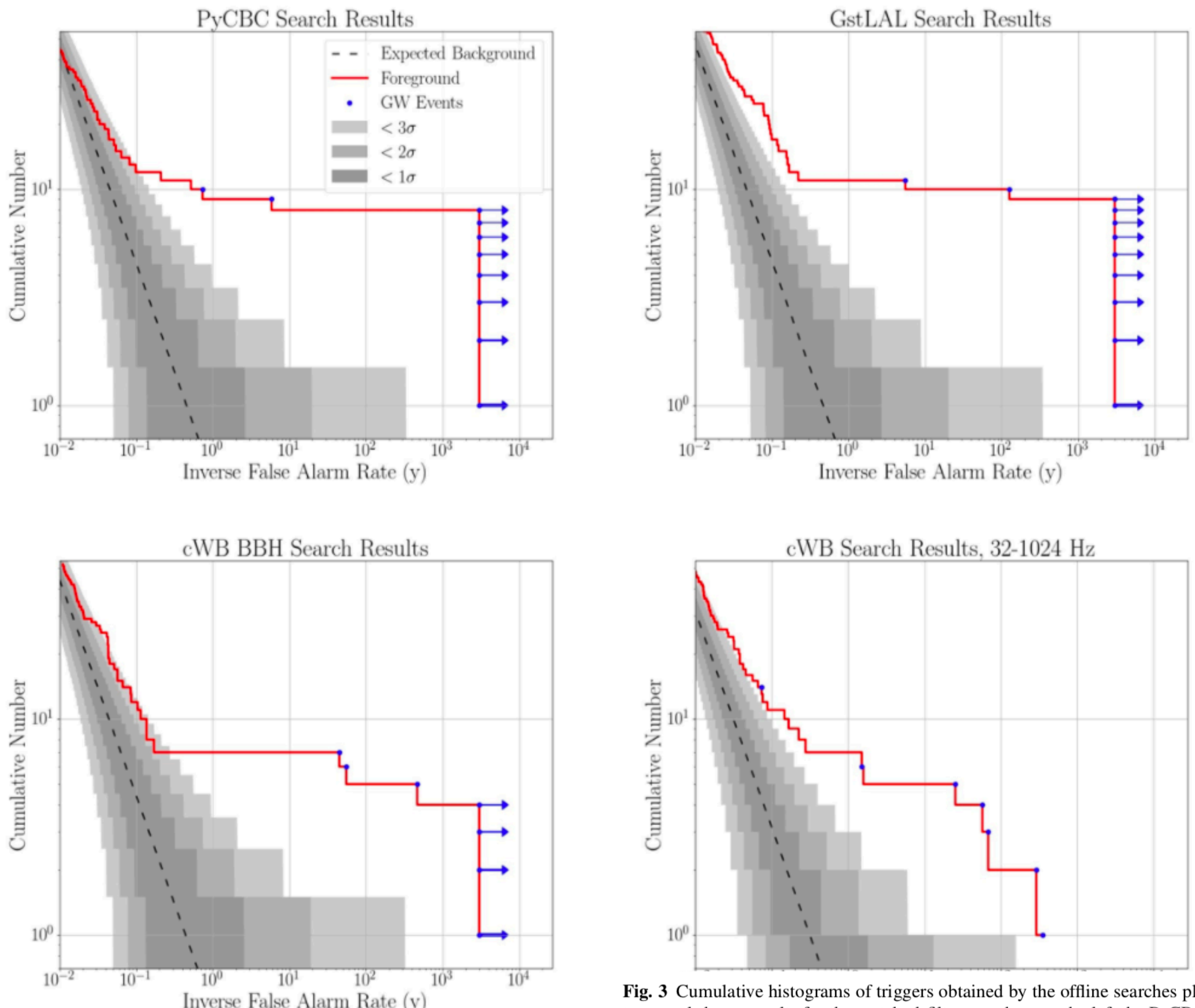

Fig. 3 Cumulative histograms of triggers obtained by the offline searches plotted versus the IFAR. The top panel shows results for the matched-filter searches; on the left the PyCBC (Dal Canton et al. 2014b; Usman et al. 2016) search pipeline, and on the right the GstLAL (Cannon et al. 2012; Privitera et al. 2014; Messick et al. 2017; Sachdev et al. 2019) search pipeline. The bottom panels show unmodeled searches performed by the cWB (Klimenko et al. 2016, 2008) pipeline; on the left looking for stellar-mass BBHs mergers, and on the right for generic transients. The dashed lines show the expected background, given the analysis time. Shaded regions denote the sigma uncertainty bounds for the Poisson statistic. The blue dots are the confident GW events found by each search. Any events with a measured or bounded inverse false alarm rate greater than 3000 yrs are shown with a right pointing arrow. The values of the FARs of the confident events can be found in Abbott et al. (2018d), Abbott et al. (2019b), and Abbott et al. (2017b).

Public Alerts

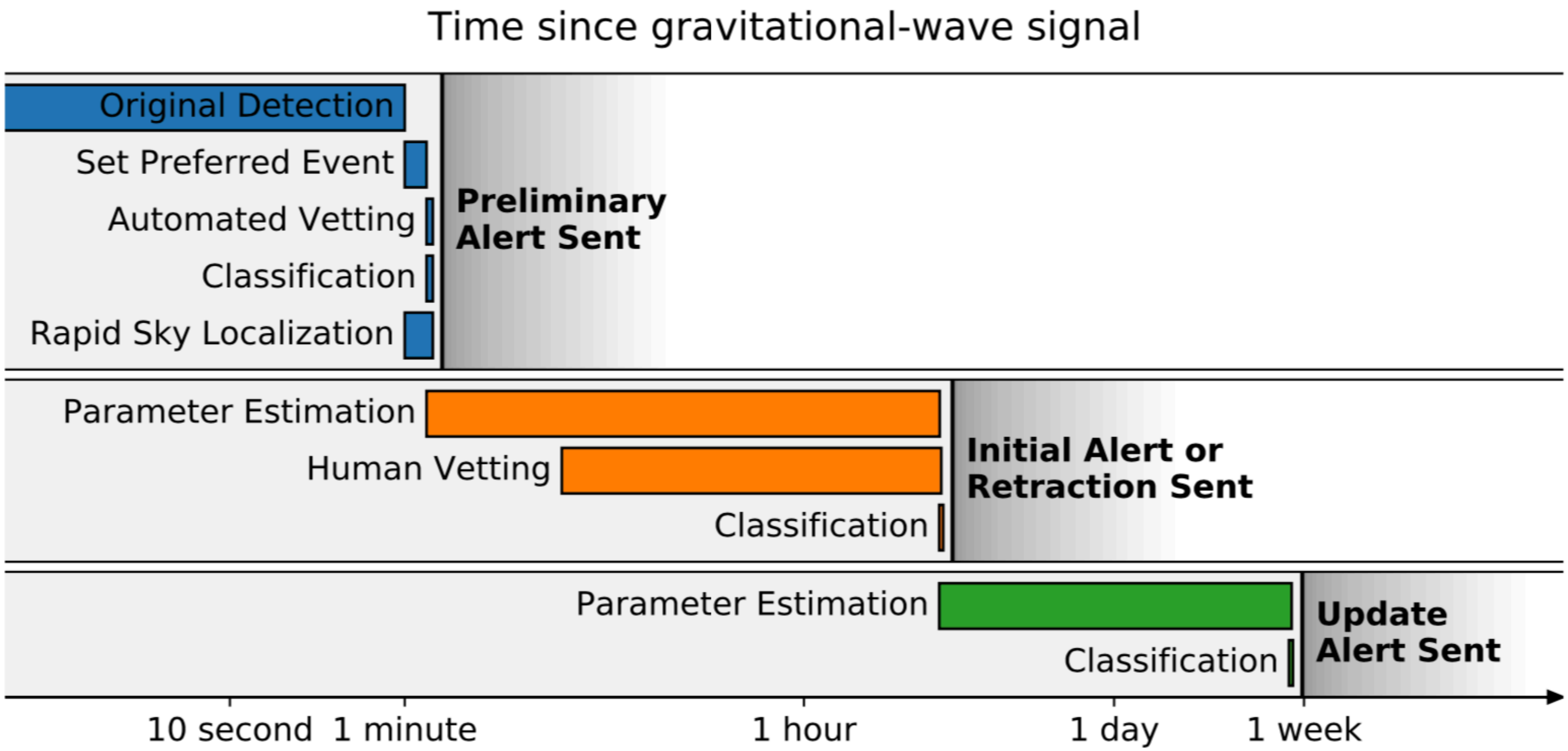

Fig. 8 Alert timeline. The *Preliminary GCN Notice* is sent autonomously within 1-10 minutes after the GW candidate trigger time. Some preliminary alerts may be retracted after human inspection for data quality, instrumental conditions, and pipeline behavior. The human vetted *Initial GCN Notice* or *Retraction GCN Notice* and associated *GCN Circular* are distributed within a few hours for BNS or NSBH sources and within one day for BBH. Update notices and circulars are sent whenever the estimate of the parameters of the signal significantly improves. Figure adapted from the LIGO/Virgo Public Alerts User Guide (see footnote 17)

https://emfollow.docs.ligo.org/userguide/

Public Alerts

GraceDB — Gravitational-Wave Candidate Event Database

HOME | PUBLIC ALERTS | SEARCH | LATEST | DOCUMENTATION | LOGIN

Latest — as of 15 February 2020 13:15:11 UTC

Test and MDC events and superevents are not included in the search results by default; see the query help for information on how to search for events and superevents in those categories.

Query:

Search for: Superevent

Search

UID	Labels	t_start	t_0	t_end	FAR (Hz)	Created (UTC)
S200213t	EM_READY ADVOK EM_Selected SKYMAP_READY EMBRIGHT_READY PASTRO_READY DQOK GCN_PRELIM_SENT	1265602257.327981	1265602258.327981	1265602259.327981	1.767e-08	2020-02-13 04:11:05 UTC
S200208q	EM_READY PE_READY ADVOK EM_Selected SKYMAP_READY EMBRIGHT_READY PASTRO_READY DQOK GCN_PRELIM_SENT	1265202094.944824	1265202095.991118	1265202096.991118	2.518e-09	2020-02-08 13:01:39 UTC
S200129m	EM_READY PE_READY ADVOK EM_Selected SKYMAP_READY EMBRIGHT_READY PASTRO_READY DQOK GCN_PRELIM_SENT	1264316115.411621	1264316116.435104	1264316117.460904	6.697e-32	2020-01-29 06:55:42 UTC
S200128d	EM_READY PE_READY ADVOK EM_Selected SKYMAP_READY EMBRIGHT_READY PASTRO_READY DQOK GCN_PRELIM_SENT	1264213228.897043	1264213229.903320	1264213230.953959	1.647e-08	2020-01-28 02:20:36 UTC
S200116ah	EM_READY PE_READY ADVNO EM_Selected SKYMAP_READY EMBRIGHT_READY PASTRO_READY DQOK GCN_PRELIM_SENT	1263211019.170712	1263211020.170712	1263211021.170712	2.029e-12	2020-01-16 11:57:11 UTC
S200115j	EM_READY PE_READY ADVOK EM_Selected SKYMAP_READY EMBRIGHT_READY PASTRO_READY DQOK GCN_PRELIM_SENT	1263097406.735840	1263097407.752869	1263097408.769043	2.094e-11	2020-01-15 04:23:40 UTC
S200114f	EM_READY ADVOK EM_Selected SKYMAP_READY DQOK GCN_PRELIM_SENT	1263002916.225766	1263002916.239300	1263002916.252885	1.226e-09	2020-01-14 02:11:12 UTC
S200112r	EM_READY PE_READY ADVOK EM_Selected SKYMAP_READY EMBRIGHT_READY PASTRO_READY DQOK GCN_PRELIM_SENT	1262879935.091777	1262879936.093931	1262879937.093931	1.283e-11	2020-01-12 15:59:06 UTC

https://gracedb.ligo.org/latest/

LV event categories

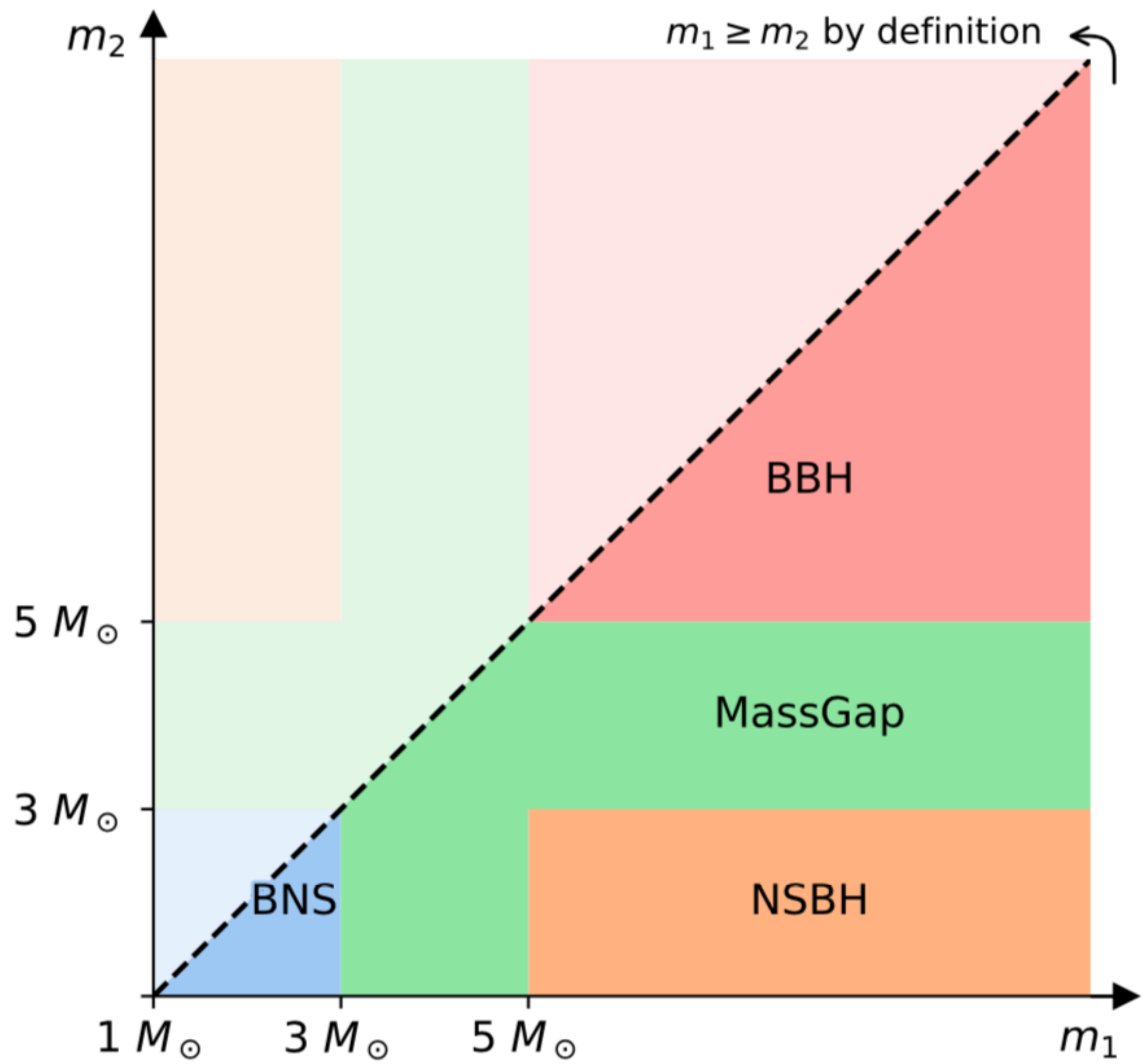

Fig. 9 The four astrophysical categories in terms (BNS, NSBH, BBH, and MassGap) of component masses *m1* and *m2*, which are used to define the source classification. By convention, the component masses are defined such that $m1 \geqslant m2$, so that the primary compact object in the binary (i.e., component 1), is always more massive than the secondary compact object (i.e., component 2). Figure adapted from the LIGO/Virgo Public Alerts User Guide (see footnote 17)

https://emfollow.docs.ligo.org/userguide/

Catalogue History

	LV	Hannover	Princeton
2018/11/1	O1 data release https://www.gw-openscience.org/about/		
2018/11/5		[1811.01921] 1-OGC	
2018/11/30	[1811.12907] GWTC-1		
2019/2/27			[1902.10331]
2019/2/27	O2 data release		
2019/4/15			[1904.07214]
			[1908.05644]
2019/10/11		2-OGC [1910.05331] https://github.com/gwastro/2-ogc	

PHYSICAL REVIEW D **100**, 023011 (2019)

New search pipeline for compact binary mergers: Results for binary black holes in the first observing run of Advanced LIGO

Tejaswi Venumadhav,[1,*] Barak Zackay,[1] Javier Roulet,[2] Liang Dai,[1] and Matias Zaldarriaga[1]
[1]*School of Natural Sciences, Institute for Advanced Study, 1 Einstein Drive, Princeton, New Jersey 08540, USA*
[2]*Department of Physics, Princeton University, Princeton, New Jersey 08540, USA*

(Received 21 March 2019; published 24 July 2019)

In this paper, we report on the construction of a new and independent pipeline for analyzing the public data from the first observing run of Advanced LIGO for mergers of compact binary systems. The pipeline incorporates different techniques and makes independent implementation choices in all its stages including the search design, the method to construct template banks, the automatic routines to detect bad data segments ("glitches") and to insulate good data from them, the procedure to account for the nonstationary nature of the detector noise, the signal-quality vetoes at the single-detector level and the methods to combine results from multiple detectors. Our pipeline enabled us to identify a new binary black hole merger GW151216 in the public LIGO data. This paper serves as a bird's eye view of the pipeline's important stages. Full details and derivations underlying the various stages will appear in accompanying papers.

DOI: 10.1103/PhysRevD.100.023011

O1
GW151216

TABLE III. Events and subthreshold candidates in all of the binary black hole banks.

Name	Bank	$\mathcal{M}(M_\odot)$[a]	GPS time[b]	ρ_H^2	ρ_L^2	FAR^{-1} (O1)[c]	$\frac{W}{\mathcal{R}(\mathrm{event}\|H_0)}$ (days)	$\mathcal{R}_{>100}(\mathrm{days}^{-1})$	p_{astro}
GW151226	BBH 1	9.74	1135136350.585	120.0	52.1	>20000	…[d]	…	1[d]
GW151012	BBH 2	18	1128678900.428	55.66	46.75	>20000	7×10^{5}[e]	0.01	0.9998[e]
GW150914	BBH 3	28	1126259462.411	396.1	184.3	>20000	…[d]	…	1[d]
GW151216[f]	BBH 3	29	1134293073.164	39.4	34.8	52	74 ± 2	0.033	0.71
151231	BBH 3	30	1135557647.145	37.5	25.2	0.98	5.4 ± 0.4	0.033	0.15
151011	BBH 4	58	1128626886.595	24.5	39.9	1.1	16 ± 1	0.01	0.14

[a]Posterior samples from parameter estimation runs for all the O1 and O2 events can be found at https://github.com/jroulet/O2_samples.
[b]Times are given as the linear free times, that is, the times corresponding to when the waveforms generated by the bank were

PHYSICAL REVIEW D **100,** 023007 (2019)

Editors' Suggestion

Highly spinning and aligned binary black hole merger in the Advanced LIGO first observing run

Barak Zackay,[1,*] Tejaswi Venumadhav,[1] Liang Dai,[1] Javier Roulet,[2] and Matias Zaldarriaga[1]

[1]*School of Natural Sciences, Institute for Advanced Study, 1 Einstein Drive, Princeton, New Jersey 08540, USA*

[2]*Department of Physics, Princeton University, Princeton, New Jersey 08540, USA*

(Received 21 March 2019; published 17 July 2019)

We report a new binary black hole merger in the publicly available LIGO first observing run (O1) data release. The event has a false alarm rate of one per six years in the detector-frame chirp-mass range $\mathcal{M}^{\rm det} \in [20, 40]M_\odot$ in a new independent analysis pipeline that we developed. Our best estimate of the probability that the event is of astrophysical origin is $P_{\rm astro} \sim 0.71$. The estimated physical parameters of the event indicate that it is the merger of two massive black holes, $\mathcal{M}^{\rm det} = 31^{+2}_{-3}M_\odot$ with an effective spin parameter, $\chi_{\rm eff} = 0.81^{+0.15}_{-0.21}$, making this the most highly spinning merger reported to date. It is also among the two highest redshift mergers observed so far. The high aligned spin of the merger supports the hypothesis that merging binary black holes can be created by binary stellar evolution.

O1

GW151216

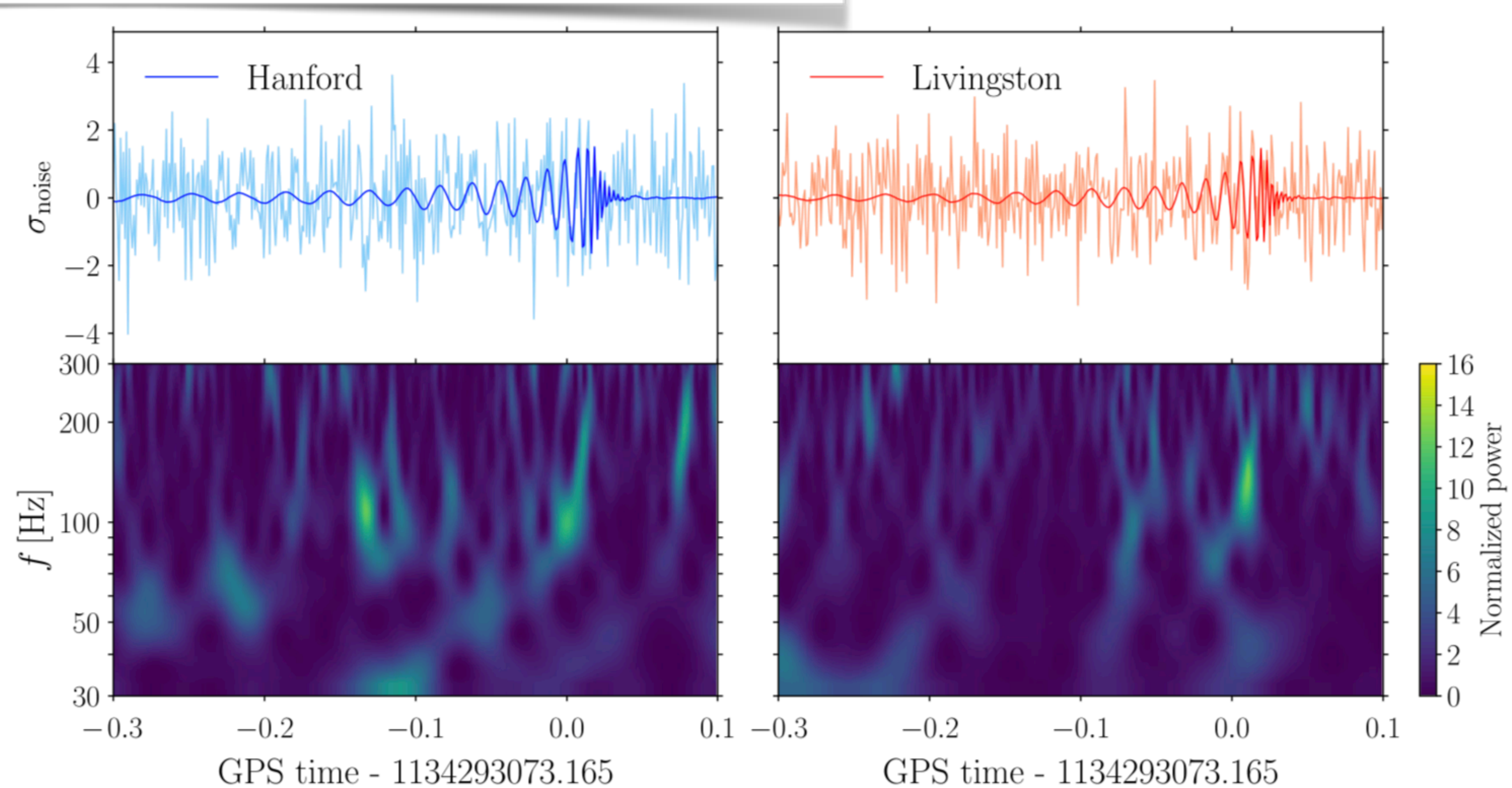

New Binary Black Hole Mergers in the Second Observing Run of Advanced LIGO and Advanced Virgo

Tejaswi Venumadhav,[1,*] Barak Zackay,[1] Javier Roulet,[2] Liang Dai,[1] and Matias Zaldarriaga[1]

[1] School of Natural Sciences, Institute for Advanced Study, 1 Einstein Drive, Princeton, NJ 08540, USA
[2] Department of Physics, Princeton University, Princeton, NJ, 08540, USA

(Dated: April 16, 2019)

TABLE I: Events already reported by the LIGO–Virgo Collaboration [2] as detected with our pipeline. The rate distributions used to compute $p_{\rm astro}$ are shown in Fig. 3. The maximum likelihood rates are $\mathcal{R}_{\rm max} = 8/\mathrm{O2}$ and $5/\mathrm{O2}$ in banks `BBH 3` and `BBH 4`, respectively.

Name	Bank	GPS time[a]	ρ_H^2	ρ_L^2	$\mathrm{FAR}^{-1}(\mathrm{O2})$[b]	$\frac{W(\mathrm{event})}{\mathcal{R}(\mathrm{event}\mid\mathcal{N})}$ (O2)	$p_{\rm astro}$
GW170104	`BBH (3,0)`	1167559936.582	85.1	104.3	$> 2 \times 10^4$	> 100	> 0.99
GW170809	`BBH (3,0)`	1186302519.740	40.5	113	$> 2 \times 10^4$	> 100	> 0.99
GW170814	`BBH (3,0)`	1186741861.519	90.2	170	$> 2 \times 10^4$	> 100	> 0.99
GW170818	`BBH (3,0)`	1187058327.075	19.4	95.1	1.7[c]	—	—[c]
GW170729	`BBH (3,1)`	1185389807.311	62.1	53.6	$> 2 \times 10^4$	> 100	> 0.99
GW170823	`BBH (3,1)`	1187529256.500	46.0	90.7	$> 2 \times 10^4$	> 100	> 0.99

[a] The times given are the ‘linear-free’ times of the best fit templates in our bank; with this time as the origin, the phase of the template is orthogonal to shifts in time, given the fiducial PSD.
[b] The FARs given are computed within each bank; our BBH analysis has 5 chirp-mass banks. The inverse FAR is given in terms of “O2” to reflect the volumetric weighting of events. Under the approximation of constant sensitivity of the detectors during the observing run, the unit “O2” corresponds to ≈ 118 days.
[c] See discussion in §III.

TABLE II: New events with astrophysical probability > 50% in all of the BBH banks. The rate distributions used to compute $p_{\rm astro}$ are shown in Fig. 3, the maximum-likelihood rates in banks `BBH 3` and `BBH 4` are $\mathcal{R}_{\rm max} = 8/\mathrm{O2}$ and $5/\mathrm{O2}$, respectively.

Name	Bank	$\mathcal{M}^{\rm det}(\mathrm{M}_\odot)$	$\chi_{\rm eff}$	z	GPS time[a]	ρ_H^2	ρ_L^2	$\mathrm{FAR}^{-1}(\mathrm{O2})$[b]	$\frac{W(\mathrm{event})}{\mathcal{R}(\mathrm{event}\mid\mathcal{N})}$ (O2)	$p_{\rm astro}$
GW170121	`BBH (3,0)`	29^{+4}_{-3}	$-0.3^{+0.3}_{-0.3}$	$0.24^{+0.14}_{-0.13}$	1169069154.565	29.4	89.7	2.8×10^3	> 30	> 0.99
GW170304	`BBH (4,0)`	47^{+8}_{-7}	$0.2^{+0.3}_{-0.3}$	$0.5^{+0.2}_{-0.2}$	1172680691.356	24.9	55.9	377	13.6	0.985
GW170727	`BBH (4,0)`	42^{+6}_{-6}	$-0.1^{+0.3}_{-0.3}$	$0.43^{+0.18}_{-0.17}$	1185152688.019	25.4	53.5	370	11.8	0.98
GW170425	`BBH (4,0)`	47^{+26}_{-10}	$0.0^{+0.4}_{-0.5}$	$0.5^{+0.4}_{-0.3}$	1177134832.178	28.6	37.5	15	0.65	0.77
GW170202	`BBH (3,0)`	$21.6^{+4.2}_{-1.4}$	$-0.2^{+0.4}_{-0.3}$	$0.27^{+0.13}_{-0.12}$	1170079035.715	26.5	41.7	6.3	0.25	0.68
GW170403	`BBH (4,1)`	48^{+9}_{-7}	$-0.7^{+0.5}_{-0.3}$	$0.45^{+0.22}_{-0.19}$	1175295989.221	31.3	31.0	4.7	0.23	0.56

[a] The times given are the ‘linear-free’ times of the best fit templates in our bank; with this time as the origin, the phase of the template is orthogonal to shifts in time, given the fiducial PSD.
[b] The FARs given are computed within each bank; our BBH analysis has 5 chirp-mass banks. The inverse FAR is given in terms of “O2” to reflect the volumetric weighting of events. Under the approximation of constant sensitivity of the detectors during the observing run, the unit “O2” corresponds to ≈ 118 days.

O2
new 6 events
170121
170202
170304
170403
170425
170727

[arXiv:1904.07214]

New Binary Black Hole Mergers in the Second Observing Run of Advanced LIGO and Advanced Virgo

Tejaswi Venumadhav,[1,*] Barak Zackay,[1] Javier Roulet,[2] Liang Dai,[1] and Matias Zaldarriaga[1]
[1]School of Natural Sciences, Institute for Advanced Study, 1 Einstein Drive, Princeton, NJ 08540, USA
[2]Department of Physics, Princeton University, Princeton, NJ, 08540, USA

(Dated: April 16, 2019)

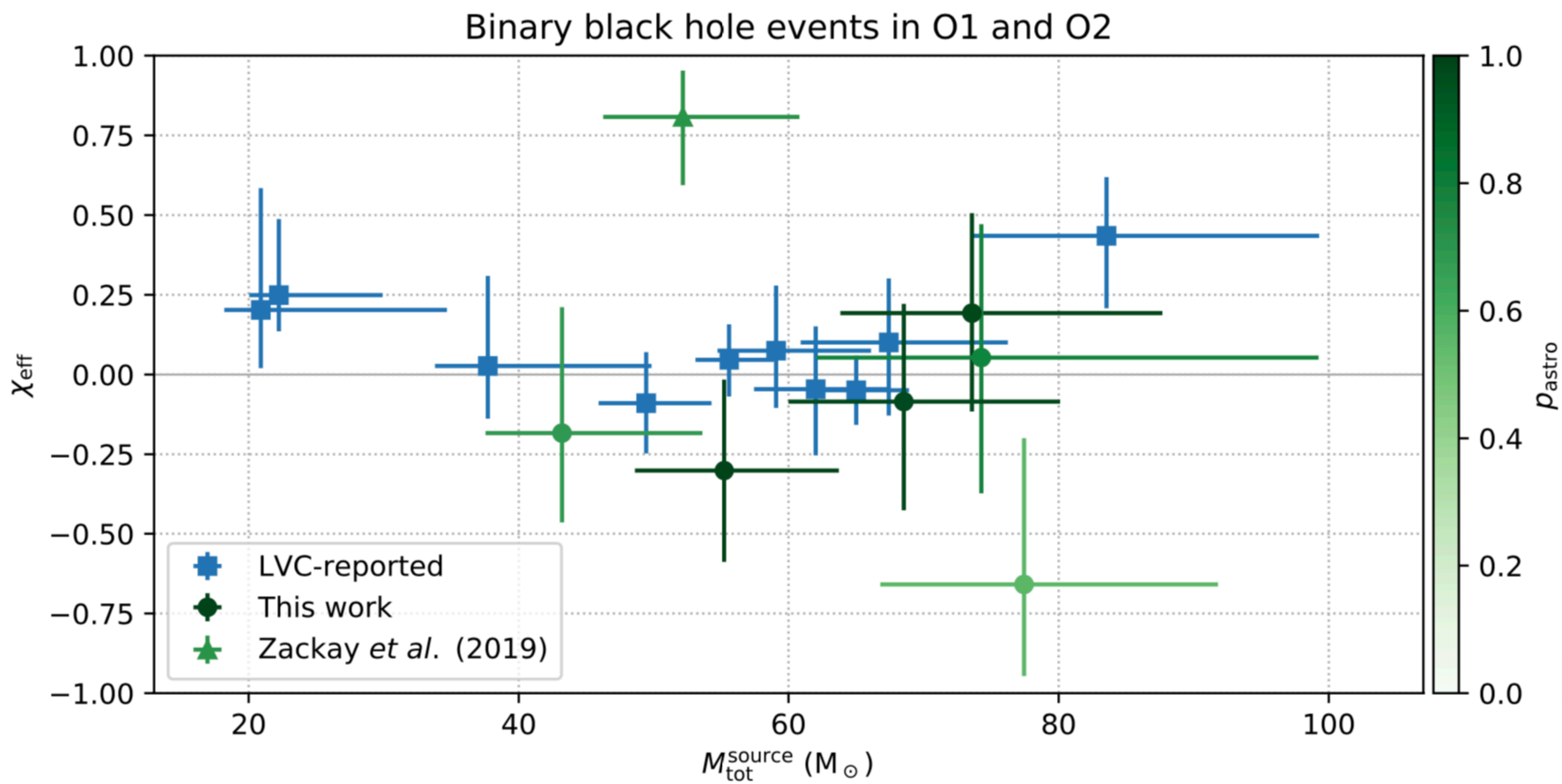

FIG. 4: Source-frame total mass and effective spin for the BBH events found in Hanford–Livingston coincidence, over O1 and O2. We recovered all the previously reported events with high confidence, $p_{\rm astro} \approx 1$, except for GW170608 and GW170818, see §III. We found seven additional events ranging from marginal triggers to confident detections: one in O1 [17] and six in O2 (this work). The dots and error bars show median and 90% confidence intervals, respectively. The spin $\chi_{\rm eff}$ and the mass can be correlated (not shown). The full posteriors can be found in Appendix A. The prior used was uniform in m_1, m_2, $\chi_{\rm eff}$, and luminosity volume.

1-OGC: The first open gravitational-wave catalog of binary mergers from analysis of public Advanced LIGO data

Alexander H. Nitz,[1,2] Collin Capano,[1,2] Alex B. Nielsen,[1,2] Steven Reyes,[3] Rebecca White,[4,3]
Duncan A. Brown,[3] and Badri Krishnan[1,2]

[1] *Max-Planck-Institut für Gravitationsphysik (Albert-Einstein-Institut), D-30167 Hannover, Germany*
[2] *Leibniz Universität Hannover, D-30167 Hannover, Germany*
[3] *Department of Physics, Syracuse University, Syracuse NY 13244, USA*
[4] *Fayetteville-Manlius High School, Manlius, NY 13104, USA*

ABSTRACT

We present the first Open Gravitational-wave Catalog (1-OGC), obtained by using the public data from Advanced LIGO's first observing run to search for compact-object binary mergers. Our analysis is based on new methods that improve the separation between signals and noise in matched-filter searches for gravitational waves from the merger of compact objects. The three most significant signals in our catalog correspond to the binary black hole mergers GW150914, GW151226, and LVT151012. We assume a common population of binary black holes for these three signals by defining a region of parameter space that is consistent with these events. Under this assumption, we find that LVT151012 has a 97.6% probability of being astrophysical in origin. No other significant binary black hole candidates are found, nor did we observe any significant binary neutron star or neutron star–black hole candidates. We make available our complete catalog of events, including the sub-threshold population of candidates.

O1

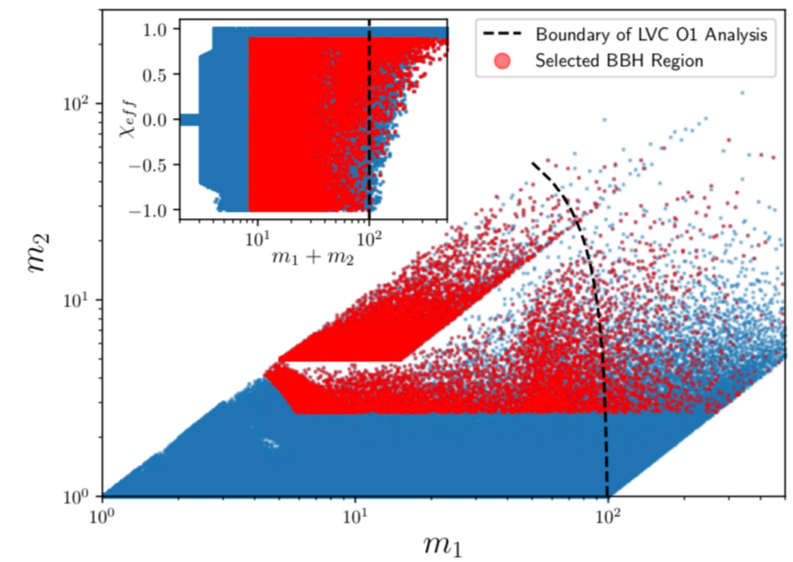

Figure 1. The component masses and spins of the templates used to search for compact binary mergers. Due to the exclusion of short duration templates, there is a dependency on the total mass searched and its effective spin. For binary black holes with negligible spin, this implies that this study only probes sources with total mass less than 200 $M_\odot$. Visible artifacts due to the procedure for constructing the template bank do not impact performance. Templates which we conservatively consider to produce binary black hole (BBH) candidates consistent with known observations are shown in red as discussed in Sec. 3. The upper mass boundary of the analysis performed by the LVC in Abbott et al. (2016a) is shown as a black dotted line.

2-OGC: Open Gravitational-wave Catalog of binary mergers from analysis of public Advanced LIGO and Virgo data

Alexander H. Nitz,[1,2] Thomas Dent,[3] Gareth S. Davies,[3] Sumit Kumar,[1,2] Collin D. Capano,[1,2] Ian Harry,[4,5] Simone Mozzon,[4] Laura Nuttall,[4] Andrew Lundgren,[4] and Marton Tápai[6]

[1] Max-Planck-Institut für Gravitationsphysik (Albert-Einstein-Institut), D-30167 Hannover, Germany
[2] Leibniz Universität Hannover, D-30167 Hannover, Germany
[3] Instituto Galego de Física de Altas Enerxías, Universidade de Santiago de Compostela, 15782 Santiago de Compostela, Galicia, Spain
[4] University of Portsmouth, Portsmouth, PO1 3FX, United Kingdom
[5] Kavli Institute of Theoretical Physics, UC Santa Barbara, CA
[6] Department of Experimental Physics, University of Szeged, Szeged, 6720 Dóm tér 9., Hungary

ABSTRACT

We present the second Open Gravitational-wave Catalog (2-OGC) of compact-binary coalescences, obtained from the complete set of public data from Advanced LIGO's first and second observing runs. For the first time we also search public data from the Virgo observatory. Our analysis is based upon updated methods to improve detection of compact binary mergers by incorporating corrections for short time variations in the detectors' noise power spectral density and instantaneous network sensitivity. We identify a population of 14 binary black hole mergers with $p_{\mathrm{astro}} > 0.5$ along with the GW170817 binary neutron star merger. We confirm the binary black hole merger observations of GW170121, GW170304, and GW170727. We also report GW151205, a new marginal binary black hole merger during the first observing run. No other individually significant binary neutron star candidates are found, nor did we observe any significant neutron star–black hole candidates. We make available our comprehensive catalog of events, including the sub-threshold population of candidates to enable deeper follow-up as our understanding of the underlying populations evolves.

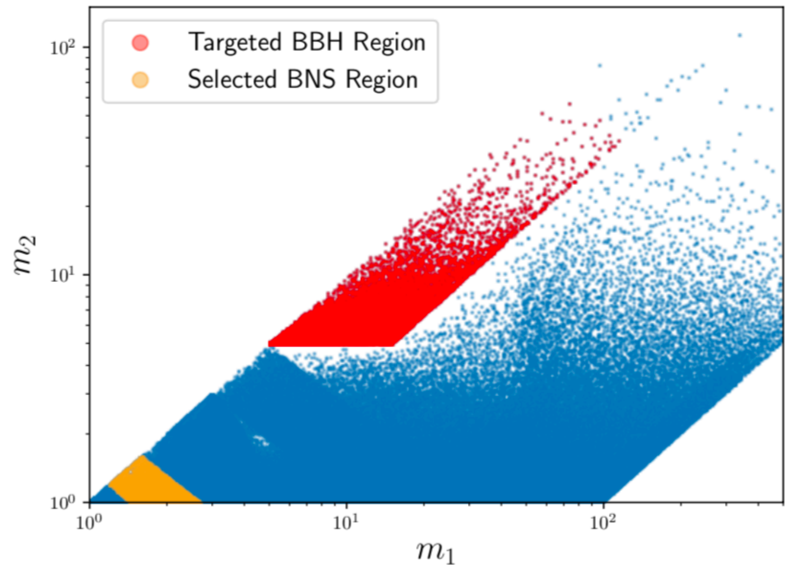

Figure 2. The component masses of templates used to search for compact binary mergers. Templates which define the targeted-binary black hole region are colored in red. Candidates which fall in the selected BNS-like region are discussed in 4.2.

O1/O2

new 4 events

151205

170121

170304

170727

自己回帰モデルを用いた重力波データ解析(2)：LIGO/Virgo O2までのカタログデータ解析

ブラックホールリングダウン波形の

真貝寿明（大阪工大）

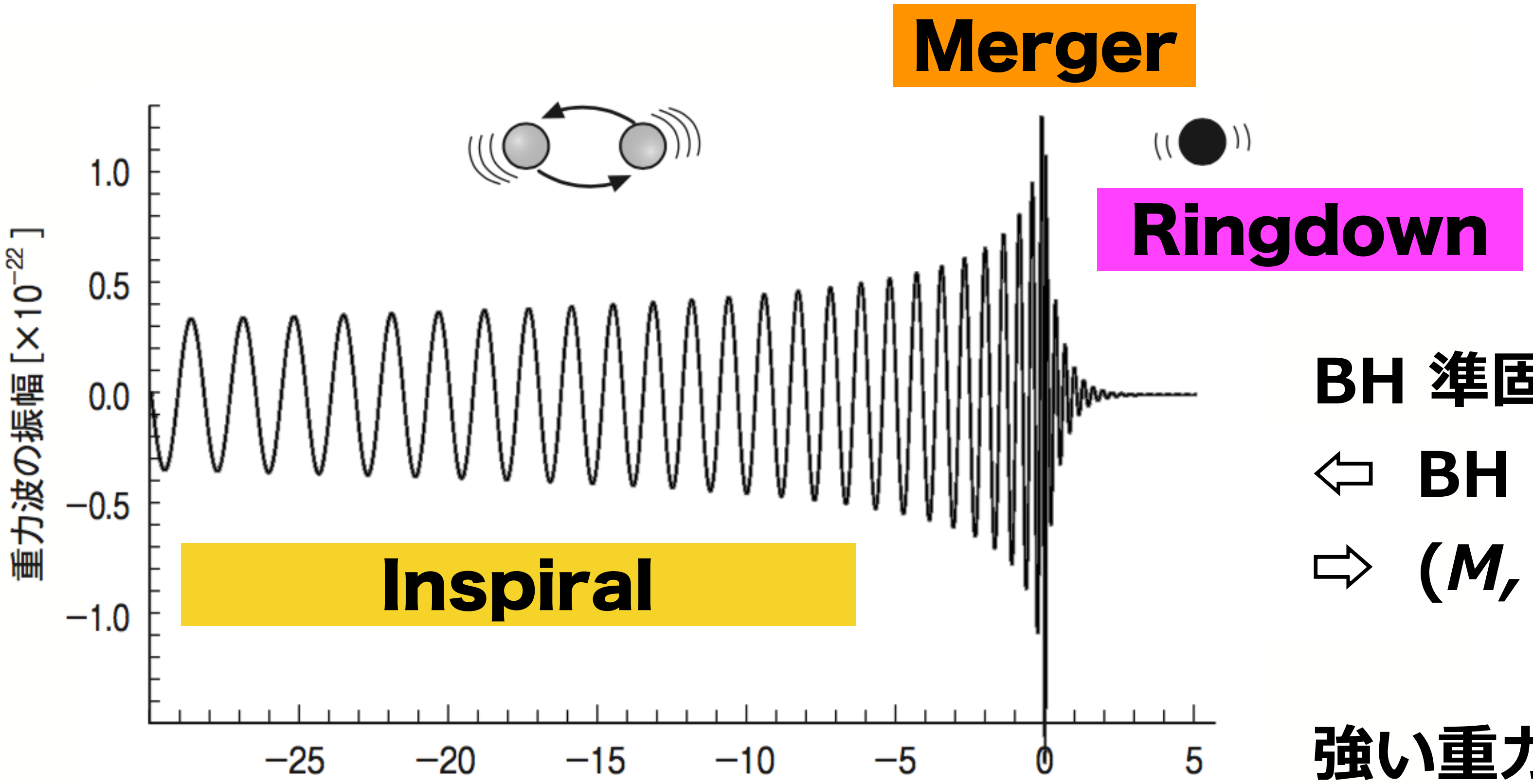

BH 準固有モード(quasi-normal modes)
⇦ BH 摂動理論
⇨ (M, a)

強い重力場の表れ
⇨ 一般相対論の検証ができる

テンプレートを使わず，データから波形を再構築.

2019/9/20 物理学会 @ 山形大学

O1/O2 カタログ

PHYSICAL REVIEW X **9,** 031040 (2019)

GWTC-1: A Gravitational-Wave Transient Catalog of Compact Binary Mergers Observed by LIGO and Virgo during the First and Second Observing Runs

B. P. Abbott *et al.**
(LIGO Scientific Collaboration and Virgo Collaboration)

(Received 14 December 2018; revised manuscript received 27 March 2019; published 4 September 2019)

O1: September 12, 2015 -- January 19, 2016

▶ GW150914 BHBH

O2: November 30, 2016 -- August 25, 2017

▶ GW170817 NSNS

▶ **GWTC-1 catalogue paper [arXiv:1811.12907]**

▶ **data released to public Feb, 2019**

O3a: April 1, 2019 -- September 30, 2019

▶ 28 alerts so far

▶ data released to public April, 2021

O3b: November 1, 2019 -- May 1, 2020

▶ KAGRA will join, “LVK collaboration”

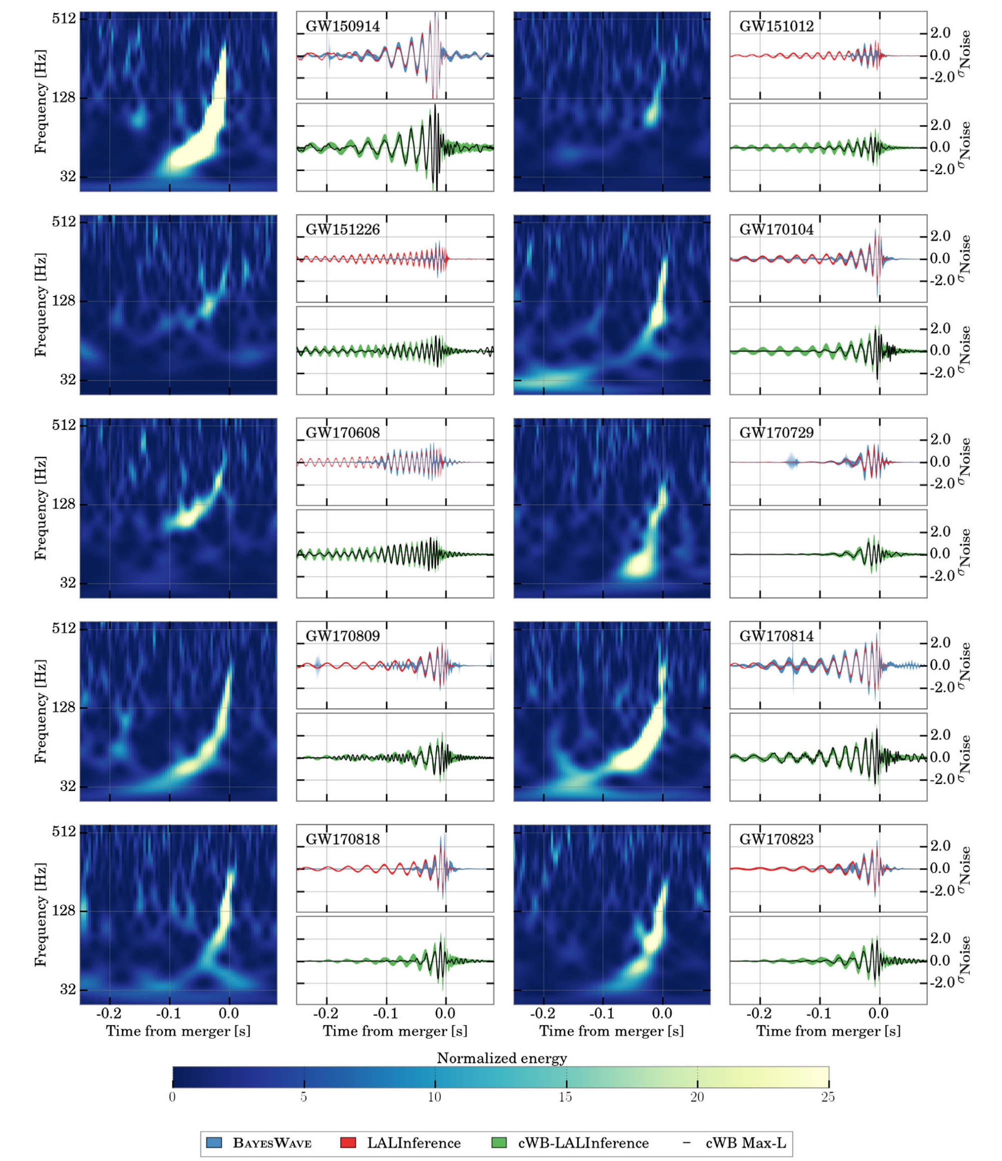

FIG. 10. Time-frequency maps and reconstructed signal waveforms for the ten BBH events. Each event is represented with three panels showing whitened data from the LIGO detector where the higher SNR is recorded. The first panel shows a normalized time-frequency power map of the GW strain. The remaining pair of panels shows time-domain reconstructions of the whitened signal, in units of the standard deviation of the noise. The upper panels show the 90% credible intervals from the posterior probability density functions of the waveform time series, inferred using CBC waveform templates from Bayesian inference (LALInference) with the PhenomP model (red band) and by the BayesWave wavelet model (blue band) [53]. The lower panels show the point estimates from the cWB search (solid lines), along with a 90% confidence interval (green band) derived from cWB analyses of simulated waveforms from the LALInference CBC parameter estimation injected into data near each event. Visible differences between the different reconstruction methods are verified to be consistent with a noise origin (see the text for details).

O1/O2 カタログ

Event	$m_1/M_\odot$	$m_2/M_\odot$	$\mathcal{M}/M_\odot$	$\chi_{\rm eff}$	$M_f/M_\odot$	a_f	$E_{\rm rad}/(M_\odot c^2)$	$\ell_{\rm peak}/({\rm erg\,s^{-1}})$	$d_L/{\rm Mpc}$	z	$\Delta\Omega/{\rm deg}^2$
GW150914	$35.6^{+4.7}_{-3.1}$	$30.6^{+3.0}_{-4.4}$	$28.6^{+1.7}_{-1.5}$	$-0.01^{+0.1}_{-0.1}$	$63.1^{+3.4}_{-3.0}$	$0.69^{+0.05}_{-0.04}$	$3.1^{+0.4}_{-0.4}$	$3.6^{+0.4}_{-0.4}\times10^{56}$	440^{+150}_{-170}	$0.09^{+0.03}_{-0.03}$	182
GW151012	$23.2^{+14.9}_{-5.5}$	$13.6^{+4.1}_{-4.8}$	$15.2^{+2.1}_{-1.2}$	$0.05^{+0.31}_{-0.20}$	$35.6^{+10.8}_{-3.8}$	$0.67^{+0.13}_{-0.11}$	$1.6^{+0.6}_{-0.5}$	$3.2^{+0.8}_{-1.7}\times10^{56}$	1080^{+550}_{-490}	$0.21^{+0.09}_{-0.09}$	1523
GW151226	$13.7^{+8.8}_{-3.2}$	$7.7^{+2.2}_{-2.5}$	$8.9^{+0.3}_{-0.3}$	$0.18^{+0.20}_{-0.12}$	$20.5^{+6.4}_{-1.5}$	$0.74^{+0.07}_{-0.05}$	$1.0^{+0.1}_{-0.2}$	$3.4^{+0.7}_{-1.7}\times10^{56}$	450^{+180}_{-190}	$0.09^{+0.04}_{-0.04}$	1033
GW170104	$30.8^{+7.3}_{-5.6}$	$20.0^{+4.9}_{-4.6}$	$21.4^{+2.2}_{-1.8}$	$-0.04^{+0.1}_{-0.21}$	$48.9^{+5.1}_{-4.0}$	$0.66^{+0.08}_{-0.11}$	$2.2^{+0.5}_{-0.5}$	$3.3^{+0.6}_{-1.0}\times10^{56}$	990^{+440}_{-430}	$0.20^{+0.08}_{-0.08}$	921
GW170608	$11.0^{+5.5}_{-1.7}$	$7.6^{+1.4}_{-2.2}$	$7.9^{+0.2}_{-0.2}$	$0.03^{+0.19}_{-0.07}$	$17.8^{+3.4}_{-0.7}$	$0.69^{+0.04}_{-0.04}$	$0.9^{+0.0}_{-0.1}$	$3.5^{+0.4}_{-1.3}\times10^{56}$	320^{+120}_{-110}	$0.07^{+0.02}_{-0.02}$	392
GW170729	$50.2^{+16.2}_{-10.2}$	$34.0^{+9.1}_{-10.1}$	$35.4^{+6.5}_{-4.8}$	$0.37^{+0.21}_{-0.25}$	$79.5^{+14.7}_{-10.2}$	$0.81^{+0.07}_{-0.13}$	$4.8^{+1.7}_{-1.7}$	$4.2^{+0.9}_{-1.5}\times10^{56}$	2840^{+1400}_{-1360}	$0.49^{+0.19}_{-0.21}$	1041
GW170809	$35.0^{+8.3}_{-5.9}$	$23.8^{+5.1}_{-5.2}$	$24.9^{+2.1}_{-1.7}$	$0.08^{+0.17}_{-0.17}$	$56.3^{+5.2}_{-3.8}$	$0.70^{+0.08}_{-0.09}$	$2.7^{+0.6}_{-0.6}$	$3.5^{+0.6}_{-0.9}\times10^{56}$	1030^{+320}_{-390}	$0.20^{+0.05}_{-0.07}$	308
GW170814	$30.6^{+5.6}_{-3.0}$	$25.2^{+2.8}_{-4.0}$	$24.1^{+1.4}_{-1.1}$	$0.07^{+0.12}_{-0.12}$	$53.2^{+3.2}_{-2.4}$	$0.72^{+0.07}_{-0.05}$	$2.7^{+0.4}_{-0.3}$	$3.7^{+0.4}_{-0.5}\times10^{56}$	600^{+150}_{-220}	$0.12^{+0.03}_{-0.04}$	87
GW170817	$1.46^{+0.12}_{-0.10}$	$1.27^{+0.09}_{-0.09}$	$1.186^{+0.001}_{-0.001}$	$0.00^{+0.02}_{-0.01}$	≤ 2.8	≤ 0.89	≥ 0.04	$\geq 0.1\times10^{56}$	40^{+7}_{-15}	$0.01^{+0.00}_{-0.00}$	16
GW170818	$35.4^{+7.5}_{-4.7}$	$26.7^{+4.3}_{-5.2}$	$26.5^{+2.1}_{-1.7}$	$-0.09^{+0.1}_{-0.21}$	$59.4^{+4.9}_{-3.8}$	$0.67^{+0.07}_{-0.08}$	$2.7^{+0.5}_{-0.5}$	$3.4^{+0.5}_{-0.7}\times10^{56}$	1060^{+420}_{-380}	$0.21^{+0.07}_{-0.07}$	スクリ
GW170823	$39.5^{+11.2}_{-6.7}$	$29.0^{+6.7}_{-7.8}$	$29.2^{+4.6}_{-3.6}$	$0.09^{+0.22}_{-0.26}$	$65.4^{+10.1}_{-7.4}$	$0.72^{+0.09}_{-0.1}$	$3.3^{+1.0}_{-0.9}$	$3.6^{+0.7}_{-1.1}\times10^{56}$	1940^{+970}_{-900}	$0.35^{+0.15}_{-0.15}$	1666

TABLE V. KL divergences (in bits) between the prior and posterior for the effective aligned spin $\chi_{\rm eff}$ and the effective precession spin χ_p. For the computation of the KL divergence for χ_p, we quote the KL divergence with the prior conditioned on the $\chi_{\rm eff}$ posterior, $D_{\rm KL}^{\chi_p}(\chi_{\rm eff})$, and without conditioning, $D_{\rm KL}^{\chi_p}$. For GW170817, $D_{\rm KL}^{\chi_p}$ is given for the high spin prior. The median and 90% interval for the KL divergences is estimated by computing the statistic for repeated draws of a subset of the posterior and prior PDFs. Single-detector optimal SNRs from parameter-estimation analyses for Hanford (H), Livingston (L), and Virgo (V).

Event	GW150914	GW151012	GW151226	GW170104	GW170608	GW170729	GW170809	GW170814	GW170817	GW170818	GW170823
$D_{\rm KL}^{\chi_{\rm eff}}$	$0.71^{+0.04}_{-0.03}$	$0.23^{+0.03}_{-0.02}$	$1.32^{+0.11}_{-0.06}$	$0.54^{+0.03}_{-0.03}$	$0.97^{+0.03}_{-0.05}$	$1.83^{+0.07}_{-0.09}$	$0.71^{+0.03}_{-0.03}$	$0.99^{+0.05}_{-0.07}$	$2.32^{+0.08}_{-0.10}$	$0.50^{+0.04}_{-0.03}$	$0.32^{+0.04}_{-0.03}$
$D_{\rm KL}^{\chi_p}$	$0.16^{+0.03}_{-0.02}$	$0.09^{+0.03}_{-0.02}$	$0.17^{+0.03}_{-0.04}$	$0.05^{+0.01}_{-0.01}$	$0.07^{+0.01}_{-0.02}$	$0.09^{+0.02}_{-0.02}$	$0.05^{+0.01}_{-0.01}$	$0.02^{+0.01}_{-0.01}$	$0.19^{+0.04}_{-0.03}$	$0.06^{+0.02}_{-0.01}$	$0.03^{+0.01}_{-0.01}$
$D_{\rm KL}^{\chi_p}(\chi_{\rm eff})$	$0.09^{+0.02}$	$0.08^{+0.02}$	$0.12^{+0.05}$	$0.07^{+0.02}$	$0.08^{+0.02}$	$0.03^{+0.01}$	$0.06^{+0.01}$	$0.13^{+0.03}$	$0.07^{+0.01}$	$0.09^{+0.02}$	$0.03^{+0.01}$
H SNR	$20.6^{+1.6}_{-1.6}$	$6.4^{+1.3}_{-1.3}$	$9.8^{+1.5}_{-1.4}$	$9.5^{+1.3}_{-1.6}$	$12.1^{+1.6}_{-1.6}$	$5.9^{+1.1}_{-1.1}$	$5.9^{+1.4}_{-1.4}$	$9.3^{+1.0}_{-1.2}$	$18.9^{+1.0}_{-1.0}$	$4.6^{+0.9}_{-0.8}$	$6.8^{+1.4}_{-1.2}$
L SNR	$14.2^{+1.6}_{-1.4}$	$5.8^{+1.2}_{-1.2}$	$6.9^{+1.2}_{-1.1}$	$9.9^{+1.5}_{-1.3}$	$9.2^{+1.5}_{-1.2}$	$8.3^{+1.4}_{-1.4}$	$10.7^{+1.6}_{-1.8}$	$14.3^{+1.5}_{-1.4}$	$26.3^{+1.4}_{-1.3}$	$9.7^{+1.5}_{-1.5}$	$9.2^{+1.7}_{-1.5}$
V SNR	...	...	...	...	...	$1.7^{+1.0}_{-1.1}$	$1.1^{+1.2}_{-0.8}$	$4.1^{+1.1}_{-1.1}$	$3.0^{+0.2}_{-0.2}$	$4.2^{+0.8}_{-0.7}$	...

Ring-down modeを独立に見つける手法の比較 (mockdata challenge)

PHYSICAL REVIEW D **99,** 124032 (2019)

Comparison of various methods to extract ringdown frequency from gravitational wave data

Hiroyuki Nakano,[1,*] Tatsuya Narikawa,[2,3,†] Ken-ichi Oohara,[4,‡] Kazuki Sakai,[5,§] Hisa-aki Shinkai,[6,∥] Hirotaka Takahashi,[7,8,¶] Takahiro Tanaka,[3,9,**] Nami Uchikata,[2,4,††] Shun Yamamoto,[6] and Takahiro S. Yamamoto[3,‡‡]

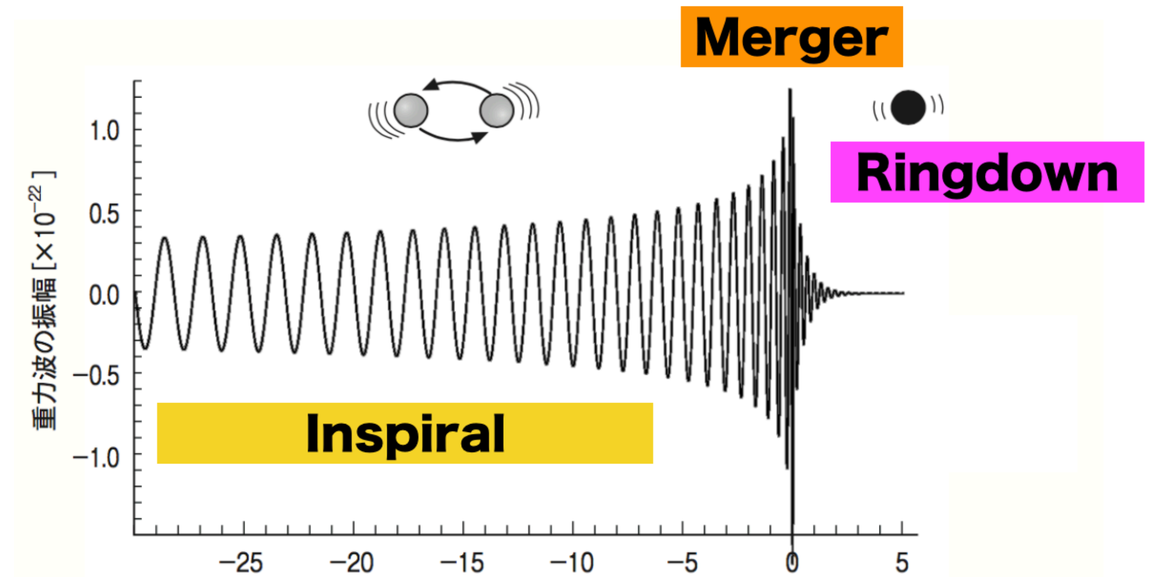

ringdown search
60 mockdata

TABLE III. We show the values of $\overline{\delta \log f_R}$, $\sigma(f_R)$, $\overline{\delta \log f_I}$, and $\sigma(f_I)$ for various methods. The results limited to set A are given on the first law of each method, while those limited to set B are on the second.

		$\overline{\delta \log f_R}$(%)	$\sigma(f_R)$(%)	$\overline{\delta \log f_I}$(%)	$\sigma(f_I)$(%)
MF-R	A	−12.88	28.36	−71.51	97.79
	B	−0.82	27.53	−46.11	75.48
MF-MR	A	6.25 (Very good)	17.27 (Good)	−12.62 (Very good)	37.9 (Very good)
	B	2.47	10.41	7.18	27.61
HHT	A	−13.38	21.91	−44.11	61.58
	B	−8.08	19.81	−28.78	49.61
AR	A	0.2 (Excellent)	9.93 (Excellent)	4.88 (Excellent)	38.75 (Good)
	B	1.91	8.57	6.2	34.64
NN	A	−6.64 (Good)	16.48 (Very good)	−15.23 (Good)	33.96 (Excellent)
	B	−6.65	11.97	9.96	23.76

matched filtering

Hilbert-Huan Transformation

Auto-Regression Method

Neural Network method

1. Auto-Regressive model (Method, general) I

Fitting data with linear func.

$$x_n = a_1 x_{n-1} + a_2 x_{n-2} + \cdots + a_M x_{n-M} + \varepsilon$$
$$= \sum_{j=1}^{M} a_j x_{n-j} + \varepsilon$$

e.g. $x_n = Ae^{-rn\Delta t}\cos(\omega n \Delta t)$

$$Z_1 = e^{-(r-j\omega)\Delta t}$$
$$Z_2 = e^{-(r+j\omega)\Delta t}$$

$$\rightarrow \quad x_n = \frac{A}{2}(Z_1^n + Z_2^n) = (Z_1 + Z_2)x_{n-1} - Z_1 Z_2 x_{n-2}$$

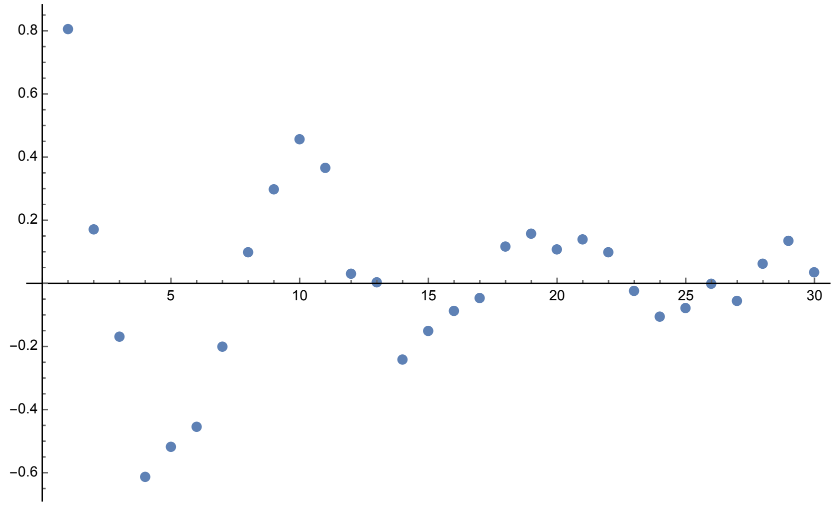

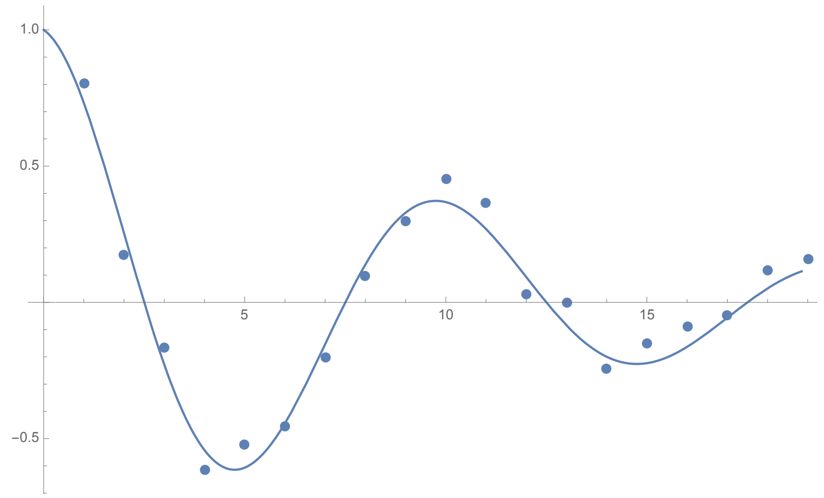

can be applied also to noisy data by adjusting *M*

1. Auto-Regressive model (Method, general) II

Fitting data with linear func.

$$x_n = a_1 x_{n-1} + a_2 x_{n-2} + \cdots + a_M x_{n-M} + \varepsilon$$
$$= \sum_{j=1}^{M} a_j x_{n-j} + \varepsilon$$

- find a_j (Burg method)
- find M (FPE final prediction error method)
- re-construct wave signal from fitted function
- apply FFT with arbitrary precision.

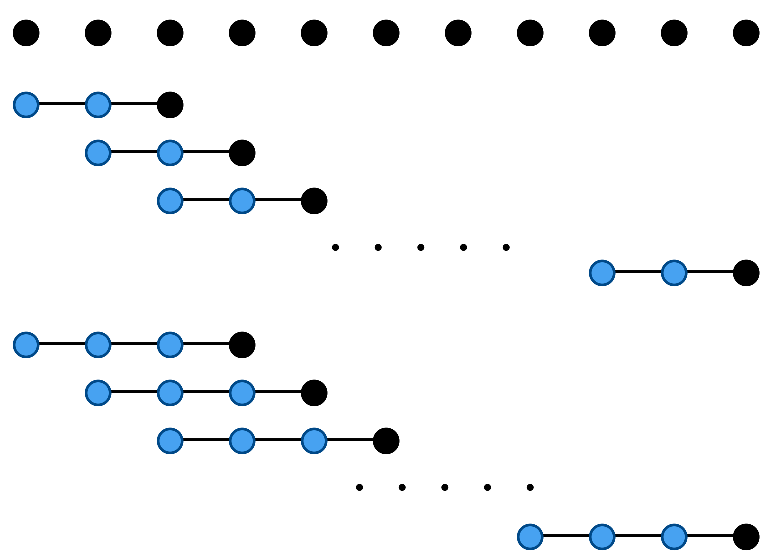

power spectrum

$$p(f) = \frac{\sigma^2}{\left| 1 - \sum_{j=1}^{M} a_j e^{-I 2\pi j f \Delta t} \right|^2}$$

Auto-Regressive model vs Short FFT

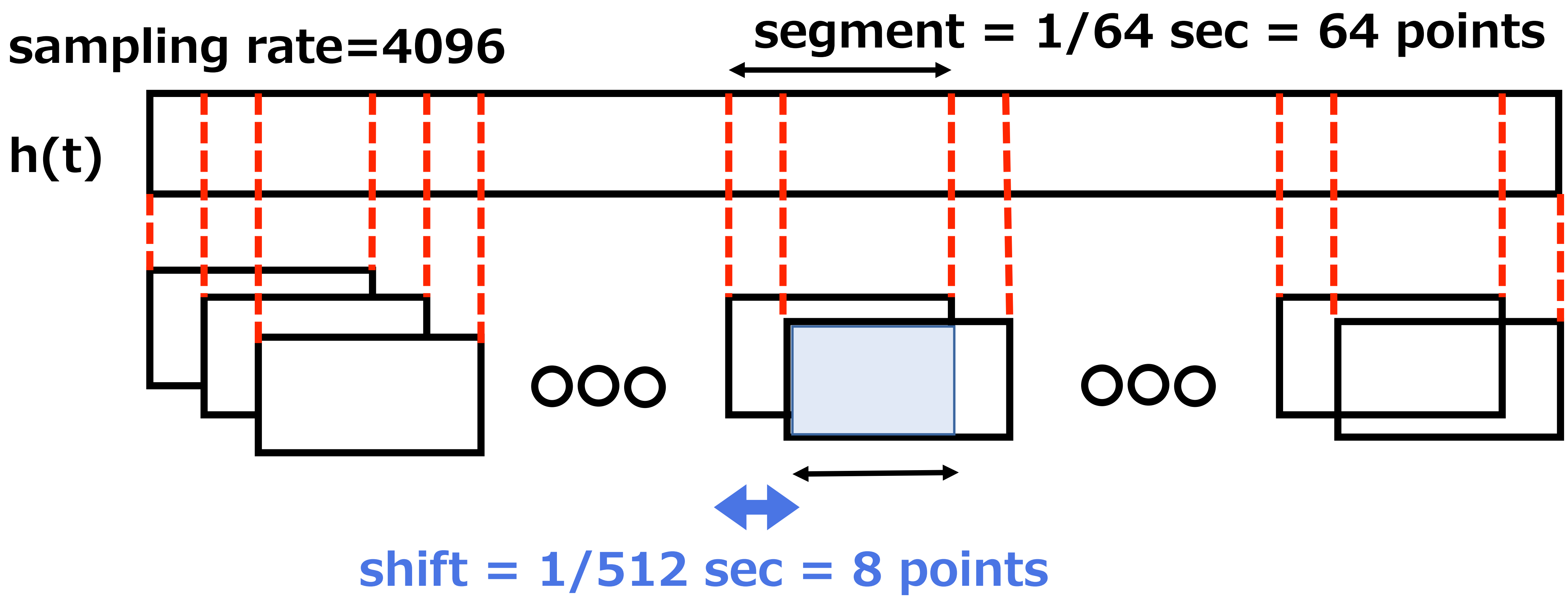

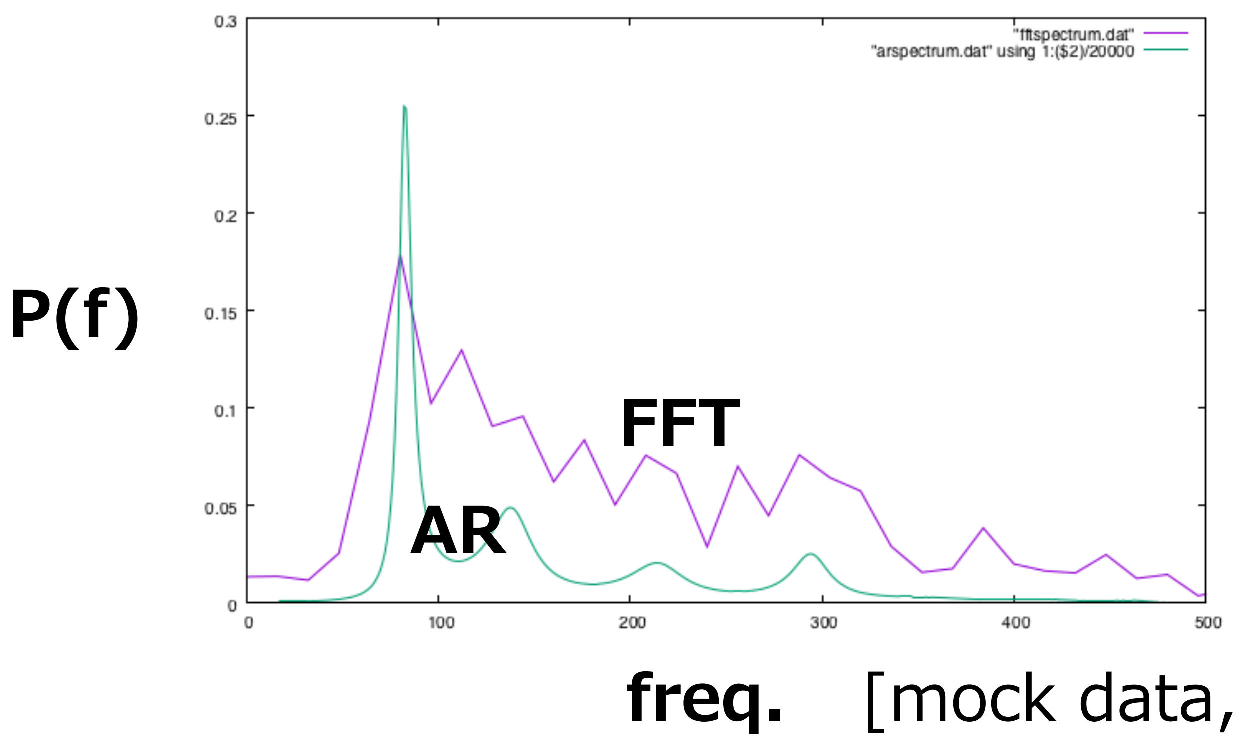

[mock data, SNR=40, inspiral part]

The order M can be fixed at 2〜8.

Even for short segment, AR model shows precise power-spectrum.

1. Auto-Regressive model (Method, general) III

Fitting data with linear func.

$$
\begin{aligned}
x_n &= a_1 x_{n-1} + a_2 x_{n-2} + \cdots + a_M x_{n-M} + \varepsilon \\
&= \sum_{j=1}^{M} a_j x_{n-j} + \varepsilon
\end{aligned}
$$

- find a_j (Burg method)
- find M (FPE final prediction error method)
- re-construct wave signal from fitted function
- apply FFT with arbitrary precision.

power spectrum

$$p(f) = \frac{\sigma^2}{\left| 1 - \sum_{j=1}^{M} a_j e^{-I 2\pi j f \Delta t} \right|^2}$$

characteristic eq.

$$f(z) = 1 - \sum_{j=1}^{M} a_j z^j = 0$$

$|z_k|$ says amplitude,
$\arg(z_k)$ says frequency.

Ringdown Search by Auto-Regressive Approach (O1/O2 public data, GWTC1 catalogue)

GW150914

LIGO paper

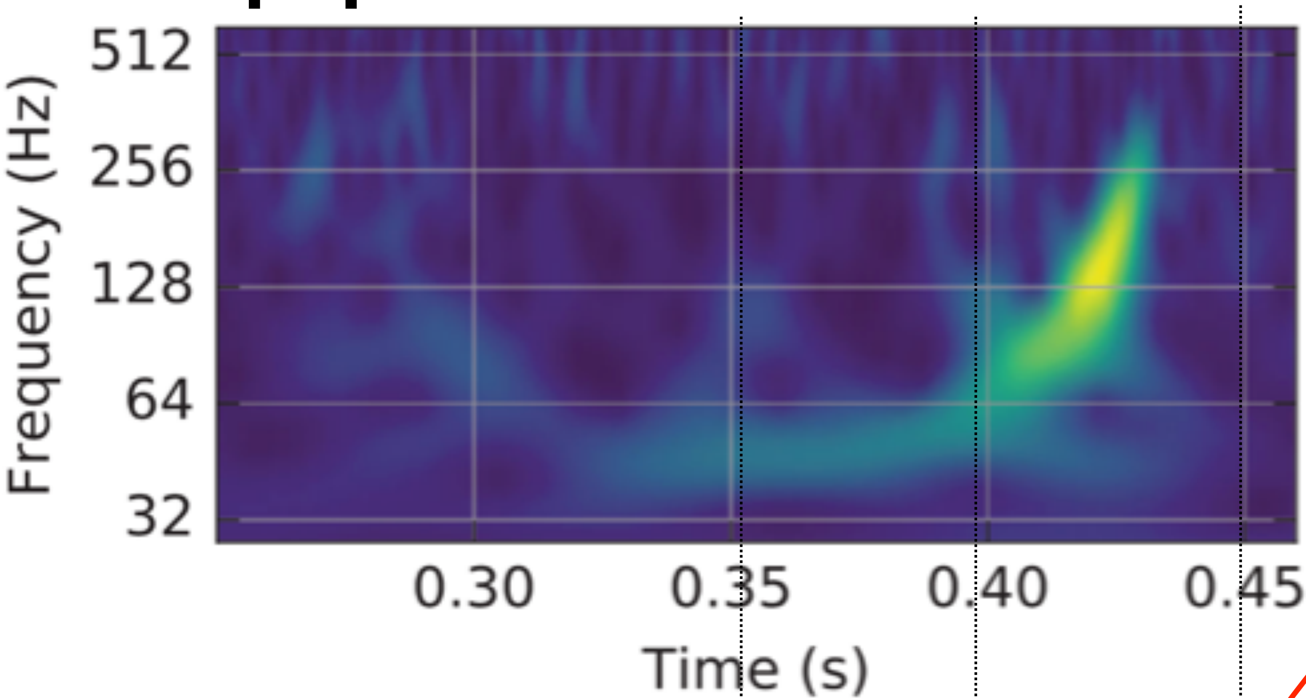

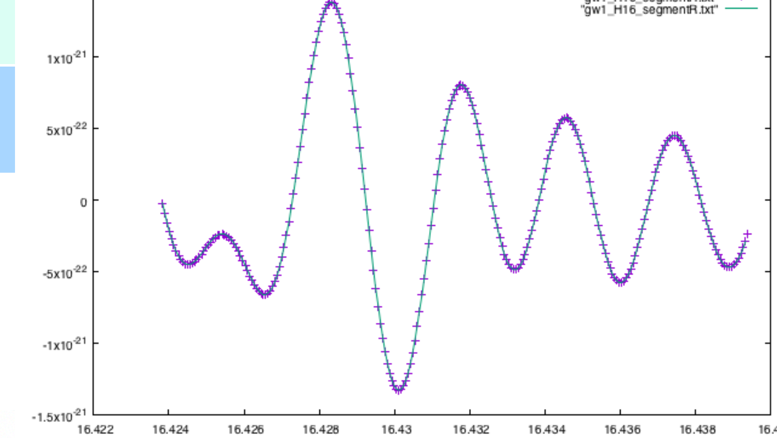

AR model Hanford

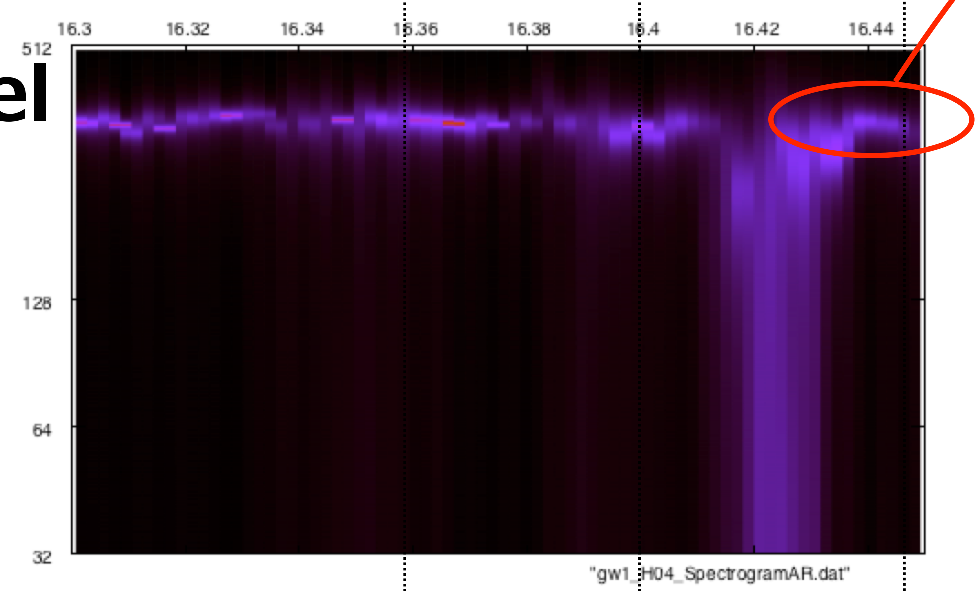

freq [Hz]

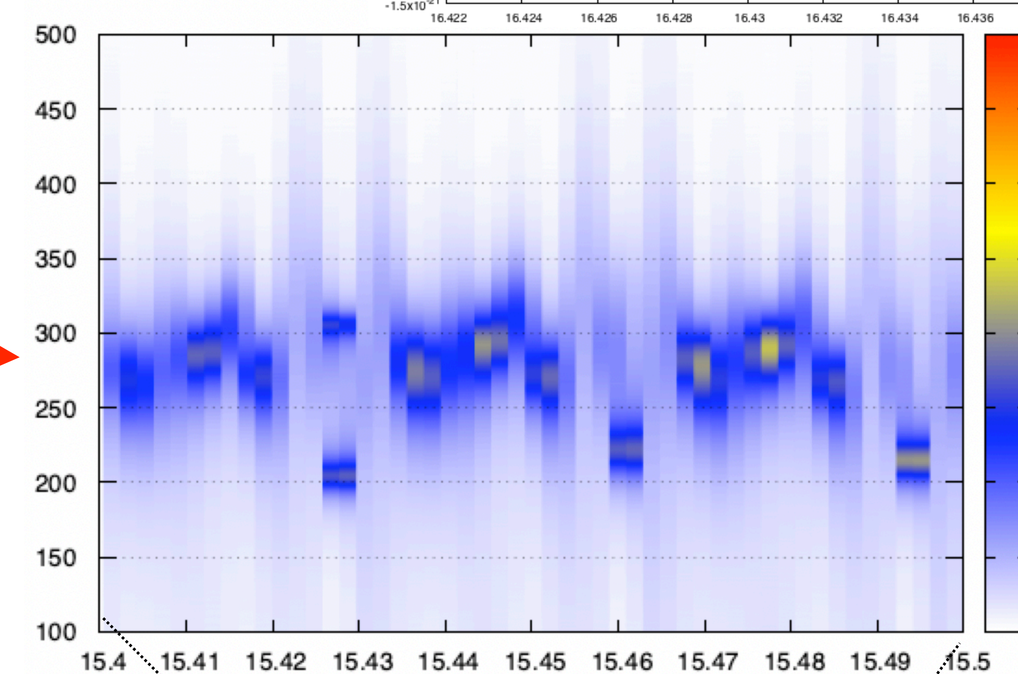

▲merger time

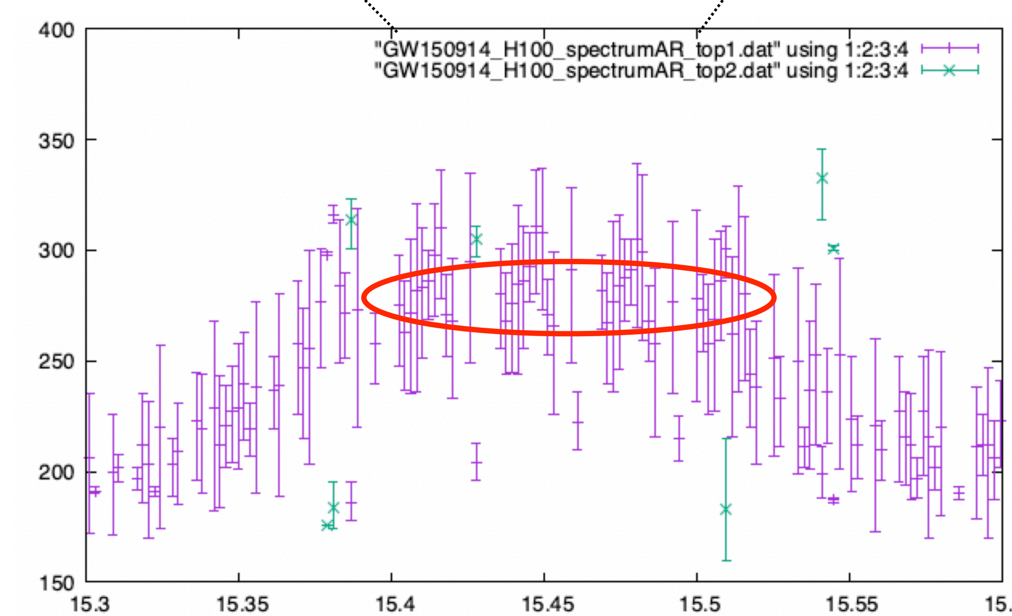

$f_{220} = 249.4$ Hz, $f_{221} = 244.0$ Hz, $f_{222} = 233.7$ Hz

$f_{210} = 349.3$ Hz, $f_{211} = 207.1$ Hz, $f_{200} = 231.9$ Hz

$f_{330} = 395.3$ Hz, $f_{331} = 392.1$ Hz, $f_{332} = 386.3$ Hz

$f_{320} = 355.9$ Hz, $f_{310} = 322.1$ Hz, $f_{300} = 293.9$ Hz

4096 sampling rate
150-450 Hz filter
1 segment = 1/64 sec= 64 points
1 shift = 1/512 sec = 8 points

GW150914

Hanford (SNR=20.6)

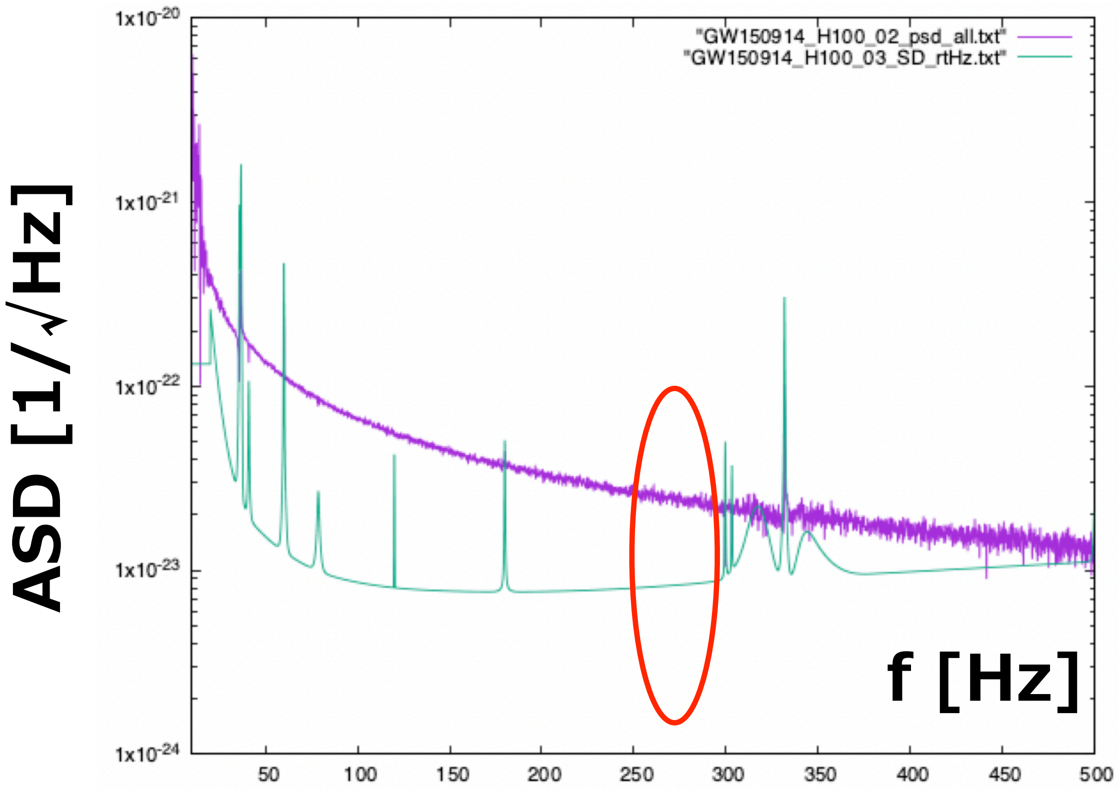

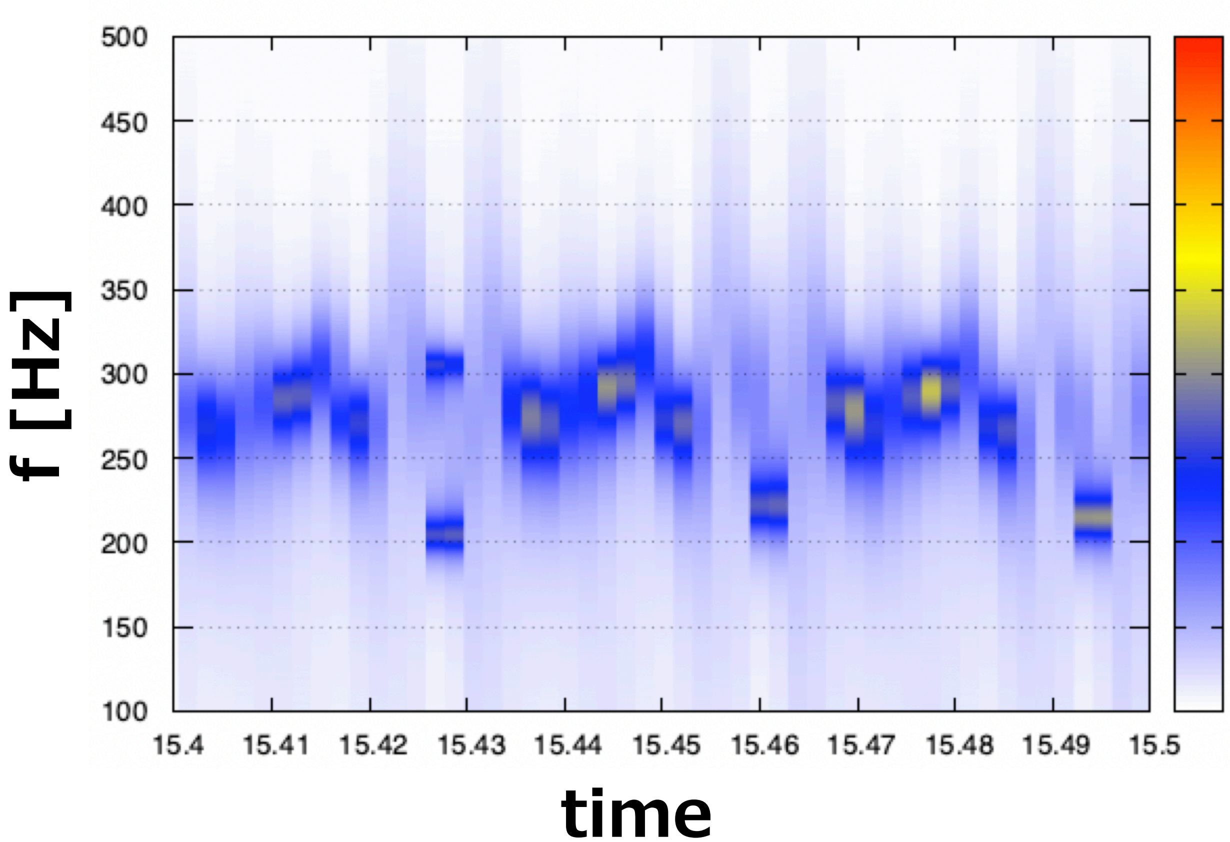

Livingston (SNR=14.2)

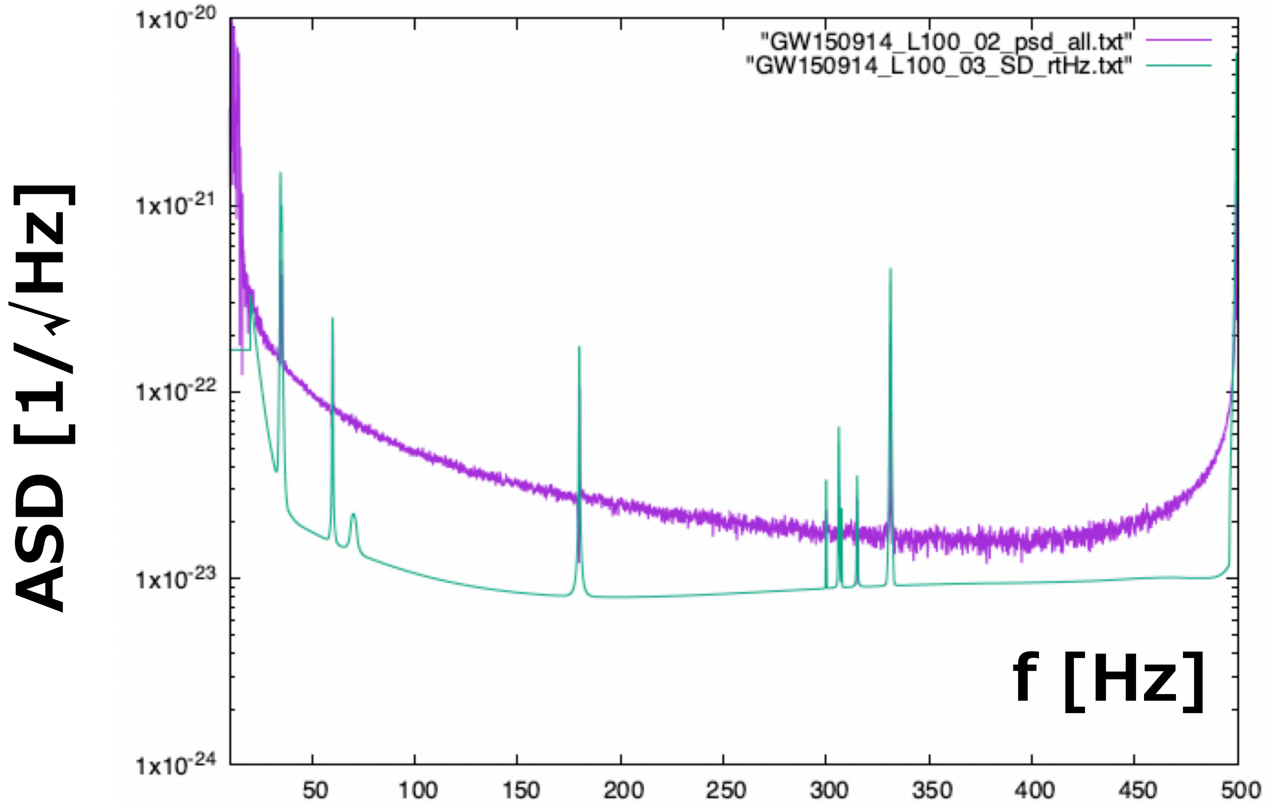

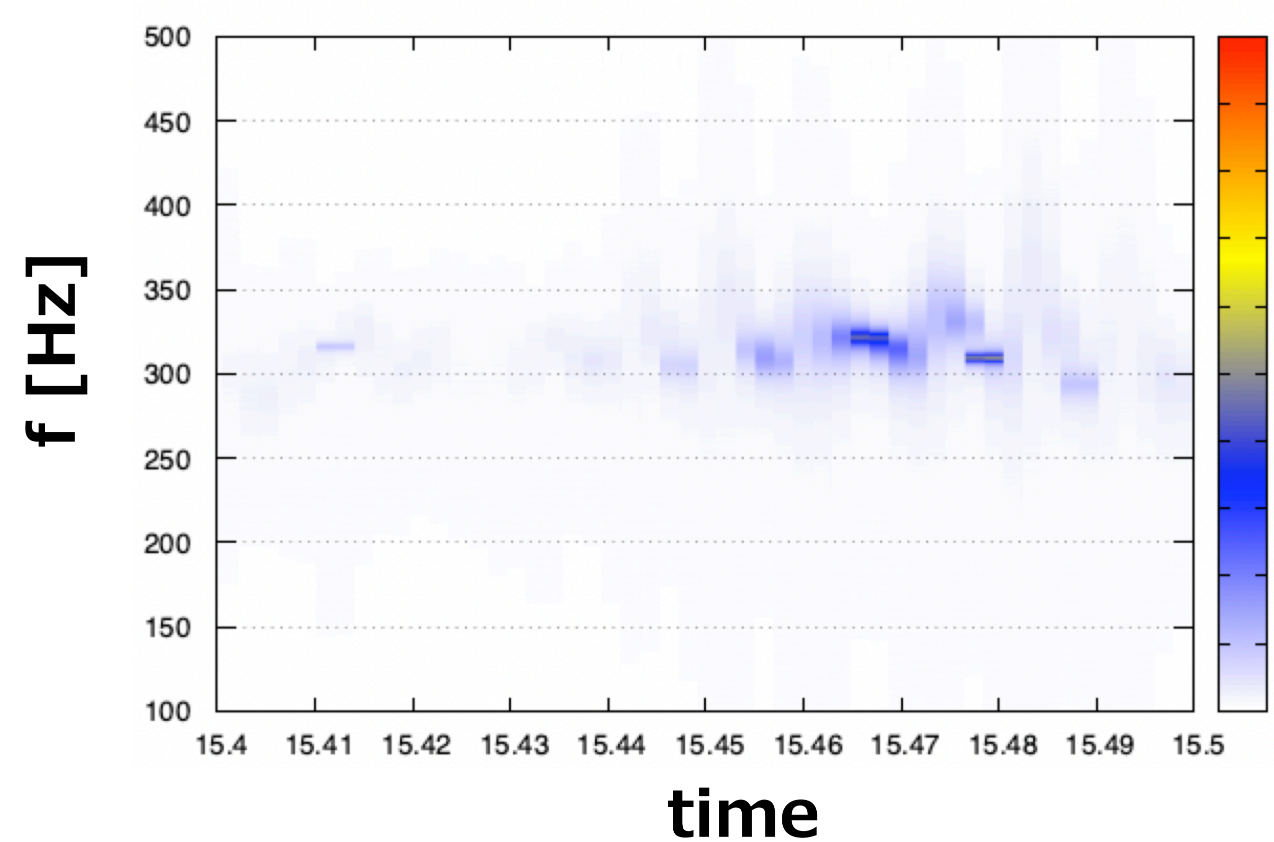

Ringdown Search by Auto-Regressive Approach (O1/O2 public data, GWTC1 catalogue)

GW150914

Hanford (SNR=20.6)

H100_SpectrogramAR

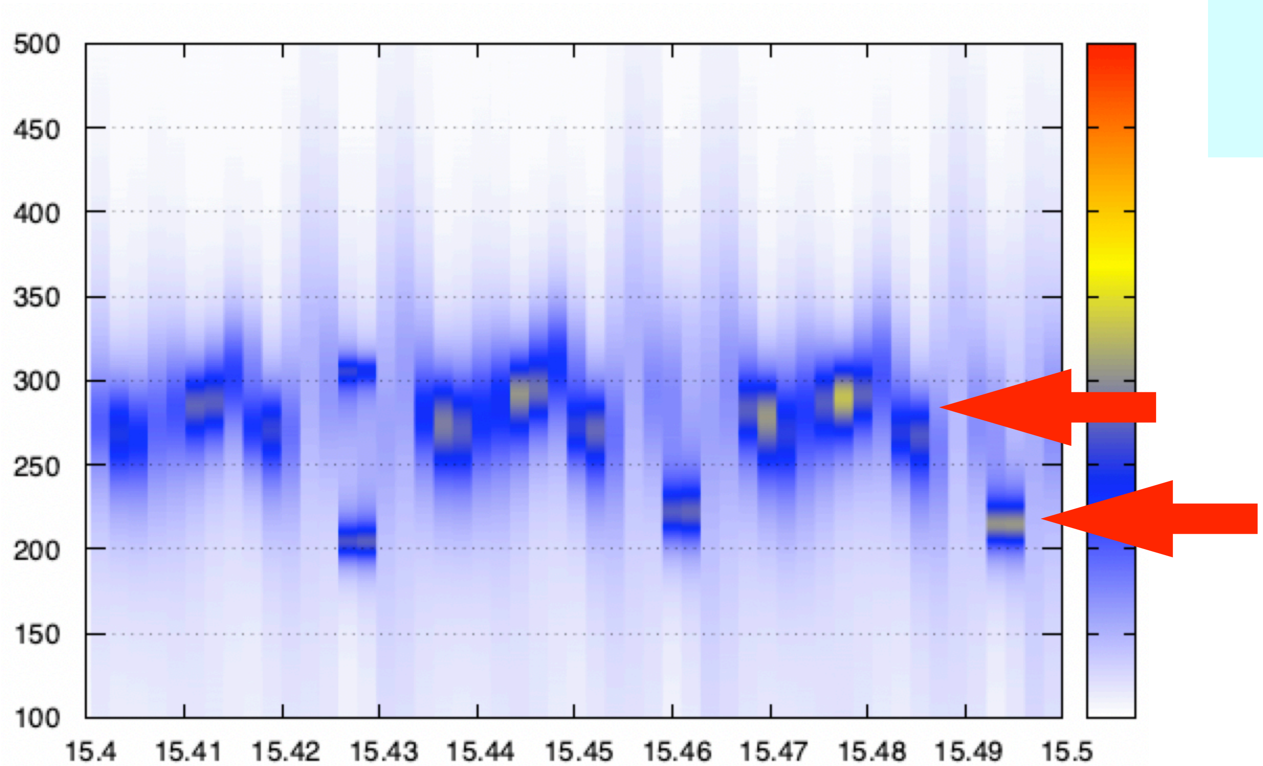

Livingston (SNR=14.2)

L100_SpectrogramAR

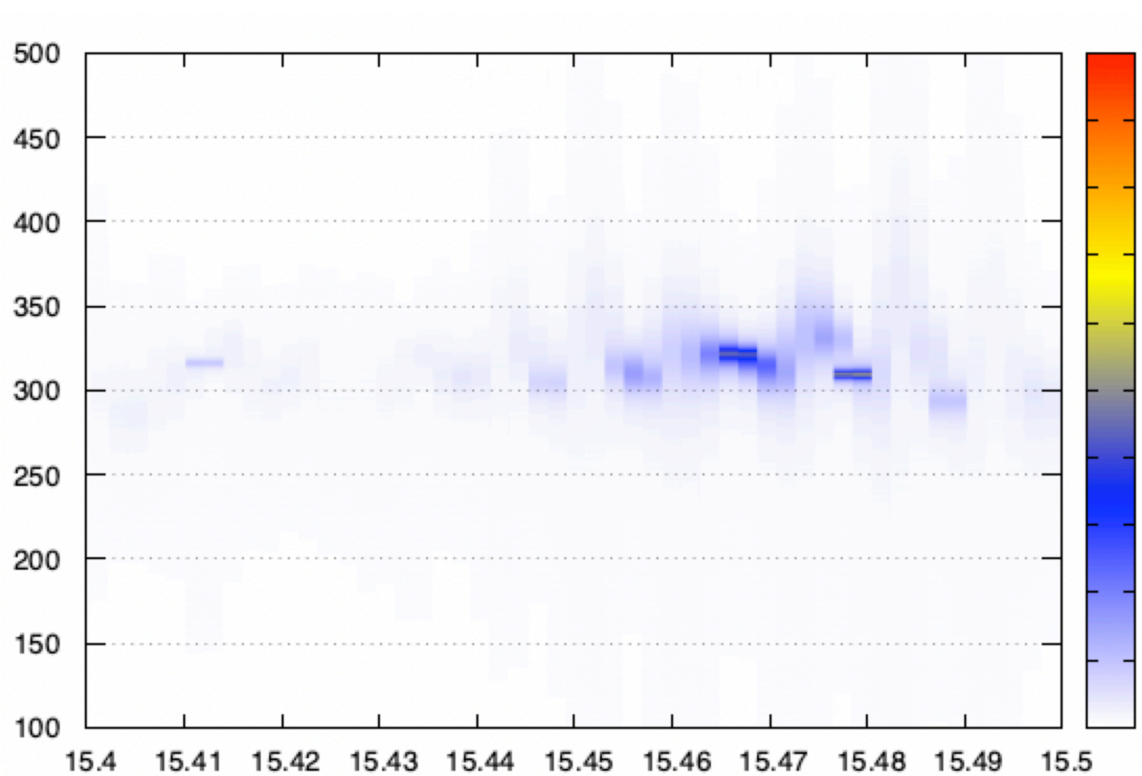

LV paper ▶ $(M, a, z) = (63.1^{+3.4}_{-3.0}, 0.69^{+0.05}_{-0.04}, 0.09^{+0.03}_{-0.03})$

f_{QNM} ▶

$f_{220} = 249.4$ Hz, $f_{221} = 244.0$ Hz, $f_{222} = 233.7$ Hz

$f_{210} = 349.3$ Hz, $f_{211} = 207.1$ Hz, $f_{200} = 231.9$ Hz

$f_{330} = 395.3$ Hz, $f_{331} = 392.1$ Hz, $f_{332} = 386.3$ Hz

$f_{320} = 355.9$ Hz, $f_{310} = 322.1$ Hz, $f_{300} = 293.9$ Hz

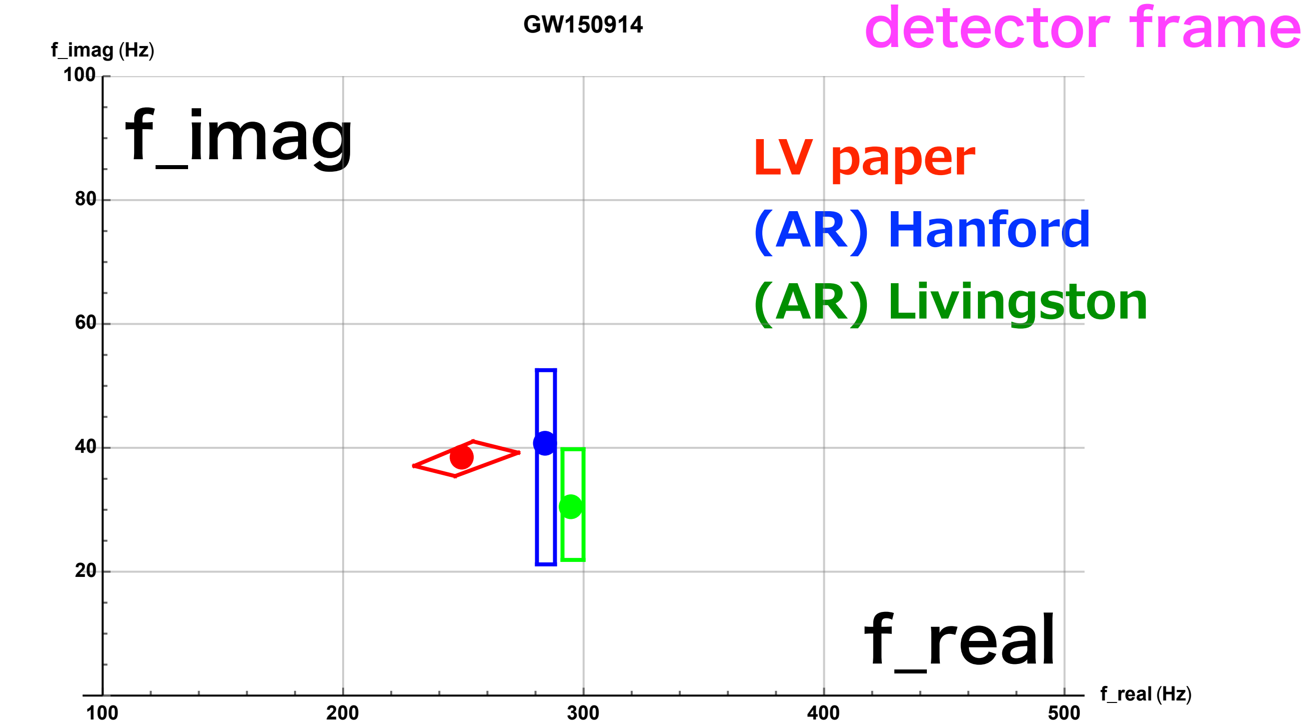

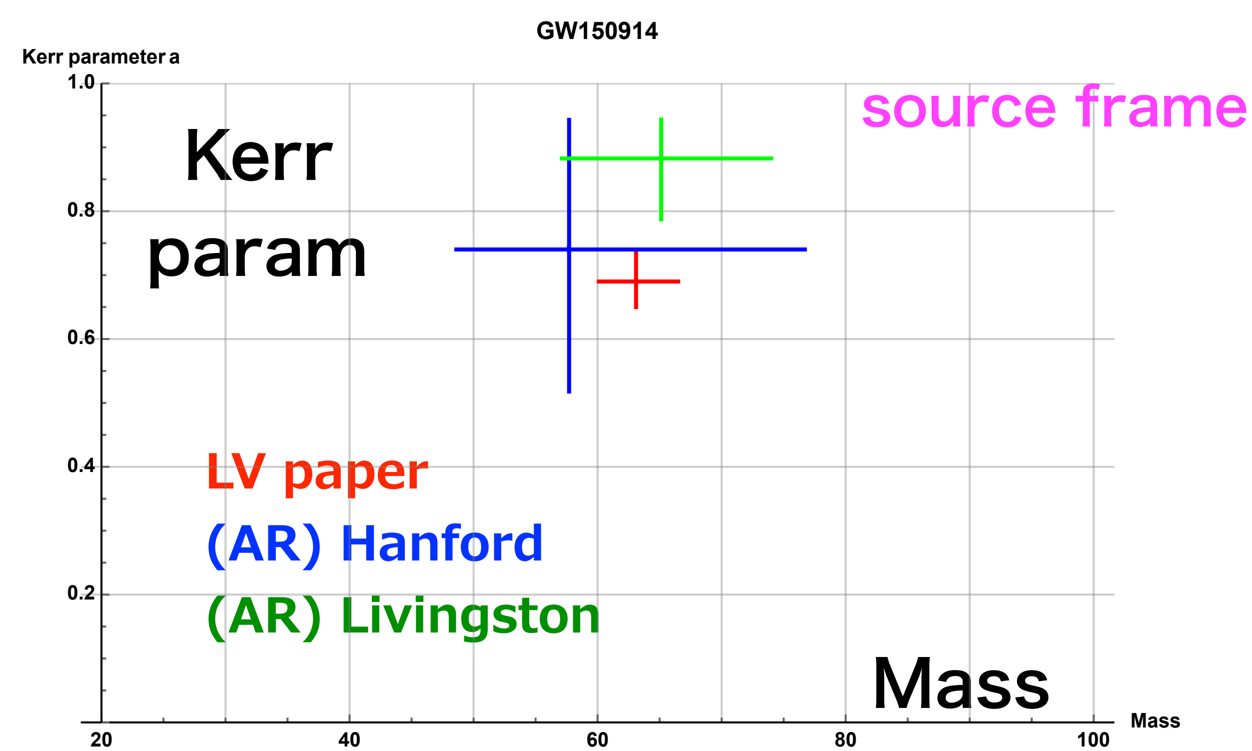

GW170104

Hanford (SNR=9.5)

H1n6_SpectrogramAR

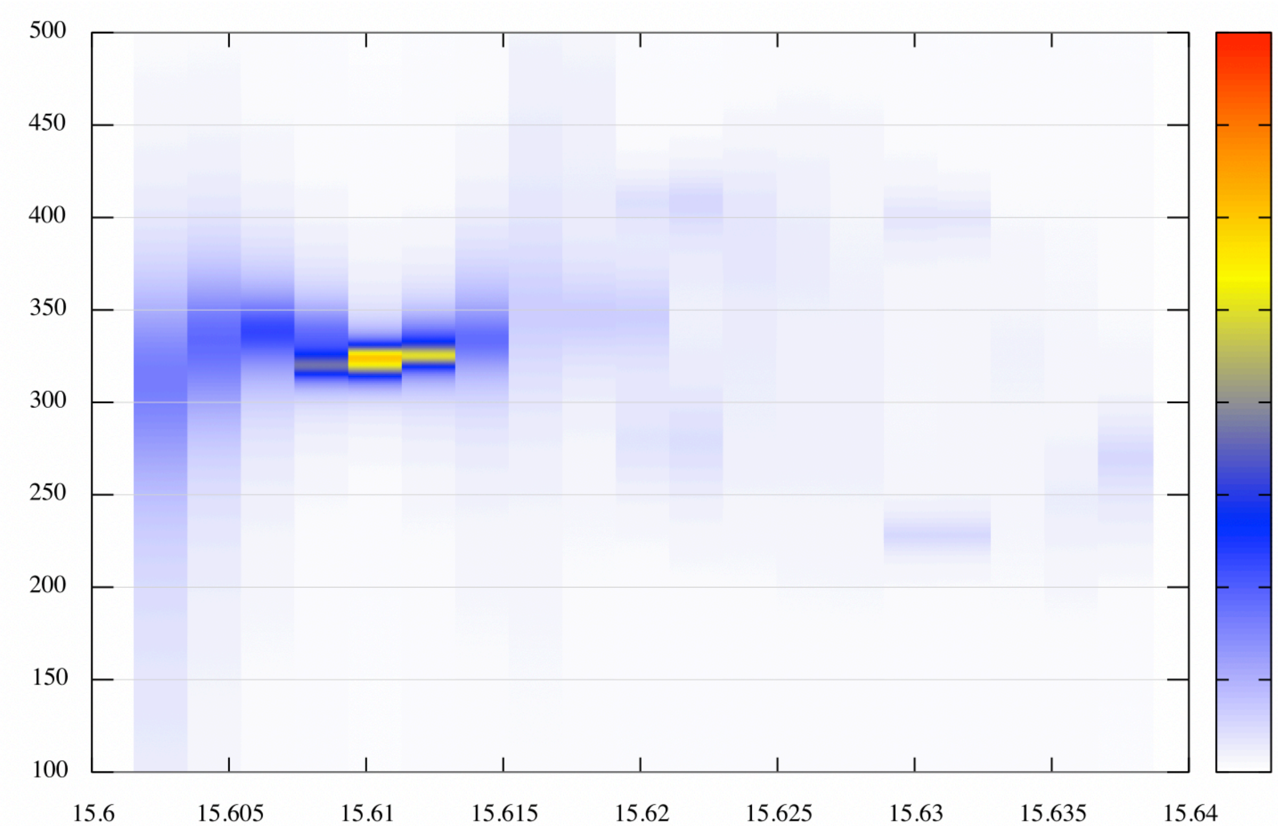

Livingston (SNR=9.9)

L1n6_SpectrogramAR

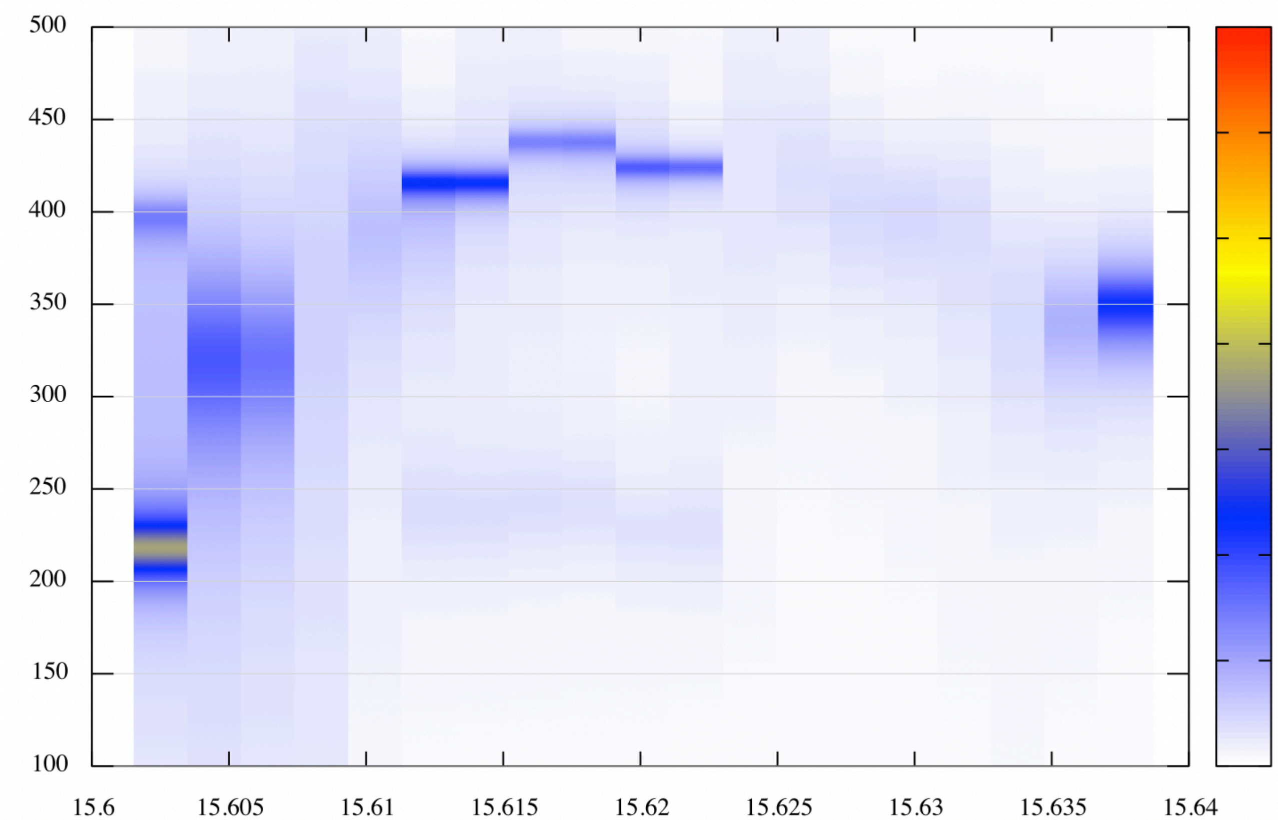

LV paper ▶ $(M, a, z) = (48.9^{+5.1}_{-4.}, 0.66^{+0.08}_{-0.11}, 0.2^{+0.08}_{-0.08})$

f_{QNM} ▶

$f_{220} = 285.7$ Hz, $f_{221} = 279.$ Hz, $f_{222} = 266.$ Hz

$f_{210} = 412.5$ Hz, $f_{211} = 239.3$ Hz, $f_{200} = 272.7$ Hz

$f_{330} = 453.5$ Hz, $f_{331} = 449.5$ Hz, $f_{332} = 442.1$ Hz

$f_{320} = 411.1$ Hz, $f_{310} = 374.4$ Hz, $f_{300} = 343.4$ Hz

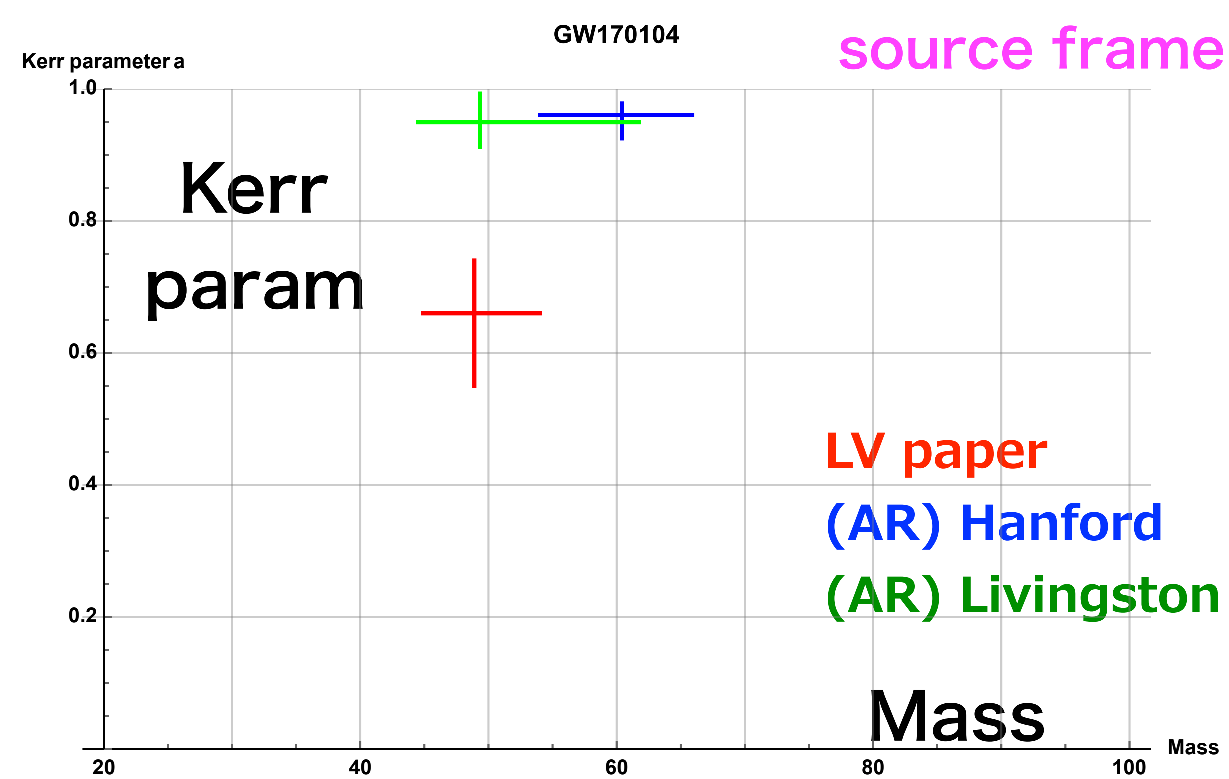

Ringdown Search by Auto-Regressive Approach (O1/O2 public data, GWTC1 catalogue)

GW170729

$$(M, a, z) = (79.5^{+14.7}_{-10.2}, 0.81^{+0.07}_{-0.13}, 0.49^{+0.19}_{-0.21})$$

$f_{220} = 161.4$ Hz, $f_{221} = 159.4$ Hz, $f_{222} = 155.3$ Hz
$f_{210} = 195.6$ Hz, $f_{211} = 128.1$ Hz, $f_{200} = 132.6$ Hz

Hanford (SNR=5.9)

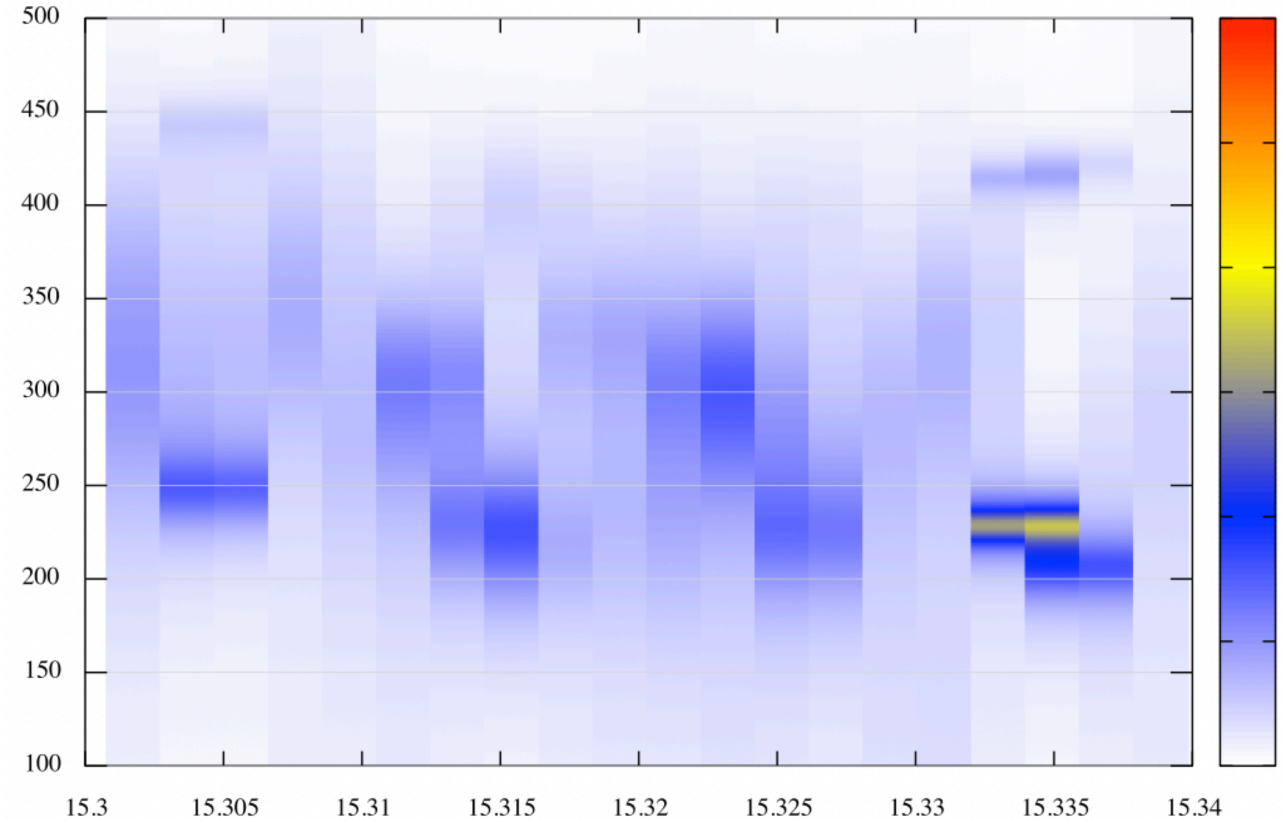

Virgo (SNR=1.7)

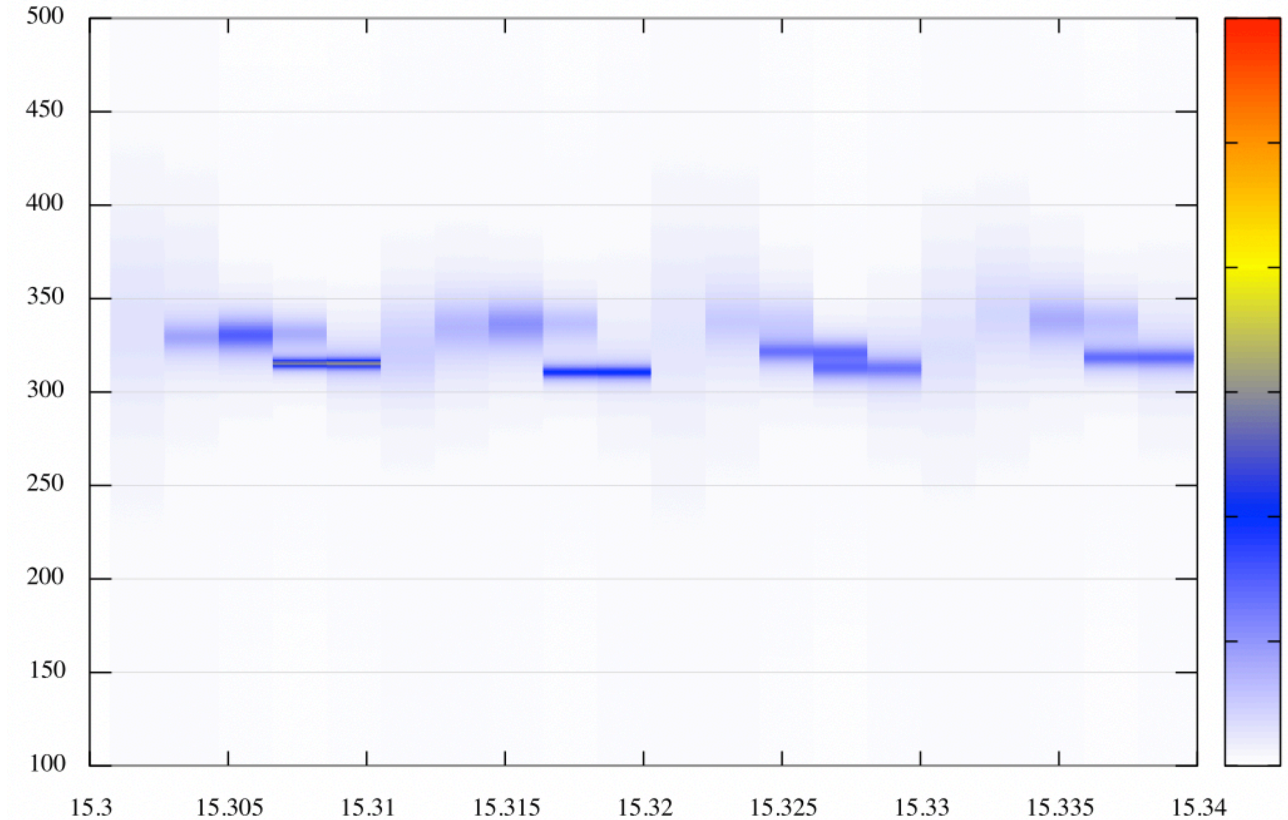

Livingston (SNR=8.3)

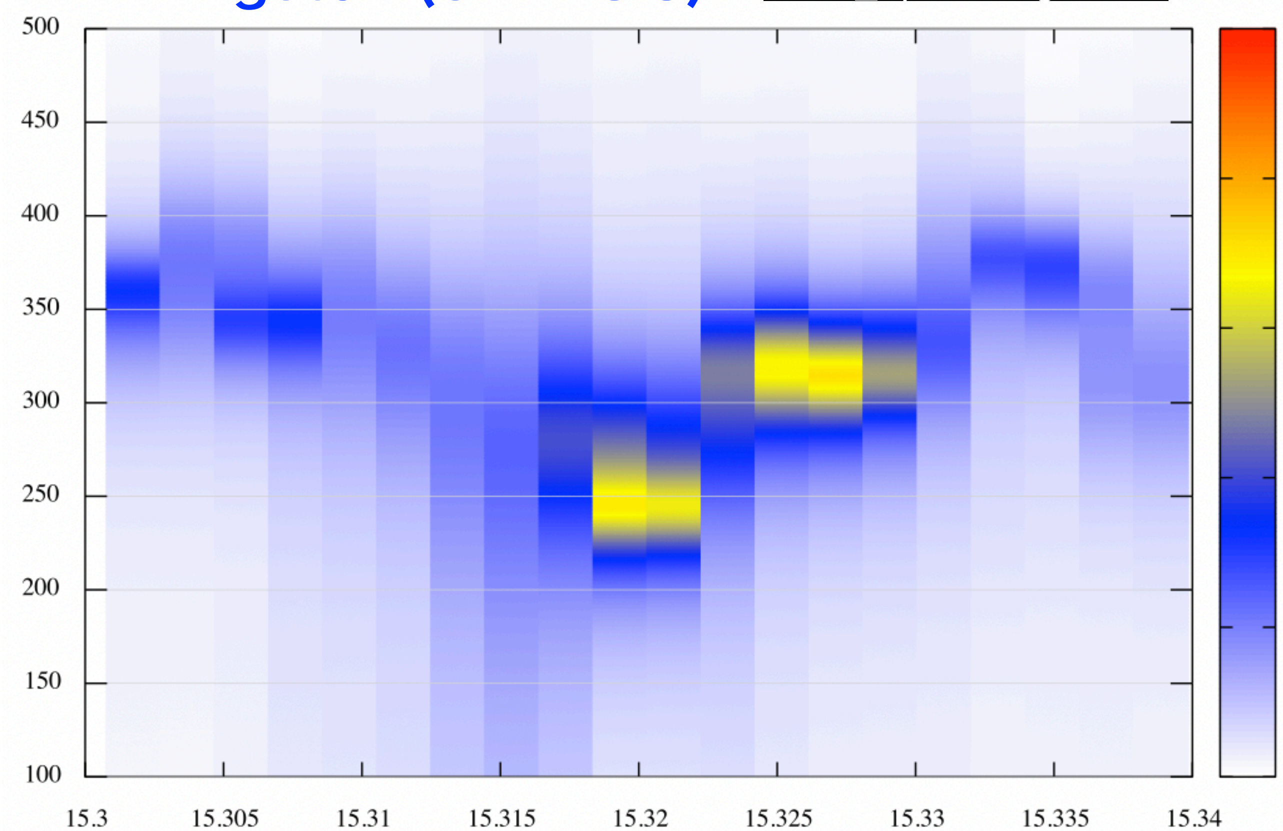

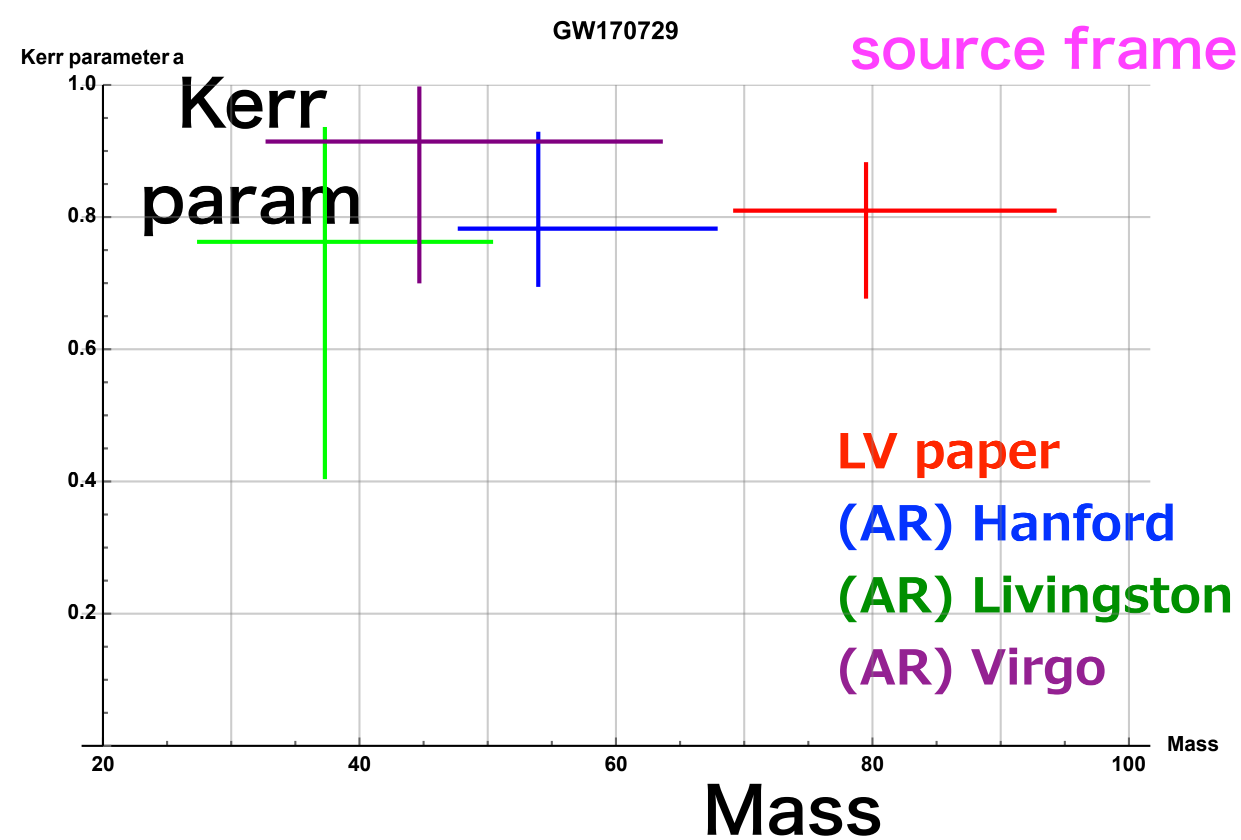

GW170809

$(M, a, z) = (56.3^{+5.2}_{-3.8}, 0.7^{+0.08}_{-0.09}, 0.2^{+0.05}_{-0.07})$

$f_{220} = 255.9$ Hz, $f_{221} = 250.6$ Hz, $f_{222} = 240.3$ Hz
$f_{210} = 354.7$ Hz, $f_{211} = 211.9$ Hz, $f_{200} = 235.8$ Hz

Hanford (SNR=5.9)

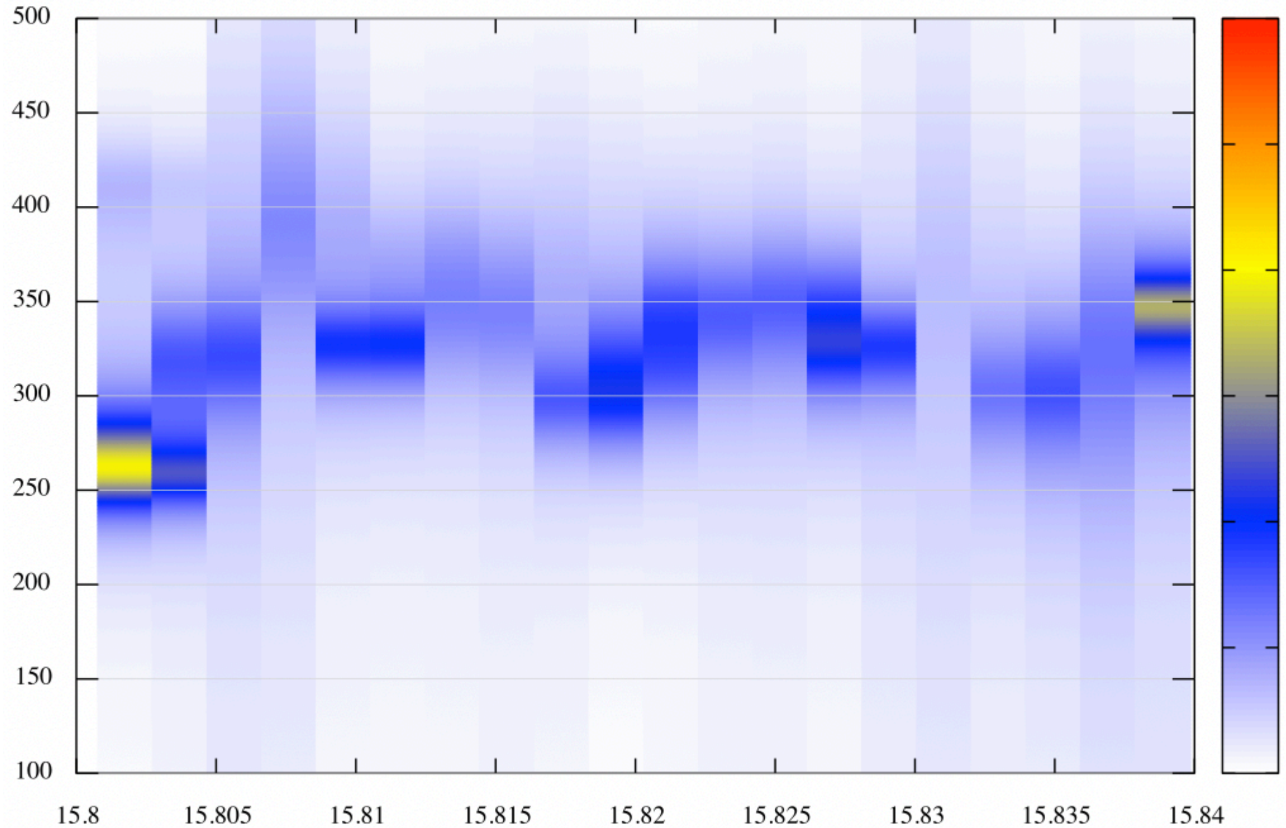

Virgo (SNR=1.1)

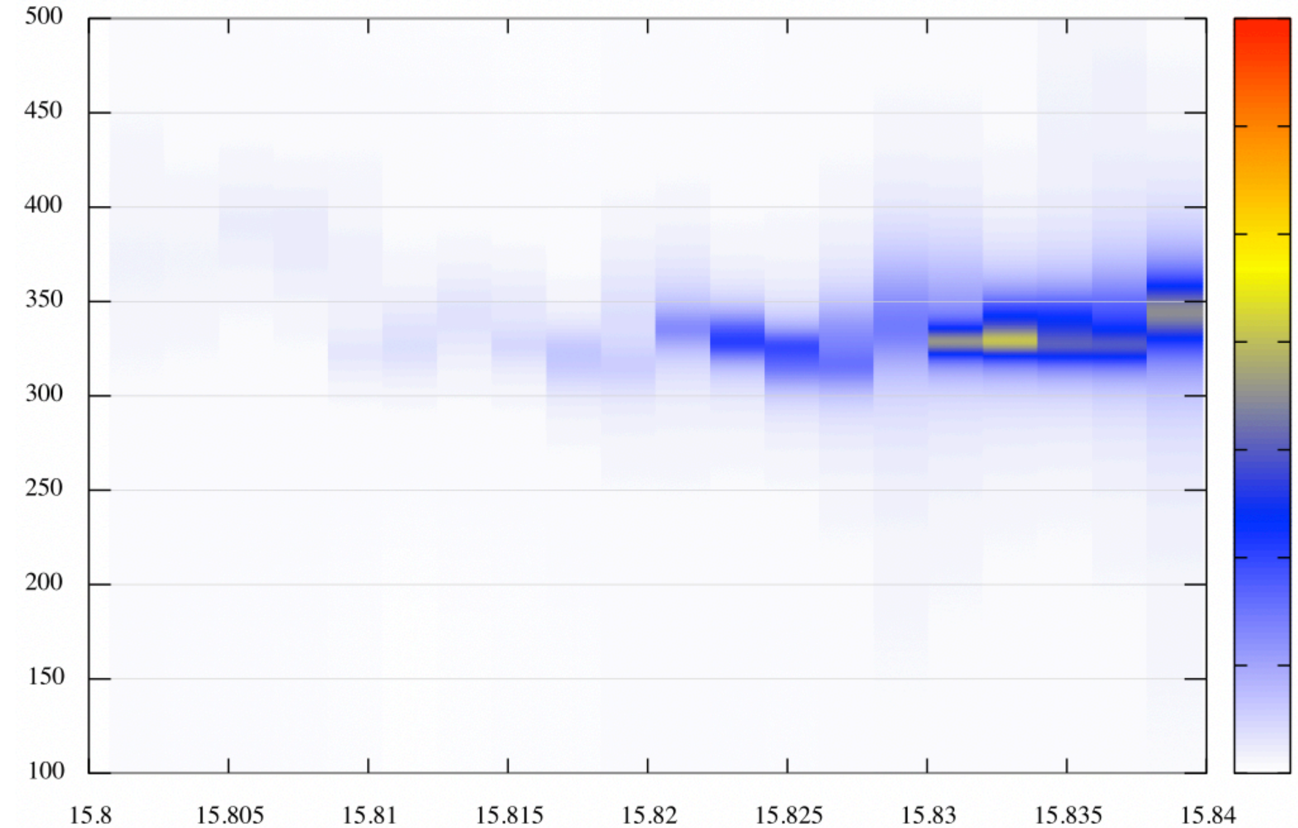

Livingston (SNR=10.7)

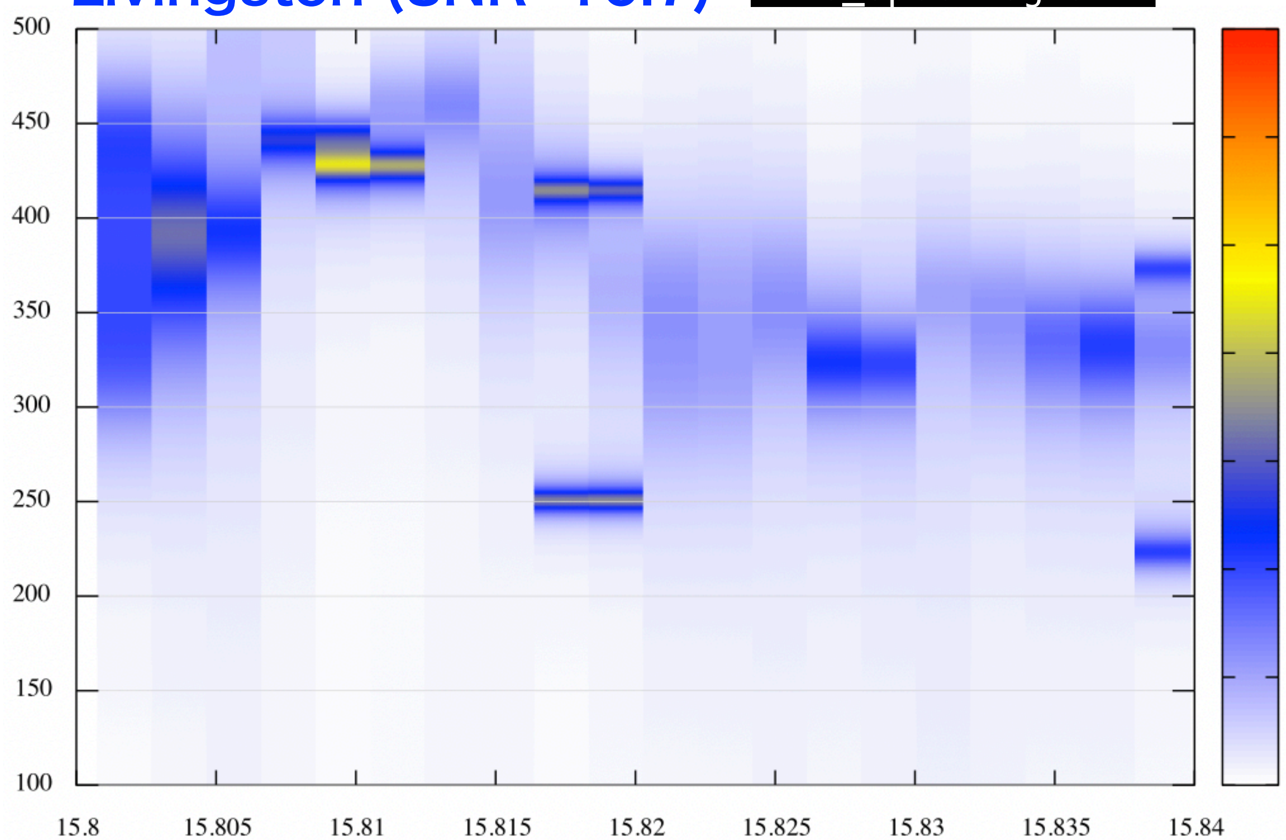

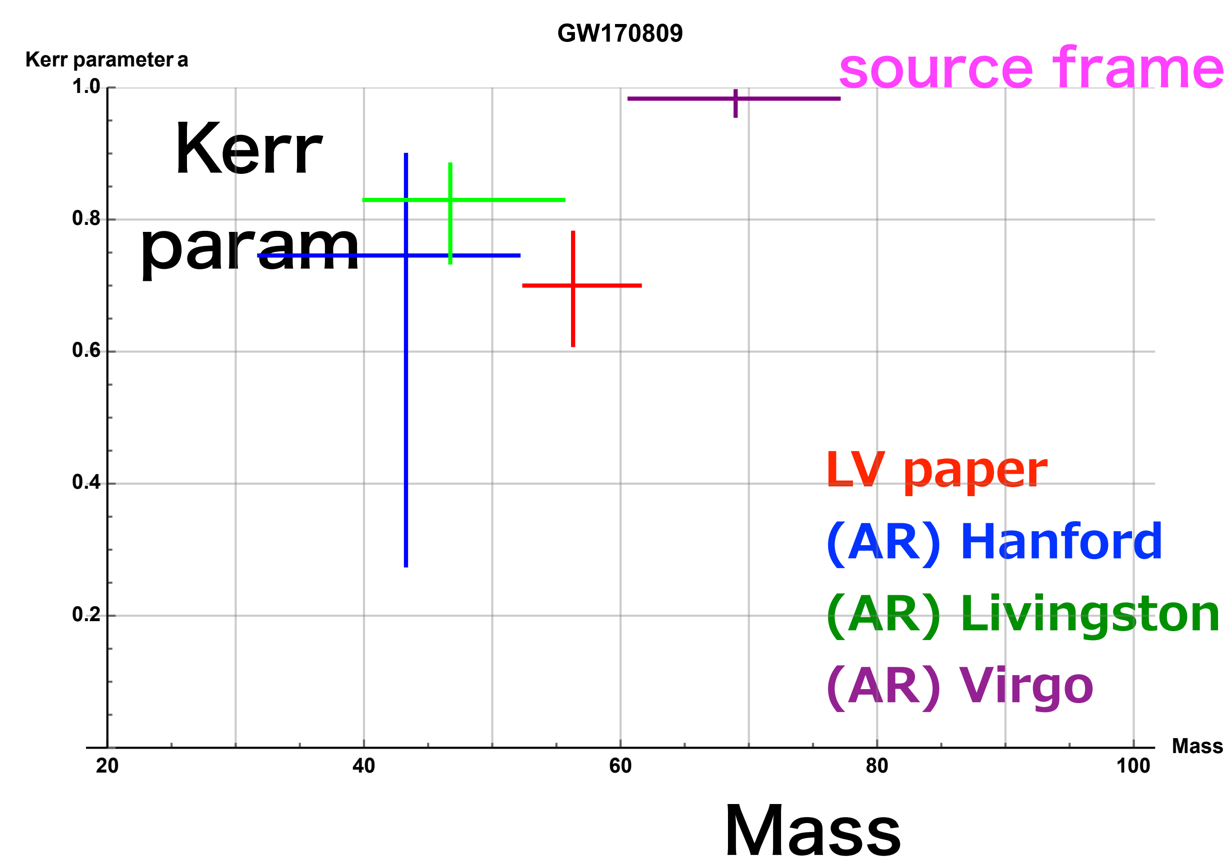

GW170814

$(M, a, z) = (53.2^{+3.2}_{-2.4}, 0.72^{+0.07}_{-0.05}, 0.12^{+0.03}_{-0.04})$

$f_{220} = 294.9$ Hz, $f_{221} = 289.2$ Hz, $f_{222} = 278.1$ Hz

$f_{210} = 400.0$ Hz, $f_{211} = 242.6$ Hz, $f_{200} = 266.8$ Hz

Hanford (SNR=9.3)

H100_SpectrogramARam

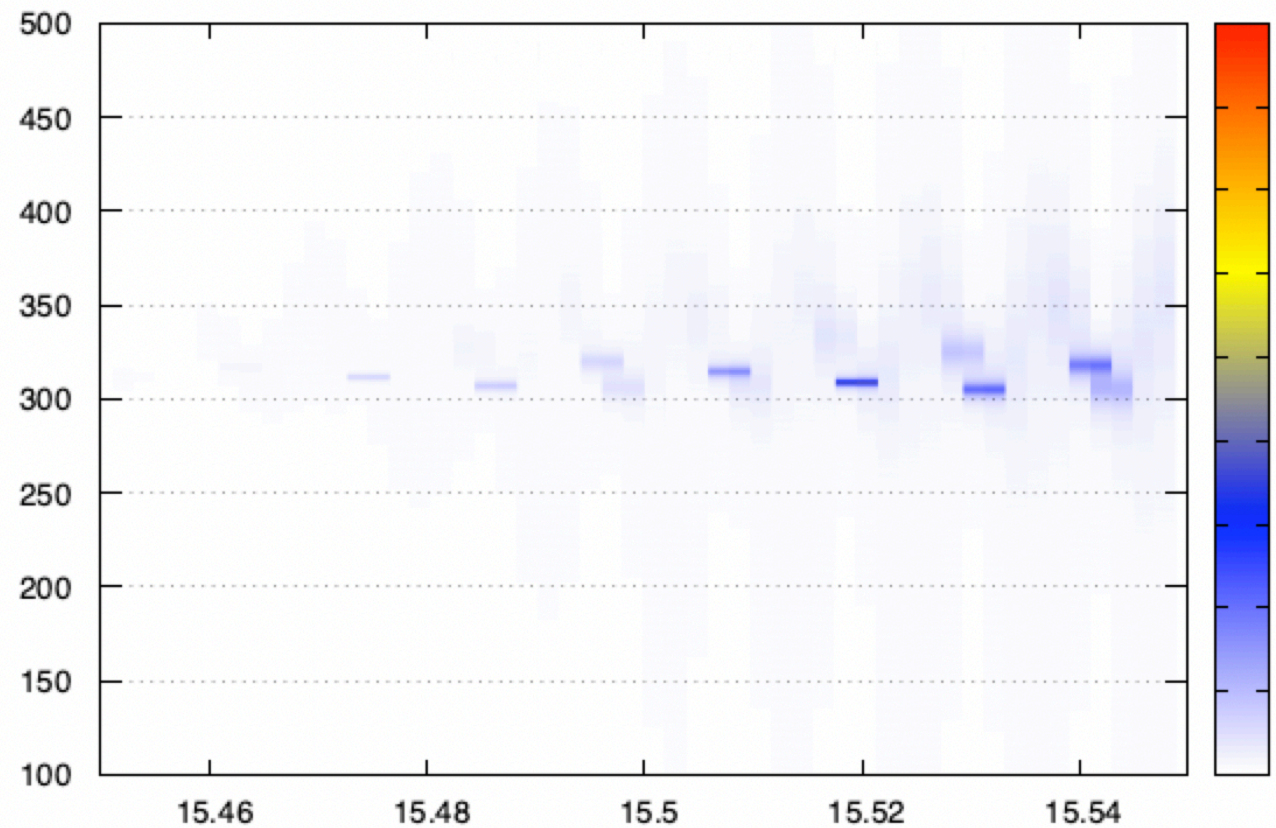

Virgo (SNR=4.1)

V1n6_SpectrogramAR

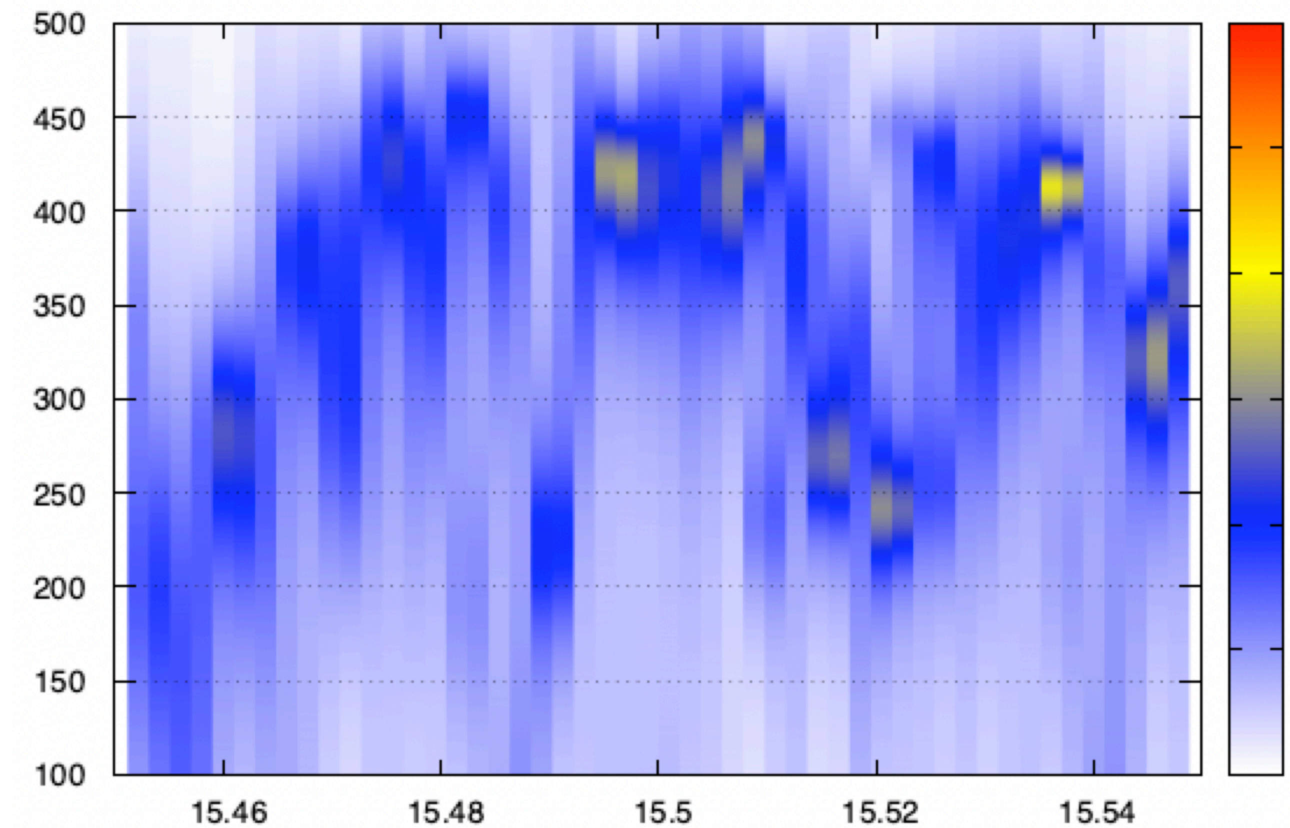

Livingston (SNR=14.3)

L100_SpectrogramARam

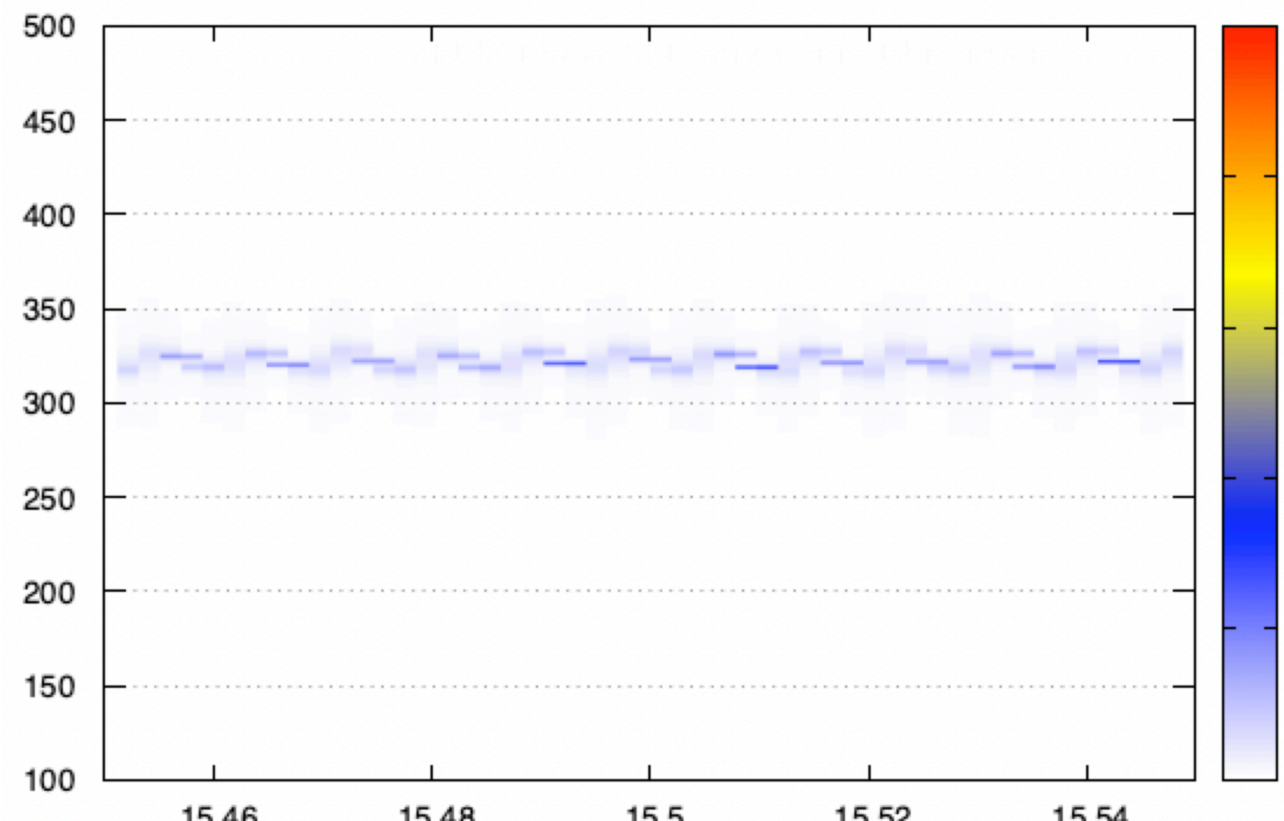

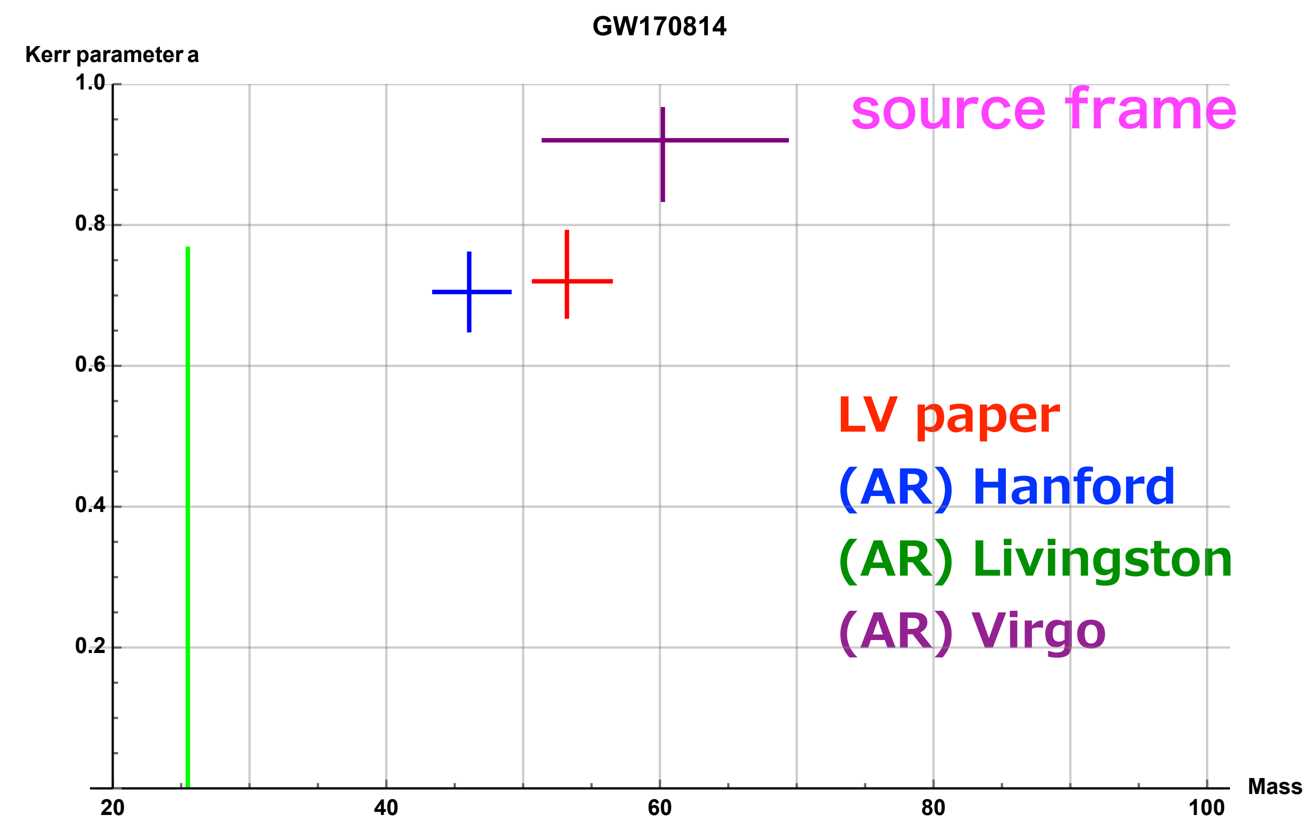

GW170818

$(M, a, z) = (59.4^{+4.9}_{-3.8}, 0.67^{+0.07}_{-0.08}, 0.21^{+0.07}_{-0.07})$

$f_{220} = 235.0$ Hz, $f_{221} = 229.6$ Hz, $f_{222} = 219.3$ Hz

$f_{210} = 336.0$ Hz, $f_{211} = 196.3$ Hz, $f_{200} = 222.4$ Hz

Hanford (SNR=4.6)

H100_SpectrogramAR

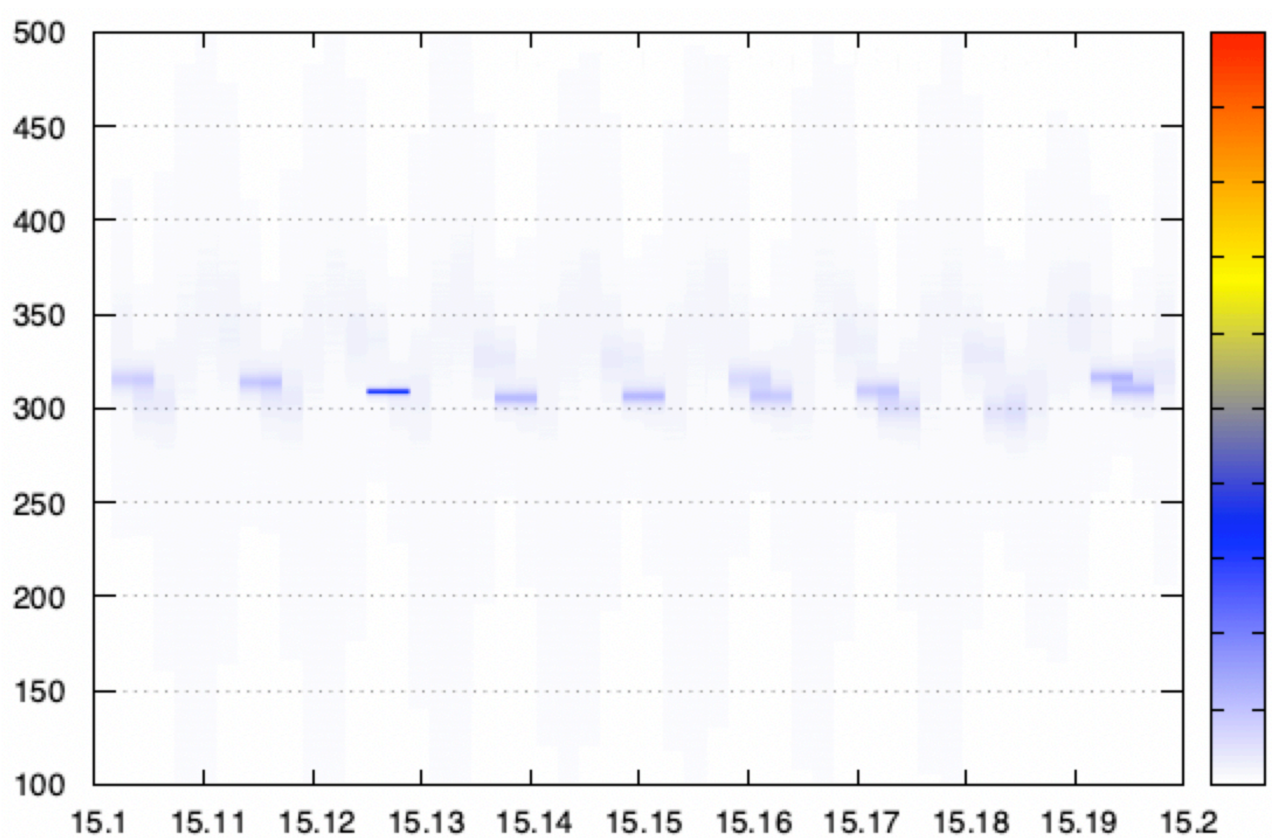

Virgo (SNR=4.2)

V100_SpectrogramAR

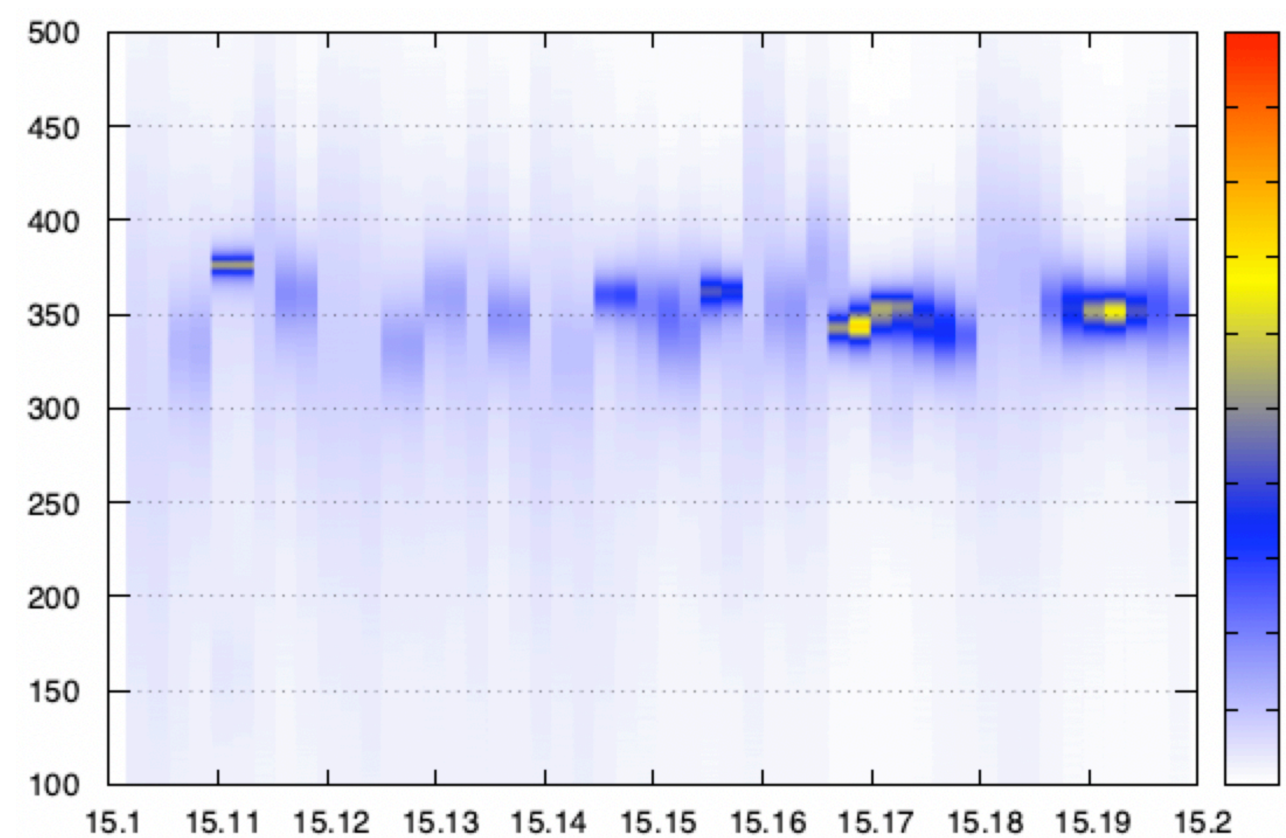

Livingston (SNR=9.7)

L100_SpectrogramAR

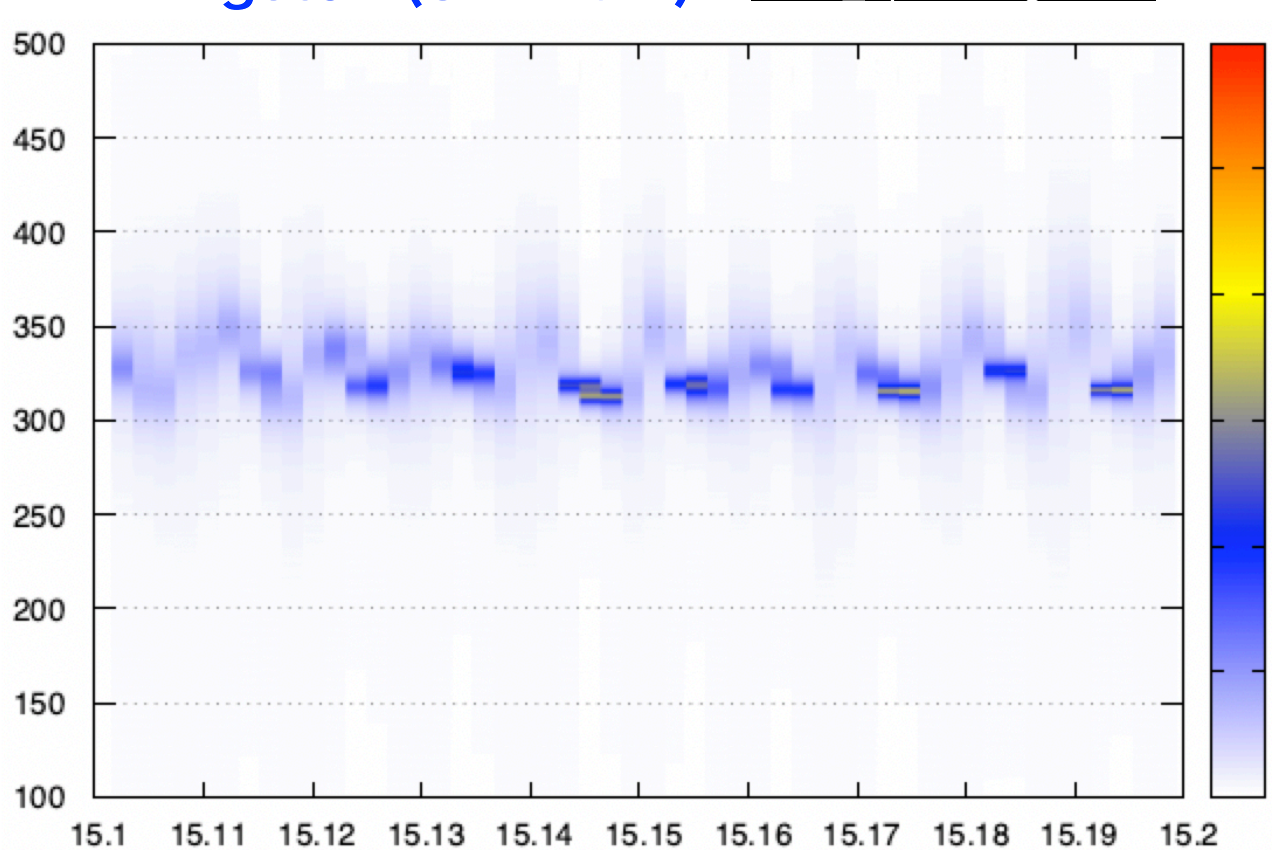

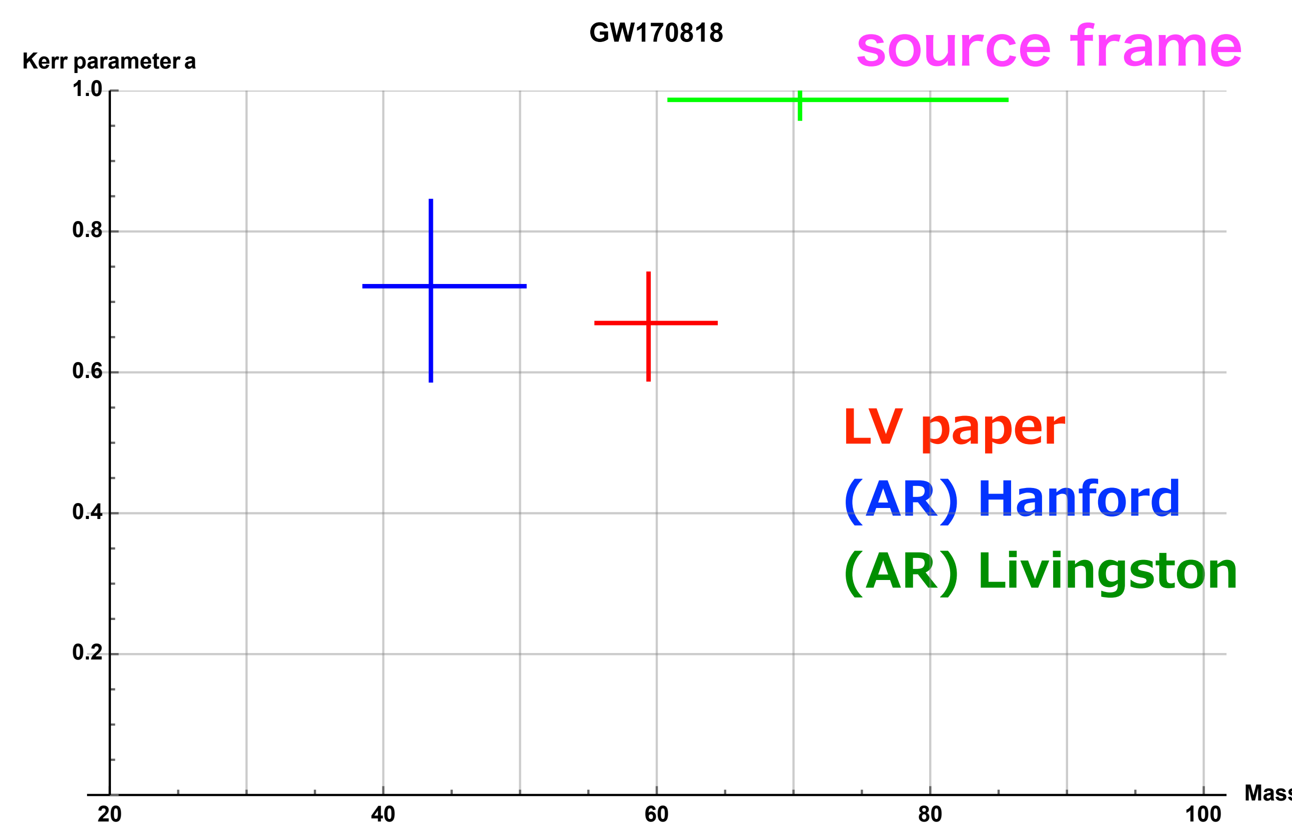

GW170823

Hanford (SNR=6.8)

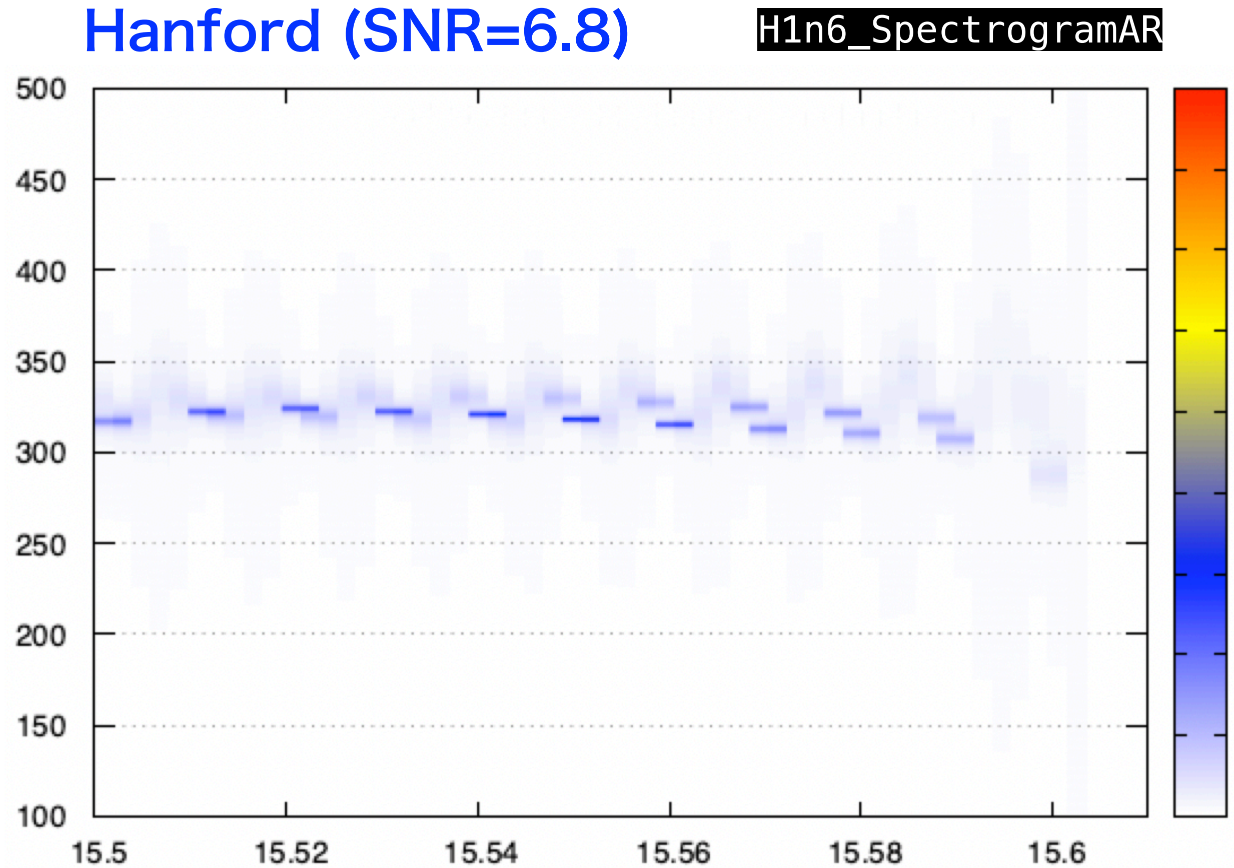

Livingston (SNR=9.2)

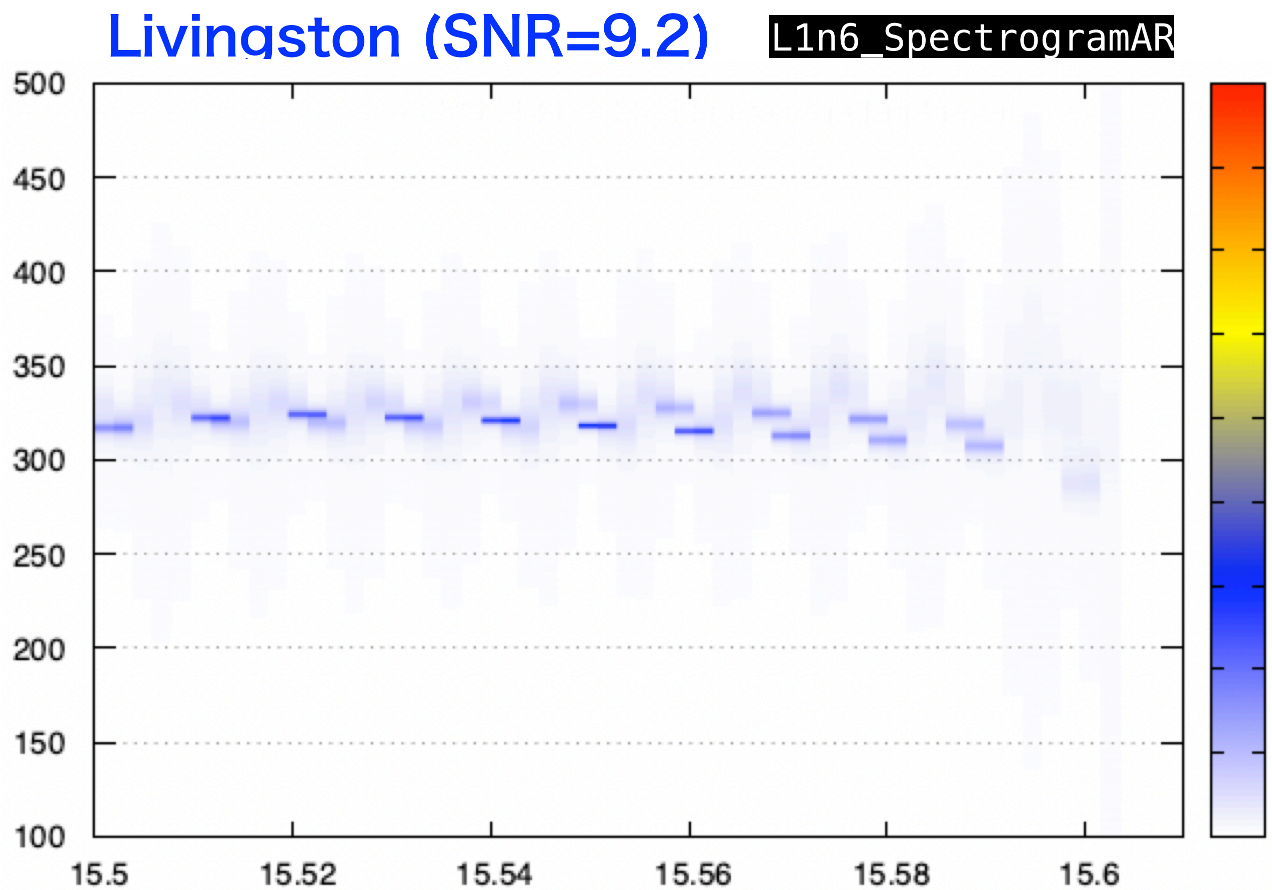

LV paper ▶ $(M, a, z) = (65.4^{+10.1}_{-7.4}, 0.72^{+0.09}_{-0.12}, 0.35^{+0.15}_{-0.15})$

f_{QNM} ▶

$f_{220} = 199.0$ Hz, $f_{221} = 195.2$ Hz, $f_{222} = 187.7$ Hz
$f_{210} = 269.9$ Hz, $f_{211} = 163.7$ Hz, $f_{200} = 180.1$ Hz
$f_{330} = 315.0$ Hz, $f_{331} = 312.8$ Hz, $f_{332} = 308.6$ Hz
$f_{320} = 281.5$ Hz, $f_{310} = 253.2$ Hz, $f_{300} = 229.7$ Hz

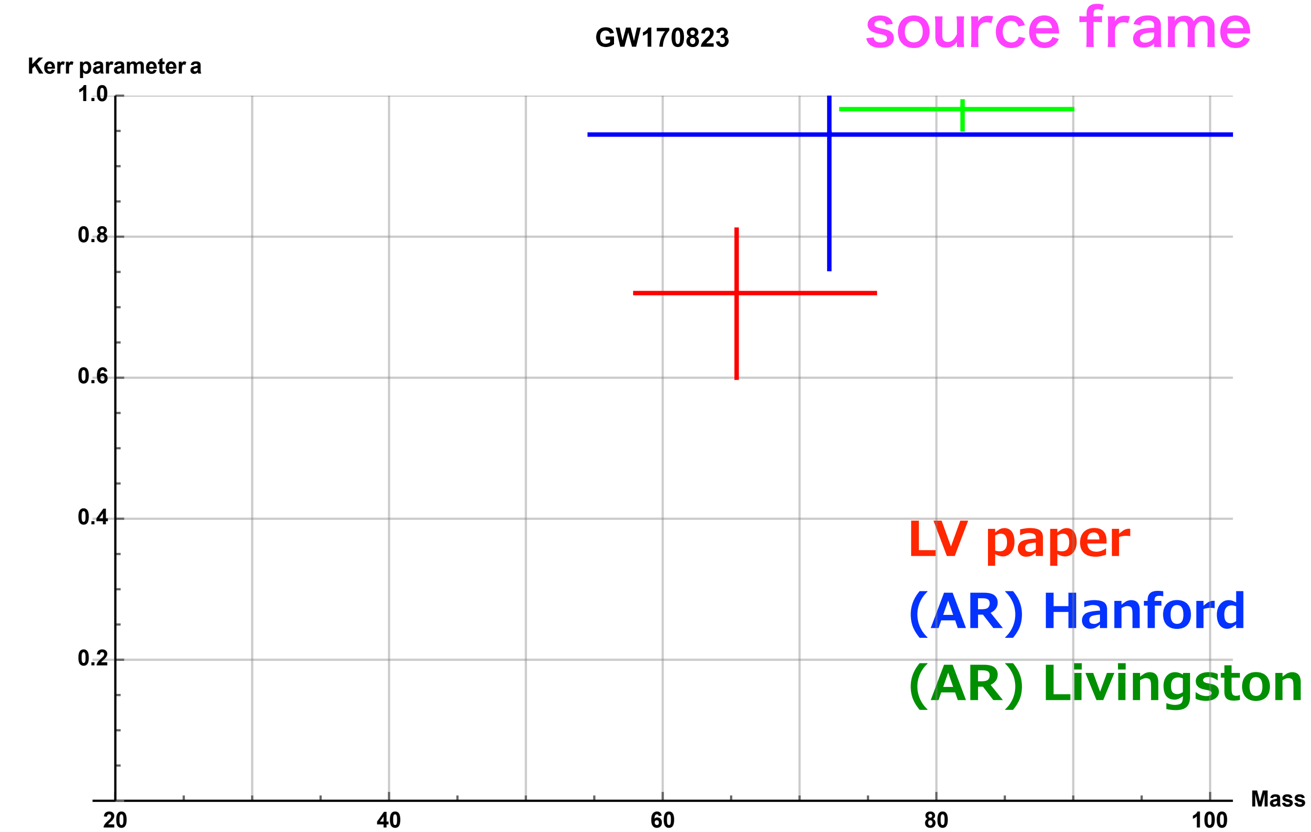

Summary & Outlook

自己回帰モデル *x(t)*

$$x_n = a_1 x_{n-1} + a_2 x_{n-2} + \cdots + a_M x_{n-M} + \varepsilon$$
$$= \sum_{j=1}^{M} a_j x_{n-j} + \varepsilon$$

短いデータ (〜 60 pts) に対しても精度よく周波数・減衰率を特定できる.
シグナルを見つけるのにテンプレートは不要.

LIGO/Virgo の O1/O2イベントデータに適用，リングダウン部分の抽出を試みた.
SN比が高ければ，独立にリングダウン部分が取り出せそうだ.

★ノイズ除去の方法や，他の方法と組み合わせ，より精密な周波数特定法を検討中.
★higher modesの検出へ，BHの特長量の特定へ，相対論検証へ.
★テンプレートを使わない方法は，今後，未知の重力波シグナルの候補検出に役立つかも.

重力波観測の将来計画

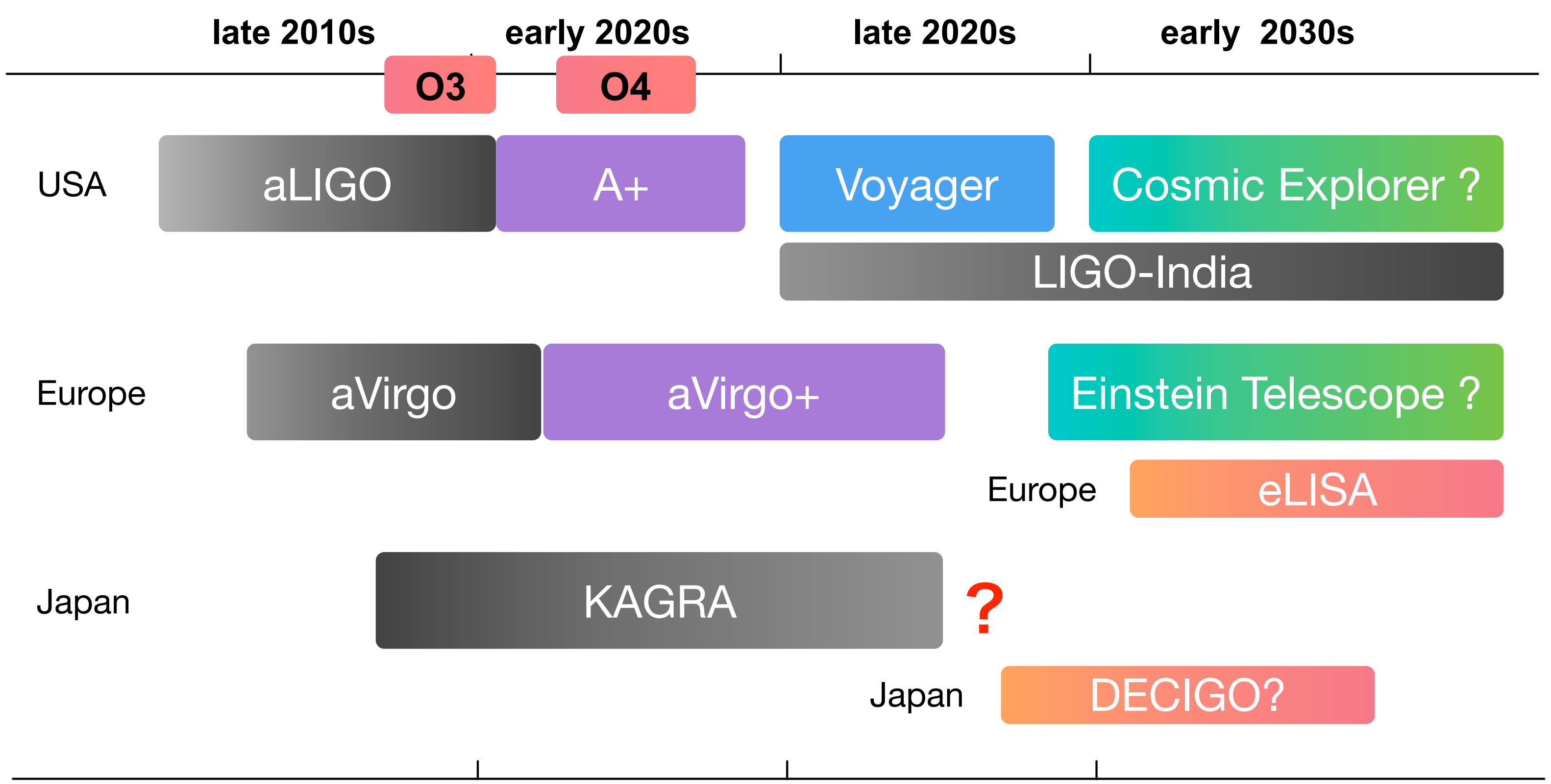

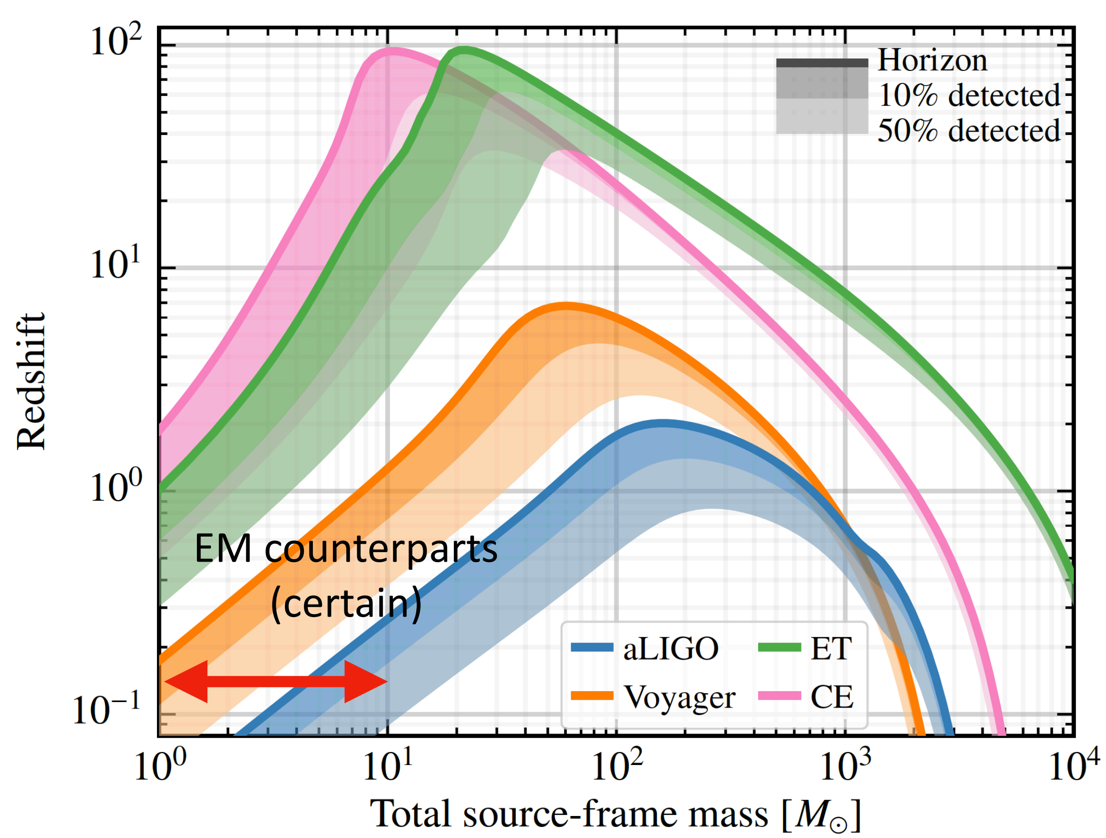

Evan Hall, MIT

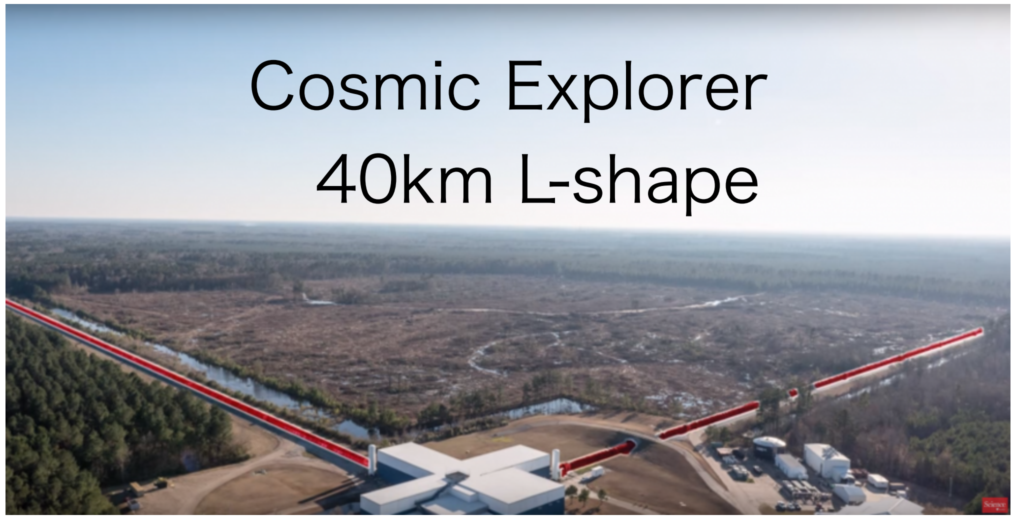

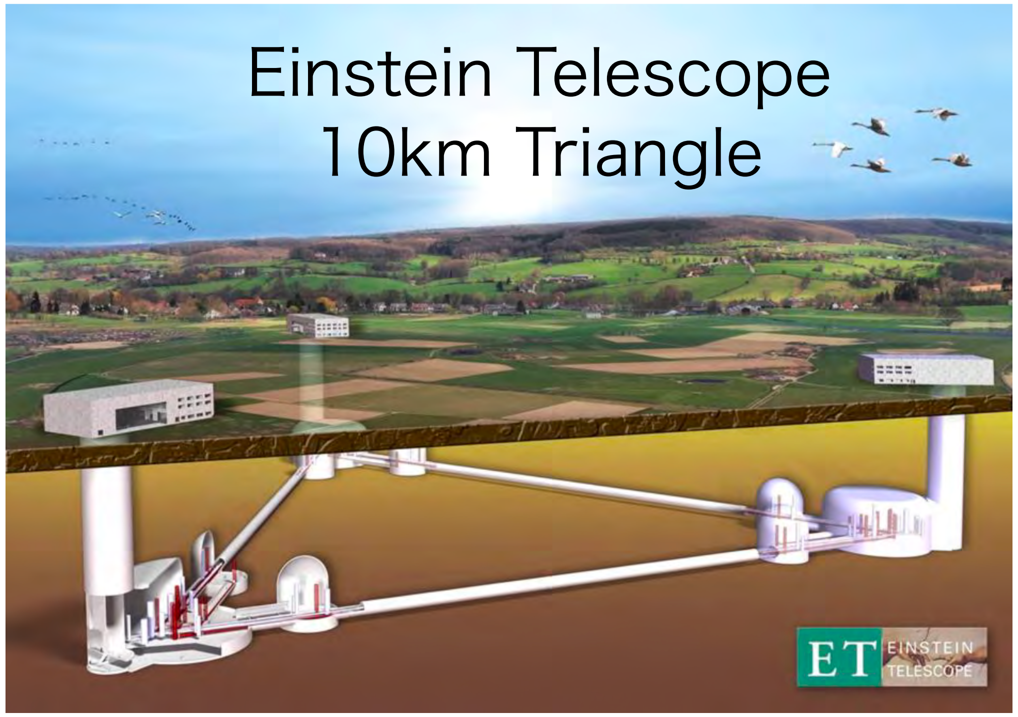

まとめ

1. **重力波観測時代がはじまった**

   BH-BH, NS-NS. 次はBH-NS? SN?

2. **日本のKAGRAも2020年2月25日から実観測開始**

   LIGO/Virgoとの共同観測体制構築.

3. **データ解析には，まだまだ試すべきアイデアがたくさんある.**

   将来計画もたくさんある. **新規参入，大歓迎！**